

**ULTRASONIC MEASUREMENT OF THE ELASTIC CONSTANTS
OF SELECTED NONLINEAR OPTICAL / SEMIORGANIC
CRYSTALS WITH ORTHORHOMBIC SYMMETRY**



THESIS SUBMITTED TO
THE COCHIN UNIVERSITY OF SCIENCE AND TECHNOLOGY
FOR THE AWARD OF THE DEGREE OF
DOCTOR OF PHILOSOPHY

A. V. ALEX

DEPARTMENT OF INSTRUMENTATION
COCHIN UNIVERSITY OF SCIENCE AND TECHNOLOGY
COCHIN-682 022


MAY - 2001

CERTIFICATE

Certified that the work presented in this thesis entitled "*Ultrasonic measurement of the elastic constants of selected nonlinear optical / semiorganic crystals with orthorhombic symmetry*" is based on the bonafide research work done by Mr. A. V. Alex under my guidance, at the Department of Instrumentation, Cochin University of Science and Technology, and has not been included in any other thesis submitted previously for the award of any other degree.

Cochin - 682 022

May 21, 2001


Dr. Jacob Philip
Supervising teacher

DEPARTMENT OF INSTRUMENTATION
Cochin University of Science & Technology
KOCHI-682 022

*

Contents

<i>Preface</i>	<i>i</i>
----------------	----------

<i>Acknowledgements</i>	<i>vii</i>
-------------------------	------------

Chapter 1	Ultrasonic measurement of the elastic constants of single crystals: A Review	
-----------	--	--

1.1	Introduction	1
1.2	The Christoffel's matrix	5
1.3	Relation between elastic constants and sound velocities	10
1.4	Elastic constants of Orthorhombic crystals	10
1.5	Measurement of elastic constants by ultrasonic methods	16
1.6	Other related elastic properties of an orthorhombic crystal	19
1.6.1	Poisson's ratios	20
1.6.2	Young's modulus	21
1.6.3	Volume compressibility and bulk modulus	22
1.6.4	Linear compressibility	23
1.6.5	Phase velocity surface and inverse velocity (slowness) surface	23
1.6.6	Group velocity surface	24
1.6.7	Computation of group velocity	27
	x-y plane	27
	y-z plane	28
	x-z plane	29
1.7	Nonlinear optical crystals: Their properties and applications	31
1.8	Summary and conclusion	35
	References	36

Chapter 2 Instrumentation

2.1	Introduction	39
2.1.1	Continuous wave methods	39
2.1.2	Low frequency methods	40
2.1.3	Pulse methods	41
2.2	The Pulse echo overlap method	42
2.3	The experimental setup	44
2.4	Sample cell and accessories	47
2.5	Low and high temperature measurements	50
2.6	Bond correction in ultrasonic measurements	50
2.7	Sample preparation techniques	55
2.7.1	Crystal growth from solution	55
	Reference	58

Chapter 3 Elastic properties of Sodium p-nitrophenolate dihydrate (NPNa) single crystals

3.1	Introduction	61
3.2	Sample preparation	65
3.3	Ultrasonic velocity measurements	68
3.4	Temperature variation of elastic constants	70
3.5	Elastic anisotropy of NPNa crystals	70
3.6	Discussion and conclusion	76
	.References	78

Chapter 4 Elastic properties of Potassium acid phthalate (KAP) single crystals

4.1	Introduction	81
4.2	Sample preparation	83
4.3	Ultrasonic velocity measurements	84
4.4	Elastic constants of KAP crystal	85
4.5	Temperature dependence of elastic constants	87
4.6	Anisotropy of elastic wave propagation in KAP crystal	88
4.7	Discussion and conclusion	95
	References	95

Chapter 5 Elastic properties of Zinc tris (thiourea) sulphate (ZTS) single crystals

5.1	Introduction	98
5.2	Sample preparation	104
5.3	Ultrasonic velocity measurements	106
5.4	Elastic constants of ZTS crystal	107
5.5	Temperature dependence of elastic constants	109
5.6	Anisotropy in elastic wave propagation in ZTS	109
5.7	Discussion and conclusion	117
	References	118

Chapter 6 Elastic properties of benzoyl glycine (BG) single crystals

6.1	Introduction	121
6.2	Sample preparation	124
6.3	Ultrasonic velocity measurements	127
6.4	Elastic constants of benzoyl glycine single crystal	128
6.5	Temperature variation of elastic constants	130
6.6	Elastic anisotropy in BG crystals	130
6.7	Discussion and conclusion	137
	References	139

Chapter 7 Elastic properties of di-Ammonium hydrogen citrate (DAHC) single crystals

7.1	Introduction	141
7.2	Sample preparation	142
7.3	Ultrasonic velocity measurements	144
7.4	Elastic constants of DAHC single crystals	145
7.5	Temperature dependence of elastic constants	147
7.6	Elastic anisotropy in DAHC crystal	148
7.7	Discussion and conclusion	154
	References	156

Chapter 8 Summary and conclusion

	Appendix I	162
--	-------------------	-----

PREFACE

Crystalline structure is the result of an orderly process of packing of atoms/ molecules and generally speaking, is the ideal form of aggregation for a solid from a thermodynamic point of view. Consequently, the study of properties of single crystals is an essential ingredient in the effort to gain a better understanding of solid materials. Single crystals are in general continuous media that are homogeneous and anisotropic. Mechanical properties of crystals depend on their response to the applied load. In the initial stage of deformation, called elastic deformation, the strain experienced by the medium is small and reversible. If deformation is irreversible, we call it plastic deformation. In the final stage of deformation we have the strength or resistance of the material to failure as the relevant material characteristic. Elastic properties of a solid depend on the behavior of the constituent particles, atoms or molecules where as the behavior of a chain of such particles decides the plastic behavior. Properties of surfaces built by these particles alone decide the strength or resistance to failure. The balance of the inter-particle forces can be disturbed by the application of mechanical stress resulting in changes in lattice spacing.

Ultrasonics is one of the most widely used techniques to determine the elastic properties of solids. Both static and dynamic properties can be measured simultaneously using this technique. Ultrasonic velocity measurements provide information about the equilibrium adiabatic properties of the system and the influence of external parameters such as temperature, pressure, different external fields etc. on it. Measurement of the elastic constants as a function of temperature enables one to locate phase transition points, determine phase diagrams and to make statements about the order of the transition involved.

Measurement of ultrasonic velocities along different symmetry directions in crystals with waves of different polarizations enables one to determine the second order elastic constants. Different techniques have been developed for the accurate measurement of ultrasonic wave velocities. Pulse interferometric techniques such as pulse echo overlap technique and pulse superposition technique are the most accurate and precise ones for these measurements. Pulse comparison technique is generally used for ultrasonic attenuation measurements.

In this thesis we present the results of our investigations of the elastic properties of three selected nonlinear optical crystals, sodium p-nitrophenolate dihydrate (NPNa), benzoyl glycine (BG) and Zinc tris(thiourea) sulphate (ZTS) and two semiorganic compounds, potassium hydrogen phthalate (KAP) and di-ammonium hydrogen citrate (DAHC). All these crystals have orthorhombic structure at room temperature.

Chapter 1 is an introductory chapter, which includes a brief introduction to the theory of elastic wave propagation through anisotropic media. Expressions for the velocity of propagation of ultrasonic waves along different symmetry directions are derived for crystals of orthorhombic symmetry. Techniques to demonstrate anisotropy in elastic wave propagation characteristics of a medium are also reviewed with theoretical support. Various other elastic properties such as Poisson's ratios, bulk modulus, volume compressibility, Young's modulus and linear compressibility are also discussed briefly. A brief introduction to the properties and applications of nonlinear optical crystals is also included for completeness.

Various techniques to measure ultrasonic wave velocity, dependence of velocity on temperature, crystal growth from solution and preparation of oriented samples for measurements, are discussed briefly in chapter 2. The McSkimin Δt correction procedure is also included with necessary theoretical support. The design

and development of a programmable temperature controller suitable for solution growth by the slow cooling technique is included and more details are given as Appendix I.

Details of the measurement of the elastic stiffness constants of NPNa crystals and dependence of the diagonal elastic constants on temperature in a limited range are discussed in chapter 3. The anisotropy in elastic wave propagation characteristics of this crystal is illustrated by plotting sections of the phase velocity, slowness and group velocity surfaces along the a-b, b-c and a-c symmetry planes. Young's modulus and linear compressibility surfaces are also plotted to demonstrate the anisotropy in elastic properties of this crystal. Various results and a brief discussion on the results presented are also included in this chapter.

Details of our investigations on the elastic properties of KAP single crystals are briefly described in chapter 4. All the nine second-order elastic constants, Poisson's ratios, bulk modulus and volume compressibility values are reported for this crystal and the anisotropy in elastic wave propagation characteristics illustrated with the help of surface plots of phase velocity, slowness and group velocity. Anisotropy in other elastic properties such as Young's modulus and linear compressibility are also demonstrated by plotting projections of the respective surfaces on a-b, b-c and a-c symmetry planes.

A potential nonlinear optical (NLO) material of current interest viz., Zinc tris(thiourea) sulphate (ZTS), is the subject of discussion in chapter 5. Crystal growth, morphology, measurement of ultrasonic wave velocity, determination of respective elastic constants and various other elastic properties such as Poisson's ratios, bulk modulus and volume compressibility are briefly discussed with experimental details. Sections of phase velocity, slowness and group velocity surfaces along the symmetry

planes demonstrating the anisotropy in elastic wave propagation characteristics of this crystal are also included in this chapter. Young's modulus and linear compressibility values are plotted for various directions in the symmetry planes a-b, b-c and a-c to illustrate the anisotropy in elastic properties of this crystal. A short discussion on the various results is given to conclude this chapter.

Chapter 6 discusses in detail, the crystal growth, preparation of oriented specimen, experimental method, and results of our measurements of the elastic properties of benzoyl glycine single crystals, which exhibit NLO activity. Elastic constants, Poisson's ratios, bulk modulus and volume compressibility of this crystal are evaluated following ultrasonic wave velocity measurements. Anisotropy in elastic properties demonstrated by projecting the surfaces of phase velocity, slowness and group velocity on the symmetry planes (a-b, b-c and a-c) is also included in this chapter with a brief discussion of the results obtained.

Results of our investigations of the elastic properties of di-ammonium hydrogen citrate single crystal are reported in chapter 7. All the nine elastic constants, Poisson's ratios and related elastic parameters are determined and anisotropy in elastic properties demonstrated using surface plots of phase velocity, slowness and group velocity in two dimensions. Young's modulus and linear compressibility values plotted for various directions in the three symmetry planes demonstrate the extent of anisotropy in its elastic properties. This chapter concludes with a brief discussion on the results outlined.

Chapter 8 is a concluding chapter, which discusses the general aspects of the above five single crystals. It also reviews the scope for future studies in the field of NLO crystals. Semi-organic or organo-metallic NLO crystals have several advantages

over crystals of the organic and inorganic constituents. Scope for future work on the elastic properties of similar materials is outlined in this chapter.

The following papers have been published / presented / communicated in different journals / conferences based on the results presented in this thesis.

1. A. V. Alex, J. Philip, S. Brahadeeswaran and H. L. Bhat, "*Ultrasonic measurement of the elastic constants of sodium p-nitrophenolate dihydrate single crystals*", Phys. Rev. B **62** (2000) 2973
2. A. V. Alex and J. Philip, "*Ultrasonic measurement of the elastic constants of potassium hydrogen phthalate single crystals*", J. Appl. Phys. **88** (2000) 2349
3. A. V. Alex and J. Philip, "*Elastic properties of zinc tris(thiourea) sulphate (ZTS) single crystals*", (Communicated to J. Appl. Phys.)
4. A. V. Alex and J. Philip, "*Elastic properties of di-ammonium hydrogen citrate single crystals: An ultrasonic study*", (Communicated to Materials science and engineering B)
5. A. V. Alex and J. Philip, "*Ultrasonic measurement of the elastic properties of benzoyl glycine single crystals*", (Communicated to Crystal Research and Technology)
6. A. V. Alex and J. Philip, "*An automated crystal growth unit employing temperature reduction under microprocessor control*", National Symposium on Instrumentation (NSI-22), 22-25 October 1997, National Physical Laboratory, New Delhi.
7. A. V. Alex, J. Philip, S. Brahadeeswaran and H. L. Bhat, "*The elastic constants of sodium p-nitrophenolate dihydrate single crystals measured by ultrasonic PEO technique*", IX National Symposium on Ultrasonics, 14-16 December 1998, Raman School of Physics, Pondicherry University. J. Pure Appl. Ultrason. **21** (1999) 47
8. A. V. Alex and J. Philip, "*Elastic constants of potassium hydrogen phthalate single crystals measured by ultrasonic PEO method*", International Conference and Exhibition on Ultrasonics (ICEU-99) 2-4 December 1999, National Physical Laboratory, New Delhi.
9. A. V. Alex "*Ultrasonic measurement of the elastic constants of selected orthorhombic crystals*", 43rd DAE-Solid State Physics Symposium, 27-31 December 2000, Guru Ghasidas University, Bilaspur (MP)
10. A. V. Alex and J. Philip, "*Ultrasonic measurement of the elastic constants of di-ammonium hydrogen citrate single crystals*", 43rd DAE-Solid State Physics Symposium, 27-31 December 2000, Guru Ghasidas University, Bilaspur (MP)

11. A. V. Alex and J. Philip, "*Ultrasonic measurement of the elastic constants of benzoyl glycine crystals*", Xth National Symposium on Ultrasonics (X-NSU), 8-9 March 2001, Department of Physics, Osmania University, Hyderabad.
12. A. V. Alex and J. Philip, "*Ultrasonic measurement of the elastic constants of zinc tris(thiourea) sulphate single crystals*", Xth National Symposium on Ultrasonics (X-NSU), 8-9 March 2001, Department of Physics, Osmania University, Hyderabad.

In addition to these, another two papers, which are not included in this thesis, have also been published during the course of this work.

1. A. Deepthy, H. L. Bhat, A. V. Alex and J. Philip, "*Ultrasonic investigation of elastic properties and phase transition in ferroelectric glycine phosphite $NH_3CH_2COOH_3PO_3$ single crystals*", Phys. Rev. **B 62** (2000) 8752
2. A. Deepthy, H. L. Bhat, A. V. Alex and J. Philip, "*Ultrasonic measurement of elastic constants of glycine phosphite crystals*", National Symposium on Acoustics-2000 (NSA-2000) 22-23 November 2000, Department of Physics, St. Joseph's College, Thiuchirappalli. J. Acous. Soc. Ind., **28** (2000) 185

Chapter 1

Ultrasonic measurement of the elastic constants of single crystals: A Review

1.1 Introduction

The study of elastic properties of a material is very important since they are directly related to various fundamental solid state parameters such as specific heat, Debye temperature, phonon dispersion, thermal expansion, Grüneisen parameters etc. Elastic waves in solids are generated by mechanical vibrations of material media, which result from collective vibrations of the atoms and molecules of the medium. Crystals are a special class of solid media, which are continuous, homogeneous and anisotropic. Mechanical properties of solids depend on their response to the load applied. The initial stage of deformation, where strain is small and reversible, is called elastic deformation. If the deformation produced is irreversible, we call it plastic deformation. In the final stage of deformation, we have the strength (or resistance to failure) as the characteristic of the material.

In solids, the linear elastic properties depend on the magnitude of the inter-atomic forces between constituent particles. The wave propagation characteristics are different for crystalline and amorphous solids. In crystalline solids, the response of a chain of particles in the direction of the applied load determines the plastic deformation and the overall response in three dimensions determine the strength or resistance to failure. If a crystal is subjected to a very small mechanical stress, the balance of the inter-particle forces gets disturbed and as a result, lattice spacing changes. Macroscopic changes in lattice spacing manifest themselves as elastic strain.

In linear elasticity theory, Hooke's law relates stress to strain as

$$\sigma = C\varepsilon \quad \text{or} \quad \varepsilon = S\sigma \quad (1.1)$$

where σ is the applied stress, ε is the strain, C is the elastic stiffness constant and S is the elastic compliance constant. Here,

$$C = \frac{1}{S} \quad (1.2)$$

Homogeneous stress and strain are tensors of rank two having nine components. If a homogeneous stress σ_{ij} is applied to a crystal, components of the resulting homogeneous strain ε_{ij} are linearly related to the stress components as

$$\varepsilon_{11} = S_{1111} \sigma_{11} + S_{1112} \sigma_{12} + S_{1113} \sigma_{13} + S_{1121} \sigma_{21} + S_{1122} \sigma_{22} + S_{1123} \sigma_{23} + S_{1131} \sigma_{31} + S_{1132} \sigma_{32} + S_{1133} \sigma_{33} \quad (1.3)$$

The generalized form of Hooke's law can be written as

$$\varepsilon_{ij} = S_{ijkl} \sigma_{kl} \quad (1.4)$$

Similarly, the components of the stress can be expressed in terms of the strain as

$$\sigma_{ij} = C_{ijkl} \varepsilon_{kl} \quad (1.5)$$

C_{ijkl} and S_{ijkl} are two fourth rank tensors having 81 components each. Stress components σ_{11} , σ_{22} and σ_{33} are called normal stresses. All other components act along the areas and are called tangential stresses or shear stresses. These tangential stresses form a coupled force, which is counteracted by another to attain equilibrium. For example, σ_{12} is counter balanced by σ_{21} to maintain equilibrium. Thus the number of independent stress and strain components reduces to six. Correspondingly, the number of independent components of stiffness and compliance get reduced to 36.

The coefficients of elasticity C_{ijkl} and S_{ijkl} (Tensor form) can be written more conveniently in the matrix form using the contracted Voigt notation [1.1,1.2]. The, four-suffix notation can be replaced by a much simpler two-suffix notation, according to the following convention

Tensor notation	11	22	33	23/32	13/31	12/21
Matrix notation	1	2	3	4	5	6

It can be obtained from the relations

$$ij \rightarrow m = i \quad \text{if } i = j$$

$$ij \rightarrow m = 9 - (i + j) \quad \text{if } i \neq j$$

This two-suffix notation is used only for the convenience of representation.

pS_{ijkl} (in the tensor notation) is equal to S_{mn} (in the matrix notation) where m and n correspond to ij and kl respectively and

$p = 1$ when both m and n are 1, 2 or 3.

$p = 2$ when either m or n are 1, 2 or 3.

$p = 4$ when both m and n are 4, 5 or 6.

Elastic stiffness constants C_{ij} can be defined, thermodynamically as

$$C_{ij} = \frac{\partial}{\partial \varepsilon_j} \left(\frac{\partial \psi}{\partial \varepsilon_i} \right) \quad (1.6)$$

where ψ is the lattice free energy. Here the order of differentiation is immaterial and hence we can show that $C_{ij} = C_{ji}$. The elastic constant matrix shows another 15 equalities among the elements due to this and hence, the total number of independent elastic constants reduces to 21.

The strain energy function [1.1] or the energy of deformation may be written in the form

$$E = E_c + gC_{ij}\varepsilon_{ij} + \frac{1}{2}C_{ijkl}\varepsilon_{ij}\varepsilon_{kl} + \frac{1}{3}C_{ijklmn}\varepsilon_{ij}\varepsilon_{kl}\varepsilon_{mn} + \dots \quad (1.7)$$

where g is a constant. If the strain energy is zero before deformation, $E_c = 0$. The second term is a potential energy corresponding to a static load or biasing stress which can be set equal to zero, when the strain is zero for zero stress. Hence

$$E = \frac{1}{2}C_{ijkl}\varepsilon_{ij}\varepsilon_{kl} + \frac{1}{3}C_{ijklmn}\varepsilon_{ij}\varepsilon_{kl}\varepsilon_{mn} + \dots \quad (1.8)$$

C_{ijkl} are the second-order elastic constants. C_{ijklmn} represent the third-order elastic constants. They form a sixth order tensor with a total of 729 components. It may be noted that, the elastic stiffness constant tensor C_{ijkl} is defined as the second order differential of the crystal potential energy function and for this reason they are called second order elastic stiffness constants. The third order elastic constants give a measure of the anharmonic (or nonlinear) form of the inter-atomic forces, or their deviation from the harmonic form of the ideal Hooke's law for solids.

Symmetry of crystals can further reduce the number of independent elastic constants significantly. This number is different for different crystal systems and is maximum, equal to 21, for the most unsymmetric (triclinic) system. For example, a cubic crystal has only three independent elastic constants, whereas an orthorhombic

crystal has nine. Table 1.1 gives the nonzero elastic constants for various crystal systems and point groups.

Table 1.1: Non-zero elastic constants for the various crystal systems and point groups.

System	Number of point groups	Point group (Herman-Mauguin) notation	Number of C_{ij} values
Triclinic	2	1, $\bar{1}$	21
Monoclinic	3	2, m , $\frac{2}{m}$	13
Orthorhombic	3	$m m 2$, $2 2 2$, $\frac{2}{m} \frac{2}{m} \frac{2}{m}$	9
Tetragonal	3	4, $\bar{4}$, $\frac{4}{m}$	7
	4	$\frac{4}{m} \frac{2}{m} \frac{2}{m}$, $\bar{4} 2 m$, $4 m m$, $4 2 2$	6
Trigonal	2	3, $\bar{3}$	7
	3	$\bar{3} \frac{2}{m}$, $3 m$, $3 2$	6
Hexagonal	7	6, $\bar{6}$, $\frac{6}{m}$, $6 m m$, $6 2 2$, $\bar{6} m 2$, $\frac{6}{m} \frac{2}{m} \frac{2}{m}$	5
Cubic	5	$\frac{4}{m} \bar{3} \frac{2}{m}$, $\bar{4} 3 m$, $4 3 2$, $\frac{2}{m} \bar{3}$, $2 3$	3

An isotropic solid has only two independent elastic constants, which are usually called the Lamé constants [1.3,1.4] λ and μ , defined as

$$\lambda = C_{12} \text{ and } \mu = C_{44}$$

where λ is the same as the shear modulus G and the bulk modulus

$$B = \lambda + \frac{2}{3}\mu.$$

C_{11} and C_{44} are directly related to velocities of propagation of longitudinal and shear waves respectively through an isotropic solid. The elastic constant matrix C_{ij} for the most unsymmetric crystal system (triclinic) is

$$C_{ij} = \begin{bmatrix} C_{11} & C_{12} & C_{13} & C_{14} & C_{15} & C_{16} \\ C_{12} & C_{22} & C_{23} & C_{24} & C_{25} & C_{26} \\ C_{13} & C_{23} & C_{33} & C_{34} & C_{35} & C_{36} \\ C_{14} & C_{24} & C_{34} & C_{44} & C_{45} & C_{46} \\ C_{15} & C_{25} & C_{35} & C_{45} & C_{55} & C_{56} \\ C_{16} & C_{26} & C_{36} & C_{46} & C_{56} & C_{66} \end{bmatrix} \quad (1.9)$$

where, we have used the relation $C_{ij} = C_{ji}$.

1.2. The Christoffel's matrix

A number of authors [1.5-1.10] have discussed in detail the theory of elastic wave propagation in crystals. In general, three different linear elastic waves may propagate with different velocities along any given direction in an an-isotropic crystal. These three waves are not usually pure modes. The particle displacement vector may have components both parallel and perpendicular to the wave normal. One of these components may be much larger. The wave with large parallel component is called quasi-longitudinal, while the wave with large perpendicular component is called quasi-shear or quasi-transverse wave. If the material is elastically isotropic or if the direction of wave propagation is elastically isotropic, all the modes become pure modes, i.e., particle displacements are either parallel or perpendicular to the wave normal, and the two transverse modes degenerate into one.

Consider a volume element of a homogeneous, continuous unbounded medium with its sides parallel to a set of Cartesian coordinate system of axes (Fig. 1.1). During the propagation of an elastic disturbance through this medium, the net unbalanced force acting in the x_1 direction is

$$\left(\frac{\partial \sigma_{11}}{\partial x_1} + \frac{\partial \sigma_{12}}{\partial x_2} + \frac{\partial \sigma_{13}}{\partial x_3} \right) \delta x_1 \delta x_2 \delta x_3 \quad (1.10)$$

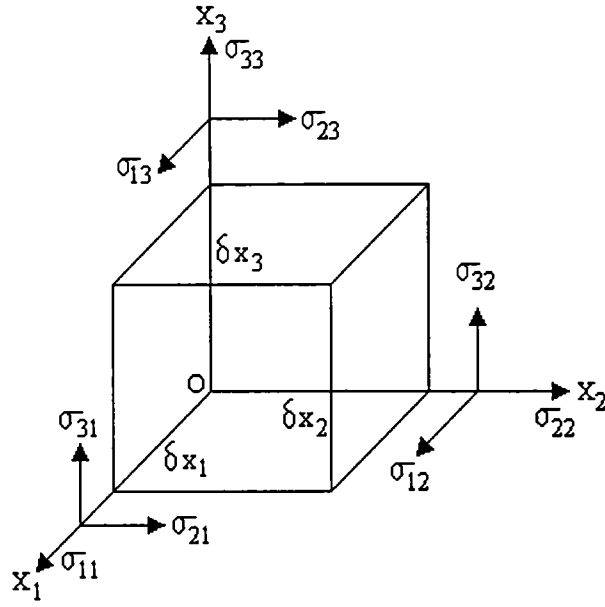


Fig. 1.1: Schematic representation of the components of stress acting on a volume element of an unbounded homogeneous continuous medium.

But from Newton's second law, this can be set equal to $(\rho \delta x_1 \delta x_2 \delta x_3) \ddot{u}$ where ρ is the mass density and u is the displacement in the x_1 direction. Hence

$$\left(\frac{\partial \sigma_{11}}{\partial x_1} + \frac{\partial \sigma_{12}}{\partial x_2} + \frac{\partial \sigma_{13}}{\partial x_3} \right) = \rho \ddot{u} \quad (1.11)$$

Similarly for the x_2 and x_3 directions, one can write

$$\left(\frac{\partial \sigma_{21}}{\partial x_1} + \frac{\partial \sigma_{22}}{\partial x_2} + \frac{\partial \sigma_{23}}{\partial x_3} \right) = \rho \ddot{v} \quad (1.12)$$

$$\left(\frac{\partial \sigma_{31}}{\partial x_1} + \frac{\partial \sigma_{32}}{\partial x_2} + \frac{\partial \sigma_{33}}{\partial x_3} \right) = \rho \ddot{w} \quad (1.13)$$

Here, v and w are the particle displacements in the y and z directions. These equations can be written more compactly as

$$\frac{\partial \sigma_{ij}}{\partial x_j} = \rho \ddot{u}_i \quad (1.14)$$

where, u_i stands for u , v and w . For a linear elastic anisotropic solid, the stress-strain relation can be written as

$$\sigma_{ij} = C_{ijkl} \varepsilon_{kl} \quad (1.15)$$

C_{ijkl} are the second order elastic constants and ε_{kl} are the strain tensor defined as

$$\varepsilon_{kl} = \frac{1}{2} \left[\frac{\partial u_k}{\partial x_l} + \frac{\partial u_l}{\partial x_k} \right] \quad (1.16)$$

Substituting Eq.(1.16) in Eq.(1.15)

$$\sigma_{ij} = \frac{1}{2} C_{ijkl} \frac{\partial u_k}{\partial x_l} + \frac{1}{2} C_{ijlk} \frac{\partial u_l}{\partial x_k} \quad (1.17)$$

The elastic constant matrix is symmetric and hence

$$C_{ijkl} = C_{ijlk} . \quad (1.18)$$

Substituting Eq. (1.18) in Eq. (1.17), we have

$$\sigma_{ij} = \frac{1}{2} C_{ijkl} \frac{\partial u_k}{\partial x_l} + \frac{1}{2} C_{ijlk} \frac{\partial u_l}{\partial x_k} . \quad (1.19)$$

k and l are dummy indices and hence we have

$$\sigma_{ij} = C_{ijkl} \frac{\partial u_k}{\partial x_l} . \quad (1.20)$$

Differentiating with respect to x_j we have

$$\frac{\partial \sigma_{ij}}{\partial x_j} = C_{ijkl} \frac{\partial^2 u_k}{\partial x_j \partial x_l} \quad (1.21)$$

Thus Eq.(1.14) can be modified as

$$C_{ijkl} \frac{\partial^2 u_k}{\partial x_j \partial x_l} = \rho \frac{\partial^2 u_i}{\partial t^2} \quad (1.22)$$

The plane wave solution for the above equation can be assumed as

$$u_i(x_k, t) = A_0 \alpha_i \exp[i(\omega t - k_m x_m)] . \quad (1.23)$$

A_0 is the amplitude of the wave, $\alpha_i (= \alpha, \beta, \gamma)$ are the direction cosines of the displacement vector, ω is the angular frequency and k_m the wave vector. The wave vector k_m can be written in terms of the direction cosines of the normal to the plane wave, $l_m (= l, m, n)$ as

$$k_m = \frac{2\pi}{\lambda} l_m = kl_m$$

Eq.(1.22) can now be rewritten incorporating all these changes, as

$$C_{ijkl} k^2 l_i l_j u_k = \rho \omega^2 u_i, \text{ or} \quad (1.24)$$

$$\left(C_{ijkl} l_i l_j - \left(\frac{\omega^2}{k^2} \right) \rho \delta_{ik} \right) \alpha_k = 0$$

$\frac{\omega}{k} = v$ is the wave velocity. δ_{ik} has the usual meaning.

$$\begin{aligned} \delta_{ik} &= 0 \quad \text{if } i \neq k \text{ and} \\ \delta_{ik} &= 1 \quad \text{if } i = k \end{aligned}$$

Let $\Gamma_{ik} = C_{ijkl} l_i l_j$ such that

$$\begin{aligned} \Gamma_{11} &= C_{1111} l_1 l_1 + C_{1112} l_1 l_2 + C_{1113} l_1 l_3 + C_{1211} l_2 l_1 + C_{1212} l_2 l_2 + \\ &C_{1213} l_2 l_3 + C_{1311} l_3 l_1 + C_{1312} l_3 l_2 + C_{1313} l_3 l_3 \end{aligned} \quad (1.25)$$

Thus Eq. (1.24) can be written as

$$\left(\Gamma_{ik} - \rho v^2 \delta_{ik} \right) \alpha_k = 0. \quad (1.26)$$

α_k is arbitrary and not necessarily zero. Hence the determinant of the coefficients of α_k must be zero. i.e.,

$$\left| \Gamma_{ik} - \rho v^2 \delta_{ik} \right| = 0 \quad (1.27)$$

Now we can adopt a much simpler notation for the direction cosines as $l_1 = l$, $l_2 = m$ and $l_3 = n$.

Eq. (1.27) can now be written in a more useful form as

$$\begin{vmatrix} \Gamma_{11} - \rho v^2 & \Gamma_{12} & \Gamma_{13} \\ \Gamma_{21} & \Gamma_{22} - \rho v^2 & \Gamma_{23} \\ \Gamma_{31} & \Gamma_{32} & \Gamma_{33} - \rho v^2 \end{vmatrix} = 0 \quad (1.28)$$

Eq. (1.26) is the Christoffel's equation. Γ_{ik} are the elements of the Christoffel matrix and are functions of the second order elastic constants and direction cosines l, m, n of the normal to the plane wave (specimen axis). Solution of Eq.(1.28) gives wave speeds (eigen values). This characteristic equation is cubic in v^2 and indicates that three plane waves may be propagated in a linear elastic homogeneous anisotropic medium.

The direction cosines α, β, γ of the particle displacements (eigen vectors) may be obtained from Eq. (1.26), which can be modified as

$$\begin{bmatrix} \Gamma_{11} & \Gamma_{12} & \Gamma_{13} \\ \Gamma_{21} & \Gamma_{22} & \Gamma_{23} \\ \Gamma_{31} & \Gamma_{32} & \Gamma_{33} \end{bmatrix} \begin{bmatrix} \alpha \\ \beta \\ \gamma \end{bmatrix} = \rho v^2 \begin{bmatrix} 1 & 0 & 0 \\ 0 & 1 & 0 \\ 0 & 0 & 1 \end{bmatrix} \begin{bmatrix} \alpha \\ \beta \\ \gamma \end{bmatrix} \quad (1.29)$$

or

$$\begin{aligned} \Gamma_{11}\alpha + \Gamma_{12}\beta + \Gamma_{13}\gamma &= \rho v^2 \alpha \\ \Gamma_{21}\alpha + \Gamma_{22}\beta + \Gamma_{23}\gamma &= \rho v^2 \beta \\ \Gamma_{31}\alpha + \Gamma_{32}\beta + \Gamma_{33}\gamma &= \rho v^2 \gamma \end{aligned} \quad (1.30)$$

First, Γ_{ik} values for a given crystallographic direction (known l, m, n) are determined and substituted in Eq. (1.28) and solved to get the three velocities of propagation. These wave speeds are in turn substituted along with Γ_{ik} and ρ in Eq. (1.30) to solve for the particle displacement direction cosines keeping in mind that

$$\alpha^2 + \beta^2 + \gamma^2 = 1 \quad (1.31)$$

Eq. (1.26) represents a set of three equations and are called the Christoffel's equations.

1.3 Relations between elastic constants and sound velocities

The determinantal equation for the propagation of elastic waves through the most unsymmetric crystals is given in Eq.(1.28). The Christoffel's coefficients Γ_{ik} can be written in the expanded form as

$$\begin{aligned}
 \Gamma_{11} &= C_{11}l^2 + C_{66}m^2 + C_{55}n^2 + 2 \cdot C_{56} m \cdot n + 2 \cdot C_{15} l \cdot n + 2 \cdot C_{16} l \cdot m \\
 \Gamma_{22} &= C_{66}l^2 + C_{22}m^2 + C_{44}n^2 + 2 \cdot C_{24} m \cdot n + 2 \cdot C_{46} l \cdot n + 2 \cdot C_{26} l \cdot m \\
 \Gamma_{33} &= C_{55}l^2 + C_{44}m^2 + C_{33}n^2 + 2 \cdot C_{34} m \cdot n + 2 \cdot C_{35} l \cdot n + 2 \cdot C_{45} l \cdot m \\
 \Gamma_{21} = \Gamma_{12} &= C_{16}l^2 + C_{26}m^2 + C_{45}n^2 + (C_{25} + C_{46})m \cdot n + (C_{14} + C_{56})l \cdot n + (C_{12} + C_{66})l \cdot m \\
 \Gamma_{23} = \Gamma_{32} &= C_{56}l^2 + C_{24}m^2 + C_{34}n^2 + (C_{23} + C_{44})m \cdot n + (C_{36} + C_{45})l \cdot n + (C_{25} + C_{46})l \cdot m \\
 \Gamma_{31} = \Gamma_{13} &= C_{15}l^2 + C_{46}m^2 + C_{35}n^2 + (C_{36} + C_{45})m \cdot n + (C_{13} + C_{55})l \cdot n + (C_{14} + C_{56})l \cdot m
 \end{aligned} \tag{1.32}$$

The general expressions, which govern ultrasonic wave propagation in crystals, get simplified when crystals of higher symmetry are considered. Some of the elastic constants become zero for higher symmetry systems. Substituting the values of Γ_{ik} terms and solving the characteristic determinantal equation, one can get the three different expressions for mode velocities. The number of terms in the general expression can be further reduced when wave propagation in any coordinate plane is considered, which allows any one of the direction cosines l , m or n to become zero.

If specific symmetry directions are considered, one more direction cosine becomes zero and a much simplified expression connecting elastic constant and velocity of propagation of elastic waves is obtained.

1.4 Elastic constants of orthorhombic crystals

The general expressions which govern ultrasonic wave propagation in crystals get more simplified when crystals of higher symmetry are considered. Some of the elastic constants and hence some of the Christoffel's coefficients can be zero when wave

propagation in a symmetry plane is considered which allows any one of the direction cosines l , m or n to become zero. Necessary equations for the orthorhombic system are derived in the following sections, since the work presented in this thesis is on crystals possessing orthorhombic symmetry.

The nonzero elastic constants of a crystals of all point groups under the orthorhombic system are C_{11} , C_{22} , C_{33} , C_{44} , C_{55} , C_{66} , C_{12} , C_{23} and C_{13} . All other elements of the general matrix are zero. The Γ_{ik} terms in the Christoffel's matrix reduce to the following form when the nonzero terms are retained in Eq.(1.32).

$$\begin{aligned}
 \Gamma_{11} &= C_{11}l^2 + C_{66}m^2 + C_{55}n^2 \\
 \Gamma_{22} &= C_{66}l^2 + C_{22}m^2 + C_{44}n^2 \\
 \Gamma_{33} &= C_{55}l^2 + C_{44}m^2 + C_{33}n^2 \\
 \Gamma_{12} &= \Gamma_{21} = (C_{12} + C_{66})l m \\
 \Gamma_{23} &= \Gamma_{32} = (C_{23} + C_{44})m n \\
 \Gamma_{13} &= \Gamma_{31} = (C_{13} + C_{55})l n
 \end{aligned} \tag{1.33}$$

A single term expression for the velocity of propagation will not be obtained since all the off-diagonal terms in the Christoffel's matrix are nonzero.

For simplicity, let us consider wave propagation in the x - y plane. For any direction in the x - y plane, $n = 0$ and hence the Γ_{ik} coefficients reduce to the following form.

$$\begin{aligned}
 \Gamma_{11} &= C_{11}l^2 + C_{66}m^2 \\
 \Gamma_{22} &= C_{66}l^2 + C_{22}m^2 \\
 \Gamma_{33} &= C_{55}l^2 + C_{44}m^2 \\
 \Gamma_{12} &= \Gamma_{21} = (C_{12} + C_{66})l m \\
 \Gamma_{23} &= \Gamma_{32} = 0 \\
 \Gamma_{13} &= \Gamma_{31} = 0
 \end{aligned} \tag{1.34}$$

The determinantal equation now becomes,

$$\begin{vmatrix} \Gamma_{11} - \rho v^2 & \Gamma_{12} & 0 \\ \Gamma_{12} & \Gamma_{22} - \rho v^2 & 0 \\ 0 & 0 & \Gamma_{33} - \rho v^2 \end{vmatrix} = 0 \quad (1.36)$$

Solving this we get

$$(\Gamma_{33} - \rho v^2)[\rho^2 v^4 - \rho v^2(\Gamma_{11} + \Gamma_{22}) + \Gamma_{11}\Gamma_{22} - \Gamma_{12}^2] = 0 \quad (1.37)$$

This is a cubic equation in ρv^2 and hence has three solutions for ρv^2 . They are

$$\begin{aligned} \rho v_0^2 &= \Gamma_{33} \\ 2\rho v_1^2 &= (\Gamma_{11} + \Gamma_{22}) + \left[(\Gamma_{11} + \Gamma_{22})^2 - 4(\Gamma_{11}\Gamma_{22} - \Gamma_{12}^2) \right]^{\frac{1}{2}} \\ 2\rho v_2^2 &= (\Gamma_{11} + \Gamma_{22}) - \left[(\Gamma_{11} + \Gamma_{22})^2 - 4(\Gamma_{11}\Gamma_{22} - \Gamma_{12}^2) \right]^{\frac{1}{2}} \end{aligned} \quad (1.37)$$

Elastic wave with velocity v_0 is a pure shear wave with polarization in the z-direction, v_1 and v_2 represents velocities of propagation of the quasi-longitudinal and quasi-shear (or quasi-transverse) waves respectively. Expressions for the velocity of propagation of these waves in terms of the elastic constants and direction cosines can be obtained by replacing the Γ_{ik} terms using Eq. (1.34). The final set of expressions for the three velocities of propagation in any direction in the x-y plane is

$$\begin{aligned} \rho v_0^2 &= C_{55}l^2 + C_{44}m^2 \\ 2\rho v_1^2 &= (C_{66} + C_{11}l^2 + C_{22}m^2) + \left[(C_{66} + C_{11}l^2 + C_{22}m^2)^2 - 4C \right]^{\frac{1}{2}} \\ 2\rho v_2^2 &= (C_{66} + C_{11}l^2 + C_{22}m^2) - \left[(C_{66} + C_{11}l^2 + C_{22}m^2)^2 - 4C \right]^{\frac{1}{2}} \end{aligned} \quad (1.38)$$

where $C = (C_{11}l^2 + C_{66}m^2)(C_{66}l^2 + C_{22}m^2) - (C_{12} + C_{66})^2 l^2 m^2$.

The normalized direction cosines l , m and n satisfy the relation ($n = 0$ in this case)

$$l^2 + m^2 + n^2 = 1 \quad (1.39)$$

Now let us consider the wave propagation in the y-z direction for which $l = 0$.

The Christoffel's coefficients can be written as

$$\begin{aligned}
\Gamma_{11} &= C_{66}m^2 + C_{55}n^2 \\
\Gamma_{22} &= C_{22}m^2 + C_{44}n^2 \\
\Gamma_{33} &= C_{44}m^2 + C_{33}n^2 \\
\Gamma_{12} &= \Gamma_{21} = 0 \\
\Gamma_{23} &= \Gamma_{32} = (C_{23} + C_{44})mn \\
\Gamma_{13} &= \Gamma_{31} = 0
\end{aligned} \tag{1.40}$$

The determinantal equation can be simplified as

$$(\Gamma_{11} - \rho v^2)[\rho^2 v^4 - \rho v^2(\Gamma_{22} + \Gamma_{33}) + \Gamma_{22}\Gamma_{33} - \Gamma_{23}^2] = 0 \tag{1.41}$$

The three solutions of this equation are

$$\begin{aligned}
\rho v_0^2 &= \Gamma_{11} \\
2\rho v_1^2 &= (\Gamma_{22} + \Gamma_{33}) + \left[(\Gamma_{22} + \Gamma_{33})^2 - 4(\Gamma_{22}\Gamma_{33} - \Gamma_{23}^2) \right]^{\frac{1}{2}} \\
2\rho v_2^2 &= (\Gamma_{22} + \Gamma_{33}) - \left[(\Gamma_{22} + \Gamma_{33})^2 - 4(\Gamma_{22}\Gamma_{33} - \Gamma_{23}^2) \right]^{\frac{1}{2}}
\end{aligned} \tag{1.42}$$

These expressions for velocities can now be rewritten in terms of the elastic constants and direction cosines as

$$\begin{aligned}
\rho v_0^2 &= C_{66}m^2 + C_{55}n^2 \\
2\rho v_1^2 &= (C_{44} + C_{22}m^2 + C_{33}n^2) + \left[(C_{44} + C_{22}m^2 + C_{33}n^2)^2 - 4C' \right]^{\frac{1}{2}} \\
2\rho v_2^2 &= (C_{44} + C_{22}m^2 + C_{33}n^2) - \left[(C_{44} + C_{22}m^2 + C_{33}n^2)^2 - 4C' \right]^{\frac{1}{2}}
\end{aligned} \tag{1.43}$$

$$\text{where } C' = (C_{22}m^2 + C_{44}n^2)(C_{44}m^2 + C_{33}n^2) - (C_{23} + C_{44})^2 m^2 n^2 .$$

The pure shear wave with velocity v_0 has polarization normal to the y-z plane.

A similar procedure can be adopted to the **x-z** symmetry plane for which $m = 0$. Corresponding coefficients of the Christoffel's matrix are

$$\begin{aligned}
\Gamma_{11} &= C_{11}l^2 + C_{55}n^2 \\
\Gamma_{22} &= C_{66}l^2 + C_{44}n^2 \\
\Gamma_{33} &= C_{55}l^2 + C_{33}n^2 \\
\Gamma_{12} &= \Gamma_{21} = 0 \\
\Gamma_{23} &= \Gamma_{32} = 0 \\
\Gamma_{13} &= \Gamma_{31} = (C_{13} + C_{55})l \cdot n
\end{aligned} \tag{1.44}$$

The determinental equation can now be expressed as

$$(\Gamma_{22} - \rho v^2) [\rho^2 v^4 - \rho v^2 (\Gamma_{11} + \Gamma_{33}) + \Gamma_{11} \Gamma_{33} - \Gamma_{13}^2] = 0 \quad (1.45)$$

Replacing the Γ_{ik} terms and simplifying, we get

$$\begin{aligned} \rho v_0^2 &= C_{66} m^2 + C_{44} n^2 \\ 2\rho v_1^2 &= (C_{55} + C_{11} l^2 + C_{33} n^2) + [(C_{55} + C_{11} l^2 + C_{33} n^2)^2 - 4C'']^{\frac{1}{2}} \\ 2\rho v_2^2 &= (C_{55} + C_{11} l^2 + C_{33} n^2) - [(C_{55} + C_{11} l^2 + C_{33} n^2)^2 - 4C'']^{\frac{1}{2}} \end{aligned} \quad (1.46)$$

$$\text{where } C'' = (C_{11} l^2 + C_{55} n^2)(C_{55} l^2 + C_{33} n^2) - (C_{13} + C_{55})^2 l^2 n^2$$

The pure shear wave having velocity v_0 has polarization along the y direction.

When we consider wave propagation in any specific symmetry direction in the above symmetry planes, one more direction cosine becomes zero and the expressions for wave velocities further get simplified. Direct relationship of elastic constants with velocities of propagation of elastic waves can be derived for experimental purpose.

Now let us consider wave propagation along the symmetry directions x, y, and z, which correspond to a, b and c directions or the [100], [010] and [001] directions respectively in a crystal belonging to the orthorhombic system.

When wave propagation is in the x direction or [100] direction, the direction cosines are $l = 1, m = 0$ and $n = 0$. The Christoffel's coefficients are

$$\begin{aligned} \Gamma_{11} &= C_{11} & \Gamma_{12} &= \Gamma_{21} = 0 \\ \Gamma_{22} &= C_{66} & \Gamma_{23} &= \Gamma_{32} = 0 \\ \Gamma_{33} &= C_{55} & \Gamma_{13} &= \Gamma_{31} = 0 \end{aligned} \quad (1.47)$$

All the off-diagonal elements are zero and hence the determinental equation simplifies to

$$(\Gamma_{11} - \rho v^2)(\Gamma_{22} - \rho v^2)(\Gamma_{33} - \rho v^2) = 0 \quad (1.48)$$

or

$$(C_{11} - \rho v^2)(C_{66} - \rho v^2)(C_{55} - \rho v^2) = 0 \quad (1.49)$$

The three velocities of propagation can be expressed as

$$\begin{aligned} \rho v_0^2 &= C_{11} \quad \text{or} \quad v_0 = \sqrt{\frac{C_{11}}{\rho}} \\ \rho v_1^2 &= C_{66} \quad \text{or} \quad v_1 = \sqrt{\frac{C_{66}}{\rho}} \\ \rho v_2^2 &= C_{55} \quad \text{or} \quad v_2 = \sqrt{\frac{C_{55}}{\rho}} \end{aligned} \quad (1.50)$$

These are pure modes. It can be easily demonstrated that v_0 is the longitudinal wave, v_1 is a transverse wave with y polarization and v_2 is a transverse wave with z polarization.

Now, let us consider wave propagation in the y [010] direction. The corresponding direction cosines are $l=0$, $m=1$ and $n=0$. The Christoffel's coefficients are

$$\begin{aligned} \Gamma_{11} &= C_{66} & \Gamma_{12} &= \Gamma_{21} = 0 \\ \Gamma_{22} &= C_{22} & \Gamma_{23} &= \Gamma_{32} = 0 \\ \Gamma_{33} &= C_{44} & \Gamma_{13} &= \Gamma_{31} = 0 \end{aligned} \quad (1.51)$$

The determinantal equation simplifies to

$$(C_{66} - \rho v^2)(C_{22} - \rho v^2)(C_{44} - \rho v^2) = 0. \quad (1.52)$$

The corresponding solutions are

$$\rho v_0^2 = C_{22} \quad \rho v_1^2 = C_{66} \quad \rho v_2^2 = C_{44} \quad (1.53)$$

These are pure mode waves. v_0 is the longitudinal wave velocity whereas v_1 and v_2 are the velocities of transverse waves with polarisations along the x and z directions respectively.

Similarly, the velocities of propagation of elastic waves in the z [001] direction ($l = 0$, $m = 0$ and $n = 1$) can be derived. The Christoffel's coefficients can be written as

$$\begin{aligned}\Gamma_{11} &= C_{55} & \Gamma_{12} &= \Gamma_{21} = 0 \\ \Gamma_{22} &= C_{44} & \Gamma_{23} &= \Gamma_{32} = 0 \\ \Gamma_{33} &= C_{33} & \Gamma_{13} &= \Gamma_{31} = 0\end{aligned}\tag{1.54}$$

The determinantal equation simplifies to

$$(C_{33} - \rho v^2)(C_{55} - \rho v^2)(C_{44} - \rho v^2) = 0.\tag{1.55}$$

$$\rho v_0^2 = C_{33}; \quad \rho v_1^2 = C_{55}; \quad \rho v_2^2 = C_{44}\tag{1.56}$$

The velocity of propagation of the longitudinal wave (v_0) is given by the relation $\rho v_0^2 = C_{33}$, whereas the transverse wave with x polarization has a velocity v_1 given by $\rho v_1^2 = C_{55}$ and the one with y polarization has a velocity v_2 given by $\rho v_2^2 = C_{44}$.

1.5 Measurement of elastic constants by ultrasonic methods

Acoustic waves of high frequencies (about 10^{11} Hz) can be considered as artificial phonons. These waves have comparatively low frequency compared to thermal vibrations at moderate temperatures. Ultrasonics is a very powerful tool in this regard and are suitable for the investigation of phonons and their interactions with other degrees of freedom in crystals; in particular, with order parameter variations or phase transitions [1.11]. Generally, acoustic waves of very short duration are excited and detected using piezoelectric transducers bonded to the end faces of the crystal sample under study. The pulse duration must be longer than the RF period but shorter than the transit time of the acoustic wave in the sample.

Ultrasonic wave velocity measurements for waves of both longitudinal and transverse polarizations along the symmetry directions allow one to evaluate all the

diagonal elements of the elastic constant matrix. In order to determine the off-diagonal elastic constants, one has to measure velocities of propagation of ultrasonic waves along any one arbitrary direction in the symmetry planes (x-y, y-z and x-z). Fortunately in ultrasonic experiments, the three different modes in any given direction can be separately excited choosing the type of the transducer. The orientation of the polarization can also be adjusted by rotating the transverse transducer.

In the previous section, expressions for the velocities of propagation of the ultrasonic waves in various symmetry planes and symmetry directions have been derived for orthorhombic crystals. For orthorhombic crystals a, b and c directions are pure mode directions and hence all the three velocities measured along each of these directions are related to only single elastic constant. The off-diagonal constants C_{12} , C_{23} and C_{13} appear in combinations with other constants. Expressions relating elastic constants with velocity measurement data are summarized in Table 1.2. The direction cosines are obtained as the sine and cosine functions of the relevant angle of rotation. The convention adopted in this work is illustrated in Fig. 1.2.

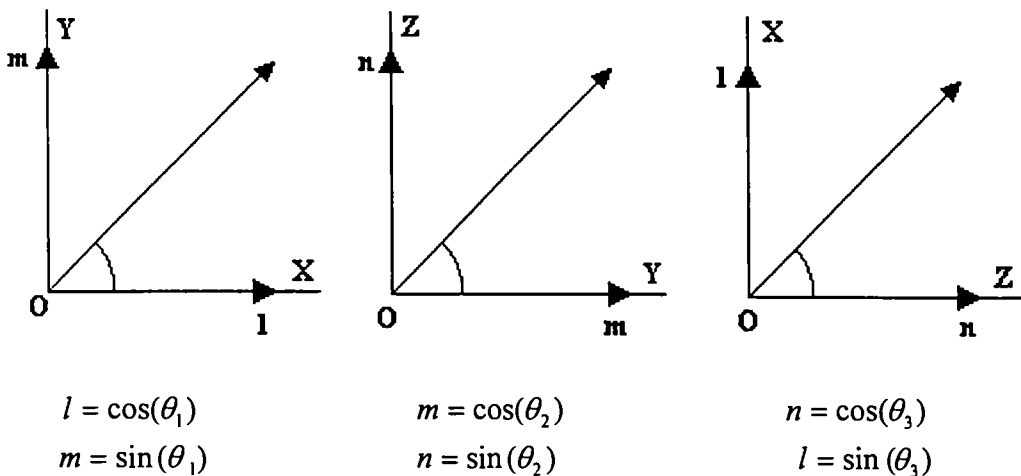


Fig. 1.2: Convention adopted in defining the direction cosines in this work

Table 1.2: Sound velocity - elastic constant relation for the orthorhombic system.

No.	Mode	Direction of propagation	Direction of polarization	Velocity-elastic constant relation
1	2	3	4	5
1	L	a [100]	a [100]	$C_{11} = \rho v^2$
2	T	a [100]	b [010]	$C_{66} = \rho v^2$
3	T	a [100]	c [001]	$C_{55} = \rho v^2$
4	L	b [010]	b [010]	$C_{22} = \rho v^2$
5	T	b [010]	a [100]	$C_{66} = \rho v^2$
6	T	b [010]	c [001]	$C_{44} = \rho v^2$
7	L	c [001]	c [001]	$C_{33} = \rho v^2$
8	T	c [001]	a [100]	$C_{55} = \rho v^2$
9	T	c [001]	b [010]	$C_{44} = \rho v^2$
10	QL	a-b plane	$\perp c$	$C_{12} = f_{ab}$
11	QT	a-b plane	$\perp c$	$C_{12} = \text{similar to } f_{ab}$
12	T	a-b plane	c	$\rho v^2 = c^2 C_{55} + s^2 C_{44}$
13	QL	b-c plane	$\perp a$	$C_{23} = f_{bc}$
14	QT	b-c plane	$\perp a$	$C_{23} = \text{similar to } f_{bc}$
15	T	b-c plane	a	$\rho v^2 = c^2 C_{66} + s^2 C_{55}$
16	QL	a-c plane	$\perp b$	$C_{13} = f_{ac}$
17	QT	a-c plane	$\perp b$	$C_{13} = \text{similar to } f_{ac}$
18	T	a-c plane	b	$\rho v^2 = s^2 C_{66} + c^2 C_{44}$

Abbreviations used in the table have the following meaning.

L - Longitudinal, T - transverse, QL - Quasi-longitudinal, QT - Quasi-transverse, c - cosine of the angle from the respective axis, s - sine of the angle from the respective axis, ρ - density of the crystal, v - velocity of propagation of the respective modes and f_{ab} , f_{bc} and f_{ac} are defined as

$$f_{ab} = \left[\frac{(c^2 C_{11} + s^2 C_{66} - \rho v^2)(c^2 C_{66} + s^2 C_{22} - \rho v^2)}{c^2 s^2} \right]^{\frac{1}{2}} - C_{66}$$

$$f_{bc} = \left[\frac{(c^2 C_{22} + s^2 C_{44} - \rho v^2)(c^2 C_{44} + s^2 C_{33} - \rho v^2)}{c^2 s^2} \right]^{\frac{1}{2}} - C_{44}$$

$$f_{ac} = \left[\frac{(s^2 C_{11} + c^2 C_{55} - \rho v^2)(s^2 C_{55} + c^2 C_{33} - \rho v^2)}{c^2 s^2} \right]^{\frac{1}{2}} - C_{55}.$$

Eighteen such mode velocity measurements are possible in a crystal belonging to the orthorhombic system along the a-b, b-c and a-c symmetry planes. Out of these, twelve mode velocity measurements are sufficient to evaluate all the nine second order elastic constants with cross checks possible on some of the values.

1.6 Other related

elastic properties of an orthorhombic crystal

Various other elastic parameters that can be determined from the elastic constant data are the Poisson's ratios, elastic compliance constants, volume compressibility, and bulk modulus. One can pictorially demonstrate anisotropy in elastic wave propagation and elastic properties by plotting two dimensional surfaces of phase velocity, slowness or inverse velocity, group velocity, Young's modulus and linear compressibility along the a-b, b-c and a-c planes.

1.6.1 Poisson's ratios

Poisson's ratio [1.3,1.7] is defined as the ratio of lateral contraction to the longitudinal extension when stress is applied uniaxially. Crystals, being elastically anisotropic produce lateral contractions different in magnitude in different directions. Consider longitudinal stress in the a-direction in an orthorhombic crystal. Longitudinal strain in the a-direction is given by

$$\begin{aligned} \varepsilon_{11} = & S_{1111}\sigma_{11} + S_{1112}\sigma_{12} + S_{1113}\sigma_{13} + S_{1121}\sigma_{21} + S_{1122}\sigma_{22} + \\ & S_{1123}\sigma_{23} + S_{1131}\sigma_{31} + S_{1132}\sigma_{32} + S_{1133}\sigma_{33} \end{aligned} \quad (1.57)$$

$\sigma_{11} \neq 0$ whereas all other $\sigma_y = 0$.

$$\varepsilon_{11} = S_{1111}\sigma_{11} \quad (1.58)$$

Lateral strain in the b [010] and c [001] directions are given as

$$\begin{aligned} \varepsilon_{22} &= S_{2211}\sigma_{11} \\ \varepsilon_{33} &= S_{3311}\sigma_{11} \end{aligned} \quad (1.59)$$

Usually ε_{22} and ε_{33} are contractions and hence the Poisson's ratios can be defined as

$$\begin{aligned} \nu_{21} &= -\frac{\varepsilon_{22}}{\varepsilon_{11}} = -\frac{S_{2211}}{S_{1111}} = -\frac{S_{21}}{S_{11}} \\ \nu_{31} &= -\frac{\varepsilon_{33}}{\varepsilon_{11}} = -\frac{S_{3311}}{S_{1111}} = -\frac{S_{31}}{S_{11}} \end{aligned} \quad (1.60)$$

Exactly in the same way, expressions for the other Poisson's ratios can be derived when uniaxial stress is applied along b [010] and c [001] directions.

$$\begin{aligned} \nu_{12} &= -\frac{\varepsilon_{11}}{\varepsilon_{21}} = -\frac{S_{12}}{S_{22}} \\ \nu_{32} &= -\frac{\varepsilon_{33}}{\varepsilon_{22}} = -\frac{S_{23}}{S_{22}} \end{aligned} \quad (1.61)$$

$$\begin{aligned}
\nu_{13} &= -\frac{\varepsilon_{11}}{\varepsilon_{33}} = -\frac{S_{13}}{S_{33}} \\
\nu_{23} &= -\frac{\varepsilon_{22}}{\varepsilon_{33}} = -\frac{S_{23}}{S_{33}}
\end{aligned}
\tag{1.62}$$

1.6.2 Young's modulus

If a material is under uniaxial stress, the Young's modulus [1.3,1.9] E of the material in the direction of stress can be defined as the ratio of longitudinal stress to longitudinal strain. Let the uniaxial stress be applied along the OX_1' (arbitrary) direction. Then the strain is

$$\varepsilon_{11}' = S'_{1111} \sigma_{11}' \tag{1.63}$$

$$E = \frac{\sigma_{11}'}{\varepsilon_{11}'} = \frac{1}{S'_{1111}} \tag{1.64}$$

S'_{1111} can be expressed in terms of the compliances S_{ij} referred to the basic symmetry axes using the transformation law as

$$S'_{1111} = a_{1i} a_{1j} a_{1k} a_{1l} S_{ijkl} = \frac{1}{E} \tag{1.65}$$

Here a_{1i} relates the arbitrary direction OX_1' to the symmetry axis OX_i . Inserting appropriate components of the compliance tensor and making use of the relations between the a_{ij} 's, one can derive the expression for the Young's modulus of a crystal belonging to the orthorhombic system for any arbitrary direction defined by the direction cosines l , m and n as

$$E = \left[S_{11}l^4 + 2S_{12}l^2m^2 + 2S_{13}l^2n^2 + S_{22}m^4 + 2S_{23}m^2n^2 + S_{33}n^4 + S_{44}m^2n^2 + S_{55}l^2n^2 + S_{66}l^2m^2 \right]^{-1} \tag{1.66}$$

In an anisotropic crystal, Young's modulus will be different in different directions and hence, the anisotropy in the Young's modulus can be illustrated by

plotting the Young's modulus values for various directions in the symmetry planes a-b, b-c and a-c so as to form sections of the Young's modulus surface lying in these planes.

1.6.3 Volume compressibility and bulk modulus

The proportionate decrease in the volume of a crystal when subjected to unit hydrostatic pressure defines volume compressibility [1.3,1.9]. Here stress is given by

$$\sigma_{kl} = -p\delta_{kl} \quad (1.67)$$

where p is the pressure applied. The corresponding strain

$$\varepsilon_{ij} = S_{ijkl} \sigma_{kl} = S_{ijkl} (-p\delta_{kl}) = -pS_{iikk} \quad (1.68)$$

During compression, material experiences volume strain given by

$$\Delta = \varepsilon_{ii} = -pS_{iikk} \quad (1.69)$$

The volume compressibility can now be written as

$$\text{Volume compressibility} = -\frac{\Delta}{p} = S_{iikk} \quad (1.70)$$

Inserting the relevant compliance constants of a crystal belonging to the orthorhombic system and simplifying, we have

$$\text{Volume compressibility} = S_{11} + S_{22} + S_{33} + 2(S_{12} + S_{23} + S_{13}) \quad (1.71)$$

It is thus the sum of the nine elements in the upper left-hand corner of the compliance matrix and is an example of an invariant formed from a tensor. Bulk modulus is defined as the reciprocal of volume compressibility.

1.6.4 Linear compressibility

The relative decrease in the length of any imaginary line in a crystal when subjected to unit hydrostatic pressure defines the linear compressibility [1.3,1.9] in that direction.

The stretch of a line in the direction of a unit vector l_i is

$$\varepsilon_{ij} l_i l_j = -p S_{ijkl} l_i l_j \quad (1.72)$$

The linear compressibility can thus be defined as

$$\beta = S_{ijkl} l_i l_j. \quad (1.73)$$

Retaining only the components of the compliance matrix for an orthorhombic system in the general expression and simplifying, we have

$$\beta = (S_{11} + S_{12} + S_{13})l^2 + (S_{12} + S_{22} + S_{23})m^2 + (S_{13} + S_{23} + S_{33})n^2. \quad (1.74)$$

Linear compressibility is also a direction dependent parameter and hence the plot of the surface of this parameter is the best way to demonstrate its anisotropy. Sections of this surface along the a-b, b-c and a-c planes can give an idea about the projection of the actual surface in three dimensions.

1.6.5 Phase velocity surface and inverse velocity (slowness) surface

Elastic wave propagation is highly anisotropic in many crystals in the sense that waves with different polarizations propagate with different velocities in different directions. Velocity of these modes calculated from elastic constant data as a function of θ (defined in Fig.1.2) can be plotted for different propagation directions lying in the symmetry planes a-b, b-c and a-c to obtain sections of the phase velocity surfaces.

In order to plot the phase velocity surfaces in the a-b plane, velocities of propagation of the pure shear, quasi-shear and quasi-longitudinal modes can be

computed for each value of θ_1 (Fig. 1.2) lying between 0 and 2π in steps of a small value (say 2°). From this, the corresponding x and y co-ordinates can be calculated using the relation $x = v \cos(\theta_1)$, $y = v \sin(\theta_1)$. The surface can be built by plotting y versus x. The same procedure can be adopted for plotting the sections of phase velocity surfaces along the b-c and a-c planes. The plot of phase velocity as a function of the direction of propagation is referred to as the phase velocity surface or simply velocity surface.

Even though the phase velocity surfaces can provide information about the anisotropy of elastic wave propagation, it is a common practice to plot the inverse of phase velocity as a function of direction of propagation. Such surfaces are usually referred to as slowness or inverse velocity surface. It denotes the locus of the end points of the radius vectors whose lengths are proportional to the refractive index. It is also known as refraction or index surface. One can trace all the features of the group velocity surface from the slowness surface. It is also a surface of three sheets and has the same degeneracies as the phase velocity surface.

1.6.6 Group velocity surface

One of the main features of elastic wave propagation in anisotropic solids is that the direction of energy flow given by the group velocity vector is not collinear with the phase velocity vector, which is parallel to the wave vector. The surface generated by plotting group velocity as a function of direction is called the group velocity surface or ray surface. The ray surface is physically the most meaningful among the three surfaces since it represents the wave front or surface of equal phase for an oscillating disturbance a unit time interval after its creation at the origin. The group velocity vector is always normal to the slowness surface. Hence the ray surface can also be

defined as the envelope of plane wave fronts with respect to the slowness surface. The analytical techniques for generating these surfaces are well established and are discussed at length by several workers [1.7,1.12-1.14]. Several papers [1.15-1.18] discussing the conditions under which cuspidal edges form in symmetry planes are available in literature. The occurrence of a cuspidal edge in the ray surface indicates that there exist two or three wave vectors corresponding to a single wave velocity vector. McCurdy [1.19] has pointed out that the directions along which cuspidal edges occur might give rise to high phonon amplification.

Ray velocity is the velocity with which energy in the wave is transported and hence ray velocity surface plots help a lot to interpret different phenomena associated with ultrasonic wave propagation, thermal conductivity, phonon transport etc. Usually the ray velocity does not coincide either in magnitude or direction with phase velocity except under special circumstances. Ray velocity can also be defined as the velocity with which the modulation envelope of a wave packet, composed of waves of slightly different k and ω propagate. It is given by

$$S = \frac{\partial \omega}{\partial k} \quad (1.75)$$

The ray surface cannot be obtained simply by inverting the slowness surface, because k and S are noncollinear. It has been shown that the group velocity must always be perpendicular to the slowness surface, i.e., k must be normal to the ray surface. Hence if ψ is the angle between the group velocity S and wave vector k , we can write $v_p = S \cos(\psi)$ where v_p is the phase velocity. This leads to a useful relation between phase velocity and ray surface. The ray surface is hence the envelope of planes normal to v_p . Each portion of the ray surface corresponds to the phase front for a plane wave with energy travelling in that direction.

The dispersion relation for plane waves is not given explicitly as $\omega = f(k_x, k_y, k_z)$ so that it is very convenient for us to calculate group velocity using the relation $S = \frac{\partial \omega}{\partial k}$. It is given in the implicit form as

$$\Omega(\omega, k_x, k_y, k_z) = |k^2 \Gamma_{ij} - \rho \omega^2| = 0 \quad (1.76)$$

In this case, the components of group velocity can be obtained by implicit differentiation of Eq. (1.76) as shown below.

$$\left(\frac{\partial \Omega}{\partial \omega} \delta \omega + \frac{\partial \Omega}{\partial k_x} \delta k_x \right)_{k_y, k_z} = 0 \quad (1.77)$$

The x component of S is obtained as

$$S_x = \left(\frac{\partial \omega}{\partial k_x} \right)_{k_y, k_z} = - \frac{\partial \Omega}{\partial k_x} \div \frac{\partial \Omega}{\partial \omega} \quad (1.78)$$

Similarly the y and z components of group velocity can be written as

$$S_y = - \frac{\partial \Omega}{\partial k_y} \div \frac{\partial \Omega}{\partial \omega} \quad (1.79)$$

$$S_z = - \frac{\partial \Omega}{\partial k_z} \div \frac{\partial \Omega}{\partial \omega}$$

The group velocity can thus be expressed as

$$S = - \frac{\nabla_k \Omega}{\left(\frac{\partial \Omega}{\partial \omega} \right)} \quad (1.80)$$

The group velocity and ray (energy) velocity are identical for acoustic waves in a lossless medium. The group velocity has a directly measurable physical meaning that is not apparent in the definition of energy velocity (v_e). If a pulse of acoustic energy is radiated by a plane wave transducer, the wave packet is limited in two dimensions by the size of the transducer and in the third dimension by the pulse length. The wave fronts travel along the direction of k which is normal to the transducer surface; but the

wave packet modulation envelope travel in a direction inclined to k . This means that the receiving transducer must be offset in order to accept the transmitted wave. Experimental evidence for this effect is reported in quartz single crystal, [1.20,1.21] where the path of the acoustic beam has been made visible by means of optical scattering.

1.6.7 Computation of group velocity

(x - y) or (a - b) plane

Direction cosine $n = 0$ for the x-y plane. The dispersion relation can be written as $\Omega = (\Gamma_{33} - \rho v^2) [(\Gamma_{11} - \rho v^2)(\Gamma_{22} - \rho v^2) - \Gamma_{12}^2] = 0$ (1.81)

The Christoffel's coefficients are given by Eq. (1.34)

Substituting the value of Γ_{ij} and expressing the equation in terms of k_x, k_y, k_z and ω

where $\frac{k_x}{k} = l, \frac{k_y}{k} = m, \frac{k_z}{k} = n$ and $\omega = kv$, the dispersion relation for the pure shear

mode can be given as

$$\Omega = C_{55}k_x^2 + C_{44}k_y^2 - \rho\omega^2 = 0 \quad (1.82)$$

$$\text{i.e., } \frac{\partial\Omega}{\partial k_x} = 2C_{55}k_x, \quad \frac{\partial\Omega}{\partial k_y} = 2C_{44}k_y, \quad \frac{\partial\Omega}{\partial k_z} = 0, \quad \frac{\partial\Omega}{\partial\omega} = -2\rho\omega \quad (1.83)$$

Thus the x, y and z components of the group velocity can be obtained. From this one can evaluate the group velocity S

For the quasi-shear and quasi-longitudinal waves, dispersion relation is given by

$$\Omega = (C_{11}k_x^2 + C_{66}k_y^2 - \rho\omega^2)(C_{66}k_x^2 + C_{22}k_y^2 - \rho\omega^2) - (C_{12} + C_{66})^2 k_x^2 k_y^2 = 0 \quad (1.84)$$

The derivatives are

$$\begin{aligned}
\frac{\partial \Omega}{\partial k_x} &= 2.C_{11}k_x(C_{66}k_x^2 + C_{22}k_y^2 - \rho\omega^2) + 2C_{66}k_x(C_{11}k_x^2 + C_{66}k_y^2 - \rho\omega^2) \\
&\quad - 2(C_{12} + C_{66})k_xk_y^2 \\
\frac{\partial \Omega}{\partial k_y} &= 2.C_{66}k_y(C_{66}k_x^2 + C_{22}k_y^2 - \rho\omega^2) + 2C_{22}k_y(C_{11}k_x^2 + C_{66}k_y^2 - \rho\omega^2) \\
&\quad - 2(C_{12} + C_{66})k_x^2k_y
\end{aligned} \tag{1.85}$$

$$\frac{\partial \Omega}{\partial k_z} = 0$$

$$\frac{\partial \Omega}{\partial \omega} = -2.\rho\omega(C_{66} + C_{11}k_x^2 + C_{22}k_y^2 - 2\rho\omega^2)$$

Substituting the appropriate values of the phase velocity, one can obtain components of the group velocity, which can be used to evaluate the group velocity in the relevant direction. The deviation of the ray from the wave normal can be determined for the a-b plane using the relation

$$\tan \psi = \frac{S_y}{S_x} \tag{1.86}$$

(y - z) or (b-c) plane

Direction cosine $l = 0$ for the b-c plane and hence the dispersion relation can be written as

$$\Omega = (\Gamma_{11} - \rho v^2) [(\Gamma_{22} - \rho v^2)(\Gamma_{33} - \rho v^2) - \Gamma_{23}^2] = 0 \tag{1.87}$$

The Christoffel's coefficients Γ_{ij} for this case are given in Eq. (1.40). Substituting Γ_{ij} values and expressing Ω in terms of k_x, k_y, k_z and ω , the dispersion relation for the pure shear mode can be obtained as

$$\Omega = C_{66}k_y^2 + C_{55}k_z^2 - \rho\omega^2 = 0 \tag{1.88}$$

The derivatives are evaluated as

$$\frac{\partial \Omega}{\partial k_x} = 0, \quad \frac{\partial \Omega}{\partial k_y} = 2C_{66}k_y, \quad \frac{\partial \Omega}{\partial k_z} = 2C_{55}k_z, \quad \frac{\partial \Omega}{\partial \omega} = -2\rho\omega \quad (1.89)$$

The x, y and z components of \mathbf{S} can be evaluated and hence the group velocity can be calculated. For the quasi-shear and quasi-longitudinal modes, Ω is given by

$$\Omega = (C_{22}k_y^2 + C_{44}k_z^2 - \rho\omega^2)(C_{44}k_y^2 + C_{33}k_z^2 - \rho\omega^2) - (C_{23} + C_{44})^2 k_y^2 k_z^2 = 0 \quad (1.90)$$

The derivatives are

$$\begin{aligned} \frac{\partial \Omega}{\partial k_x} &= 0 \\ \frac{\partial \Omega}{\partial k_y} &= 2C_{22}k_y(C_{44}k_y^2 + C_{33}k_z^2 - \rho\omega^2) + 2C_{44}k_y(C_{22}k_y^2 + C_{44}k_z^2 - \rho\omega^2) \\ &\quad - 2(C_{23} + C_{44})k_y k_z^2 \\ \frac{\partial \Omega}{\partial k_z} &= 2C_{44}k_z(C_{44}k_y^2 + C_{33}k_z^2 - \rho\omega^2) + 2C_{33}k_z(C_{22}k_y^2 + C_{44}k_z^2 - \rho\omega^2) \\ &\quad - 2(C_{23} + C_{44})k_y^2 k_z \\ \frac{\partial \Omega}{\partial \omega} &= -2\rho\omega(C_{44} + C_{22}k_y^2 + C_{33}k_z^2 - 2\rho\omega^2) \end{aligned} \quad (1.91)$$

The relevant value of phase velocity can be substituted to get the components of the group velocity. The angle of deviation of the group velocity vector from wave normal can be determined for this plane using the relation

$$\tan \psi = \frac{S_y}{S_z} \quad (1.92)$$

(x - z) or (a - c) plane

The dispersion relation for the x-z plane ($m = 0$) can be written as

$$\Omega = (\Gamma_{22} - \rho v^2) [(\Gamma_{11} - \rho v^2)(\Gamma_{33} - \rho v^2) - \Gamma_{13}^2] = 0 \quad (1.93)$$

The Christoffel's coefficients Γ_{ij} are defined in Eq. (1.44). Substituting Γ_{ij} values and rewriting Ω in terms of k_x, k_y, k_z and ω , we have the dispersion relation for the pure shear mode as

$$\Omega = C_{66}k_x^2 + C_{44}k_z^2 - \rho\omega^2 = 0 \quad (1.94)$$

The derivatives are

$$\frac{\partial\Omega}{\partial k_x} = 2C_{66}k_x, \quad \frac{\partial\Omega}{\partial k_y} = 0, \quad \frac{\partial\Omega}{\partial k_z} = 2C_{44}k_z, \quad \frac{\partial\Omega}{\partial\omega} = -2\rho\omega \quad (1.95)$$

From this, one can obtain the value of group velocity by substituting the value of phase velocity. For the quasi-shear and quasi-longitudinal modes, Ω is given by

$$\Omega = (C_{11}k_x^2 + C_{55}k_z^2 - \rho\omega^2)(C_{55}k_x^2 + C_{33}k_z^2 - \rho\omega^2) - (C_{13} + C_{55})^2 k_x^2 k_z^2 = 0 \quad (1.96)$$

The derivatives are

$$\begin{aligned} \frac{\partial\Omega}{\partial k_x} &= 2C_{11}k_x(C_{55}k_x^2 + C_{33}k_z^2 - \rho\omega^2) + 2C_{55}k_x(C_{11}k_x^2 + C_{55}k_z^2 - \rho\omega^2) \\ &\quad - 2(C_{13} + C_{55})k_x k_z^2 \\ \frac{\partial\Omega}{\partial k_y} &= 0 \\ \frac{\partial\Omega}{\partial k_z} &= 2C_{55}k_z(C_{55}k_x^2 + C_{33}k_z^2 - \rho\omega^2) + 2C_{33}k_z(C_{11}k_x^2 + C_{55}k_z^2 - \rho\omega^2) \\ &\quad - 2(C_{13} + C_{55})k_x^2 k_z \\ \frac{\partial\Omega}{\partial\omega} &= -2\rho\omega(C_{55} + C_{11}k_x^2 + C_{33}k_z^2 - 2\rho\omega^2) \end{aligned} \quad (1.97)$$

The components of the group velocity can be evaluated by substituting the relevant phase velocity values. The angle of deviation of the group velocity vector from wave normal can be determined for this plane using the relation

$$\tan\psi = \frac{S_x}{S_z} \quad (1.98)$$

These expressions can be used to calculate and plot the various surfaces listed above.

1.7 Nonlinear optical crystals:

Their properties and applications

The interaction of the electromagnetic field of an intense light beam with a nonlinear optical (NLO) material can result in the generation of new electromagnetic fields. The inherent charges in the medium can alter the phase, frequency and amplitude or polarization of the incident light when it passes through it. The study of such interactions is the field of nonlinear optics. NLO crystals find wide applications [1.22,1.23] in the field of optical harmonic generation, optical modulation, telecommunications, computer and optical signal processing etc. Optical signal processing is through optical phase conjugation and image processing, optical switching (transmission of light depending on refractive index), optical data processing through very rapid data movements and new frequency generation.

The heart of these very important NLO devices developed are crystals suitable to generate the second and higher (up to sixth) optical harmonics of laser radiation, sum frequency generation and difference frequency generation, parametric light oscillation as a tool for generating tunable radiation, stimulated Raman scattering and picosecond continuum generation.

The electric field of the incident beam induces polarization in a medium. With small fields, the strength of the applied field is proportional to the displacement of the electron density from the nucleus resulting in a dipole moment μ such that

$$\mu = \alpha E \quad (1.99)$$

where α is the linear polarisability of the atom or molecule. If the field oscillates with a frequency, the induced dipole moment also oscillates with the same frequency and

phase. For a bulk or macroscopic crystal, the polarization

$$P = \chi E \quad (1.100)$$

where, χ is the linear susceptibility of the medium. If such molecules are subjected to very intense electric fields of intense laser sources, the molecular polarisability goes beyond the linear regime. The molecular polarization can then be written as

$$P_M = \alpha E + \beta E^2 + \gamma E^3 + \Lambda \quad (1.101)$$

β is the first molecular hyper polarizability which determines the second order effect and γ is the second molecular hyper polarisability which determines the third order effect. As the field strength increases, nonlinear effect becomes more and more important because of the higher power of E. Usually α is much greater than β and γ .

The polarisation of the material can also be expressed in a similar way as

$$P = P_0 + \chi^{(1)} E + \chi^{(2)} E^2 + \chi^{(3)} E^3 + \dots \quad (1.102)$$

where $\chi^{(n)}$ is the n^{th} order NLO susceptibility. Local field effects, which are consequences of the surrounding medium, are also taken into account here. The molecules of the crystalline medium must be noncentrosymmetric for β (or $\chi^{(2)}$) to be non-zero. The induced polarization in a medium with noncentrosymmetric molecule is $+\beta E^2$ irrespective of the direction in which E is applied. A medium with centrosymmetric molecules should have a polarization $-\beta E^2$ on the reversal of field. This demands β to be zero in a centrosymmetric crystalline medium. Thus γ is the first nonzero nonlinear term in centrosymmetric case to produce γE^3 for E and $-\gamma E^3$ for $-E$.

The principle of second harmonic generation (SHG) is that, if an intense light beam passes through a second order NLO specimen, light at twice the input frequency

will be generated. This can be mathematically be shown by the following simple steps.

Let, the electric field of the incident beam be

$$E = E_0 \cos(\omega t). \quad (1.103)$$

The polarisation of the material can be written as

$$P = P_0 + \chi^{(1)} E_0 \cos(\omega t) + \chi^{(2)} E_0^2 \cos^2(\omega t) + \chi^{(3)} E_0^3 \cos^3(\omega t) + \dots \quad (1.104)$$

$\cos^2(\omega t)$ can be replaced by $\frac{1}{2}[1 + \cos(2\omega t)]$ so that

$$P = P_0 + \frac{1}{2} \chi^{(2)} E_0^2 + \chi^{(1)} E_0 \cos(\omega t) + \frac{1}{2} \chi^{(2)} E_0^2 \cos(2\omega t) + \dots \quad (1.105)$$

The polarization now consists of a new frequency doubled component. This is called three wave mixing, since two photons of frequency ω generate a new photon of frequency 2ω . This analysis can be extended to third and higher order terms. A third order process involves four-wave mixing. If two beams of different frequencies interact with NLO medium, the second order term of the material polarization becomes

$$\begin{aligned} \chi^{(2)} E_1 \cos(\omega_1 t) E_2 \cos(\omega_2 t) &= \frac{1}{2} \chi^{(2)} E_1 E_2 \cos[(\omega_1 + \omega_2) t] + \\ &\quad \frac{1}{2} \chi^{(2)} E_1 E_2 \cos[(\omega_1 - \omega_2) t] \end{aligned} \quad (1.106)$$

This indicates that polarization occurs at sum $(\omega_1 + \omega_2)$ and difference $(\omega_1 - \omega_2)$ frequencies. When these frequencies are equal, second harmonic generation (SHG) occurs.

Third order nonlinearity results from the introduction of a quartic term. The even order term in the expression for polarization will be zero for centrosymmetric molecules so that,

$$\mu = \mu_0 + \alpha E_0 \cos(\omega t) + \frac{\gamma}{6} E_0^3 \cos^3(\omega t) + \dots \quad (1.107)$$

$$\text{But, } \frac{1}{6} \cos^3(\omega t) = \frac{1}{6} \left[\frac{3}{4} \cos(\omega t) + \frac{1}{4} \cos(3\omega t) \right] \quad (1.108)$$

Substituting Eq.(1.108) in Eq.(1.107) and simplifying, we get

$$\mu = \mu_0 + \alpha E_0 \cos(\omega t) + \frac{\gamma}{8} E_0^3 \cos(\omega t) + \frac{\gamma}{24} E_0^3 \cos(3\omega t) + \dots \quad (1.109)$$

Thus the interaction of an intense beam of light with a third order NLO material creates polarization component at the third harmonic. In the bulk material, the third harmonic is decided by $\chi^{(3)}$, the third order material susceptibility.

Several experimental techniques have already been developed to investigate the NLO activity of a material. The Kurtz's powder technique is the simplest one to detect NLO activity and to determine the efficiency of second harmonic generation of powdered samples. The efficiency thus measured depends upon both the molecular (β) and bulk ($\chi^{(2)}$) polarisabilities, but this is not a reliable probe of structure-property relationships.

Applications of NLO crystals in nonlinear optical device fabrication include generation of second and higher (up to sixth) optical harmonics of laser radiation from different types of sources, sum-frequency generation (SFG), difference-frequency generation (DFG), optical parametric oscillation (OPO) or parametric luminescence (PL), stimulated Raman scattering and pico-second continuum generation.

The wavelength of lasers are either fixed or tunable over a small range. Nonlinear optical media allow us to widen the range of wavelengths generated by laser sources by several techniques such as generation of harmonics, generation of sum and difference frequencies etc. In normal cases, the efficiency of generation of second harmonic is very low because of the phase mismatch of the waves at the fundamental and doubled frequencies, while propagating through the NLO crystal. The refractive indices of these waves of different polarizations in an optically anisotropic (uniaxial or biaxial) nonlinear crystal will be different and this property can be made use of in

matching the phase velocities. This phase matching technique can be used to enhance the efficiency of harmonic generation.

The generation of combination frequencies viz. sum and difference of frequencies of radiation from two laser sources, sum and difference of frequencies of a laser and a non-coherent source have been some other achievements in this field. Optical parametric oscillation (OPO) allows us to generate radiation with a tunable frequency. Very high intense (10^7 - 10^{10} W-cm⁻²) short duration (nano and picosecond) sources are required for optical parametric oscillation. Stimulated Raman scattering (SRS) is the main mechanism of nonlinear losses which significantly reduces the conversion efficiency. The generation of a wide band radiation called picosecond continuum is observed along with SRS. This picosecond continuum generated has been successfully used in kinetic spectroscopy as probe radiation. Properties of such nonlinear optical crystals are discussed in detail in the Handbook of nonlinear optical crystals and several reviews have appeared in literature [1.22,1.24,1.25].

1.8 Summary and conclusion

Ultrasonics is a good tool to investigate the elastic properties of crystals. It enables one to determine all the elastic constants, Poisson's ratios, volume compressibility and bulk modulus of crystals from velocity measurements. It also enables one to demonstrate the anisotropy of elastic properties by plotting sections of the surfaces of phase velocity, slowness, group velocity, Young's modulus and linear compressibility along the a-b, b-c and a-c planes. They also help one to understand more about phonon amplification and helps to interpret various phenomena associated with ultrasonic wave propagation, thermal conductivity, phonon transport etc.

Study of nonlinear optical crystals is very important from an application point of view. Hundreds of new NLO materials are synthesized to meet the requirements for various applications. Inorganic, organic and organometallic or semiorganic class of compounds have been studied for several reasons. Semiorganic compounds have some advantages over their inorganic and inorganic counterparts with regard to their mechanical properties. High damage resistance, high melting point, good transparency and non-hygroscopy are some of the basic requirements for a material to be suitable for device fabrication. New NLO materials are being synthesized and investigation of the mechanical and elastic properties of these crystals is very important to test the suitability of these materials for technological applications.

References

- 1.1 R. Truell, C. Elbaum and B. B. Chick, in *Ultrasonic methods in solid state physics*, (Academic Press, New York 1969)
- 1.2 E. Schreiber, O. L. Anderson and N. Soga, in *Elastic constants and their measurements*, (McGraw Hill, New York 1973)
- 1.3 C. N. Reid, in *Deformation geometry for materials scientists*, (Pergamon Press, New York 1973)
- 1.4 R. E. Green, Jr., in *Treatise on materials science and technology Vol. 3, Ultrasonic investigation of mechanical properties*, (Academic Press, New York 1973)
- 1.5 F. I. Fedorov, in *Theory of elastic waves in crystals*, (Plenum Press, New York 1968)
- 1.6 H. B. Huntington, in *The elastic constants of crystals*, (Academic press, New York 1958)

- 1.7 M. J. P. Musgrave, in *Crystal Acoustics: Introduction to the study of elastic waves and vibrations in crystals*, (Holden Day, San Francisco 1970)
- 1.8 B. A. Auld, in *Acoustic fields and waves in solids*, Vol. 1, (John Wiley and Sons, New York 1973)
- 1.9 J. F. Nye, in *Physical properties of crystals*, (Oxford University Press, London 1957)
- 1.10 L. A. Shuvalov (ed.) *Modern Crystallography IV, Physical properties of crystals*, (Springer Verlag, Berlin 1988)
- 1.11 M. Borissov (ed.) *Optical and acoustic waves in solids – Modern topics*, Proceedings of the 2nd international school on condensed matter physics, Varna, Bulgaria 23-30 Sept 1982 (World Scientific, Singapore 1983)
- 1.12 G. F. Miller and M. J. P. Musgrave, Proc. R. Soc. London Ser. A **236** (1956) 352
- 1.13 F. Rosch and O Weiss, Z. Phys. **B25** (1976) 101; **B25** (1976) 115
- 1.14 J. Philip and K. S. Viswanathan, Pramana - J. Phys. **8** (1977) 348
- 1.15 M. J. P. Musgrave, Proc. Cambridge Philos. Soc. **53** (1957) 897
- 1.16 M. J. P. Musgrave, J. Elastic **9** (1979) 105
- 1.17 S R. P. Nayar and K. S. Viswanathan, Can. J. Phys. **50** (1972) 1903
- 1.18 H. J. Maris, J. Acoust. Soc. Am. **50** (1971) 812
- 1.19 A. K. McCurdy, Phys. Rev. **B9** (1974) 466
- 1.20 L. G. Merkulov and L. A. Yakovlev, Sov. Phys.-Acoust. **8** (1962) 72
- 1.21 J. H. Staudt and B. D. Cook, J. Acoust. Soc. Am. **41** (1967) 1547
- 1.22 N. J. Long, Angew. Chem, Int. Ed. Engl. **34** (1995) 21
- 1.23 V. G. Dmitriev, G. G. Gurzadyan, D. N. Nikogosyan in *Handboof of nonlinear optical crystals* (Springer-Verlag, Berlin 1997)

- 1.24 D. S. Chemla and J. Zyss (ed.) *Nonlinear optical properties of organic molecules and crystals* (Academic Press, New York 1986) Vol. **1 & 2**
- 1.24 R. A. Hann and D. Bloor (ed.) *Organic materials for nonlinear optics* (Royal Society of Chemistry, 1989)

Chapter 2

Instrumentation

2.1 Introduction

The science and technology of producing and transmitting sound waves through materials has become an important area of research with many practical applications. Ultrasound waves have been used in many physical investigations. A detailed description of the early history and applications of ultrasonics is available in literature [2.1]. A partial list of the large number of physical applications of ultrasound is given in the above review article. Ultrasonics is very useful in the investigation of the elastic properties of materials in the solid state.

Ultrasonic techniques used to investigate the elastic properties of materials can, in general, be classified into the following.

- (1) continuous wave methods
- (2) low frequency methods
- (3) pulse methods

The pulse methods are more popular because of the high measurement accuracy that can be attained owing to the fact that these techniques are essentially interferometric.

2.1.1 Continuous wave methods

Standing wave resonances can be excited in crystals using quartz transducers similar to that in a Fabry-perot interferometer and this technique has been successfully applied to

various problems in physical acoustics. The number of resonances excited for a frequency f in a sample of length L can be written as $n = \frac{2Lf}{v}$ where, v is the velocity of propagation of sound through the sample. Frequency modulation techniques can be applied to attain more sensitivity in velocity and attenuation measurements. More detailed description of the various methods in this category is available in few review articles [2.2,2.3].

2.1.2 Low frequency methods

Techniques using low frequency are discussed in detail by Read *et al.* [2.4]. These methods are particularly suitable for piezoelectric materials, which can be excited into mechanical resonances by an electric field directly without transducers [2.5]. The lower limit is determined by the sample dimensions. Mostly, these samples are excited into resonance in the fundamental mode. In this case, elastic compliances (Young's modulus E and shear modulus G) are determined by continuous wave resonance method or by measuring flexural and torsional oscillations. In a similar way piezoelectric crystals can be studied by applying an additional DC bias field employing electro-strictive effects [2.6]. Low frequency dynamic resonance methods are described in detailed by Schreiber *et al.* [2.7].

Transparent single crystals can be studied by the Schaefer-Bergmann [2.8] method. The interaction of a monochromatic beam of light with a system of elastic standing waves setup in a vibrating crystal is employed here. Vibrations in a crystal can be excited either directly by an electric field (for piezoelectric crystals) or by means of a piezoelectric transducer. The light, while passing through the vibrating crystal gets diffracted and a peculiar optical pattern is revealed which consists of closed curved lines. These curves are generally sections of the surface of inverted

sound velocities and hence this is a good method to study the anisotropy of elastic wave propagation in crystals.

2.1.3 Pulse methods

Pulse methods are essentially phase sensitive techniques. A brief description of ultrasonic pulse techniques is given below.

Ultrasonic wave pulses of very short duration, generated by a piezoelectric transducer, are admitted into the sample to be investigated through one of the parallel faces. Crystal samples in the form of rectangular parallelepipeds with a pair of parallel faces perpendicular to the required direction are prepared. The piezoelectric transducer is bonded to the crystal surface using a suitable bonding medium. These ultrasonic wave pulses get multiply reflected from the opposite face of the sample and the same transducer detects these echo pulses. Electric signals thus generated are amplified and displayed on an oscilloscope or processed otherwise. The transit time of the pulse in the sample and the decay rate of the pulse amplitude can be used to evaluate the ultrasonic wave velocity and attenuation respectively. There are various kinds of phase sensitive methods such as pulse superposition [2.9,2.10], phase comparison [2.11], sing-around [2.12,2.13] method and pulse echo overlap method [2.14]. More details of these techniques are discussed at length in some review articles [2.15-2.19]. In ultrasonic experiment the frequency is usually in the range 10MHz to 100MHz. The plainness and parallelism of the reflecting end faces determine the higher limit of the ultrasonic frequency. Also the duration of the ultrasonic wave pulse must be longer than the RF period, but shorter than the transit time of the acoustic wave in the sample. This restricts the lower limit of the RF frequency.

In the whole of the work presented in this thesis, the ultrasonic pulse echo overlap technique has been employed to measure ultrasonic velocities in solids. So a

detailed description of the technical details of this method is given in the following section.

2.2 The pulse echo overlap method

The pulse echo overlap (PEO) method is a very versatile and highly accurate technique for measuring the round trip travel time of ultrasonic waves in materials. This method was first invented by John E. May [2.20] in 1958 and was modified to the present form by Emmanuel P. Papadakis [2.14] in 1964. This modification was based on the principle of pulse superposition developed by McSkimin [2.9,2.10]. Now the PEO method is the most widely used technique to measure the velocity of propagation of ultrasonic waves through solids. The presence of a bonding medium between the transducer and sample alters the phase of the propagating wave and can introduce errors. Also the identification of the correct cycle-to-cycle matching of the overlapped echoes can be erroneous and hence the travel time measured need not be correct. McSkimin developed a technique by which these errors can be rectified and high absolute accuracy can be obtained in these measurements. The block diagram of the PEO setup is shown in Fig. 2.1. A highly precise continuous wave oscillator generating square pulses determines the accuracy that can be attained using this setup.

The output of the CW oscillator is fed into a frequency divider, which divides the input frequency by 10, 100 or even 1000. This divided output from the divider unit triggers an RF pulsed oscillator to produce RF wave pulses, which are synchronous with the divided trigger generated. It is not of the gated type so that it generates wave pulses of the same initial phase angle. These RF wave pulses are applied to the quartz transducer bonded to the sample surface using a suitable bonding medium. The piezoelectric transducer converts these electrical signals into mechanical vibrations and

they are admitted into the sample through the bonding medium. These mechanical wave pulses get reflected from the rear end of the sample successively so that a series of echoes are generated. The same transducer detects these echoes and are fed to the echo amplifier. The period of the divider output must be sufficiently large compared to the round trip travel time in the sample. The echo pattern is displayed using a CRO.

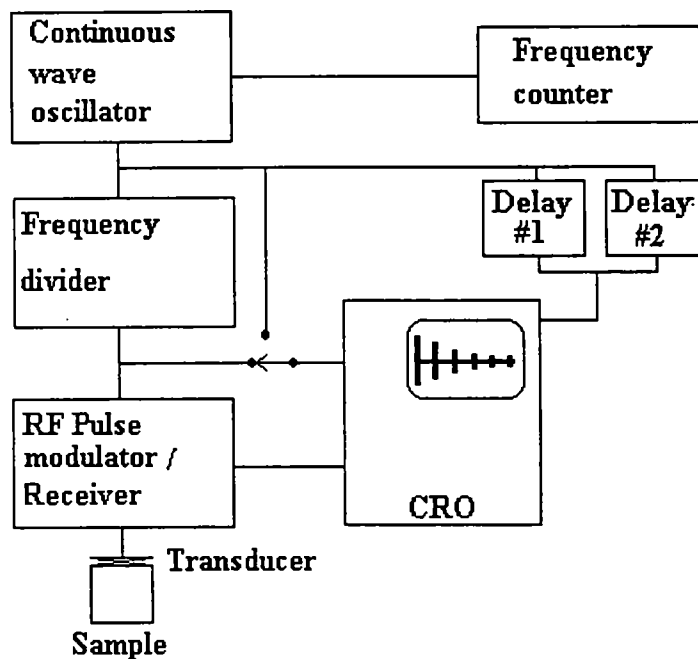


Fig. 2.1: Block diagram of the pulse echo overlap setup

The SYNC input signal of the CRO normally triggers the x-axis sweep, when it is operated in the linear sweep mode. If the output of the divider unit is given as the SYNC input signal to the CRO, one RF pulse and all the successive echoes with exponentially decreasing amplitudes are visible on the CRO screen. Two time delay units are provided to generate two pulses of proper separation and width to be given as the z-input to the CRO to intensify the two echoes of interest. When the CRO is triggered by the output of the CW oscillator, the x-axis sweep is triggered every time a pulse is received as the input. If the CW frequency is suitably adjusted so that the

period of the trigger signal is exactly equal to the round trip travel time of the ultrasonic waves in the sample, echoes appear on the screen one after the other on successive sweeps. The echoes will appear overlapped one over the other due to persistence of vision. If the amplitudes of the intensifying pulses are properly adjusted, the echoes of interest alone can be made visible in the overlapped condition. If the overlap is exact, the period of the CW output is exactly equal to the round trip travel time of the ultrasonic wave pulse in the sample.

The echoes appear on the screen in an expanded form with RF cycles in the echo visibly resolved and a perfect cycle-to-cycle matching of the overlapped echoes as shown in Fig. 2.2 can be achieved by fine tuning of the CW oscillator.

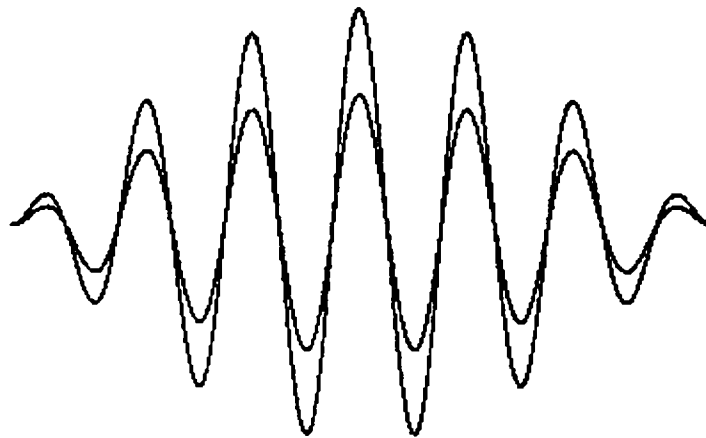


Fig. 2.2: Echo pair in the overlapped condition

2.3 The experimental setup

The basic experimental setup consists of the PEO system, the temperature measurement and control-setup, an oven for high temperature studies and a cryostat for low temperature measurements.

The PEO system includes a MATEC Model 7700 pulse modulator with Model 760V RF plug-in, Model 110 high resolution frequency source, Model 122B decade divider and dual delay generator, Model 2470B attenuation recorder, Model 70 impedance matching network etc. A 100MHz oscilloscope (HIL Model 5022) with z-axis intensification input is used to display the echo pattern. An HIL (India) Model-2722 frequency counter displays the CW frequency output. The block diagram of the experimental setup is shown in Fig. 2.3. The tunable CW source (Model-110) employs a highly stable high frequency oscillator tunable from 12 to 50MHz. The built-in frequency divider network generates low frequency CW signals for the PEO setup when required. The high frequency undivided signal is fed to the frequency counter and the divided signal is applied to the dual delay and divider unit (Model 122B). This divider network divides the input frequency by 10, 100 or 1000, which can be set suitably. Model 122B also provides the trigger signal to the CRO. It can be the signal frequency before division or frequency after division and a front panel switch allows one to select it suitably. Always the CRO is operated in the external sweep trigger mode. This unit also generates two pulses to intensify the two echoes of interest by feeding it as the z-input to the CRO. The position, duration and amplitude of these pulses can be adjusted accordingly using front panel controls. The divided output signal is directly fed to the Model-7700 pulse modulator with the RF plug-in Model 760V.

Model 760V is a RF oscillator, which can be tuned continuously from 10 to 90MHz, can be modulated by applying a modulation pulse. An RF wave pulse of peak power 1kW can be generated at the output. The amplitude of the RF output can be adjusted properly using the Model 50HT42 Alan attenuator for proper pulse shape. RF

wave pulses thus generated are fed to the piezoelectric transducer through the impedance matching network (Model 70).

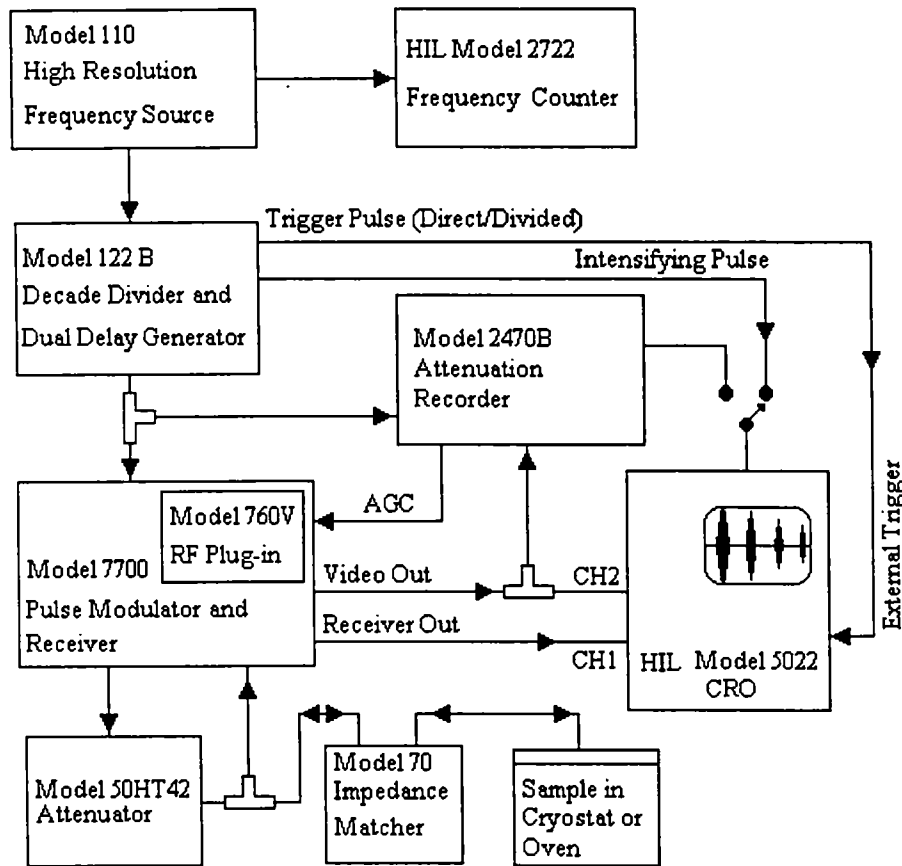


Fig. 2.3: Block diagram of the experimental setup

The same transducer detects the successive echo pulses and the detected echoes are amplified by the echo-amplifier. These signals corresponding to the echo pulses are given as the Channel 1 input for the CRO.

Model 2470 B attenuation recorder is a very useful unit to study small variation in ultrasonic attenuation. Two gates with variable delay are setup to sample the echoes of interest. The amplitude of the first echo is held constant by AVC circuitry and the amplitude of the second echo is sampled at its peak. A calibrated logarithmic amplifier converts the sampled echo amplitude to decibels relative to the constant amplitude of

the first echo. It can be recorded using a strip chart recorder when dependence of attenuation on temperature is studied.

The timing diagram of various signals in the measurement system is shown in Fig. 2.4. The first and second echoes are shown as the selected ones in the figure.

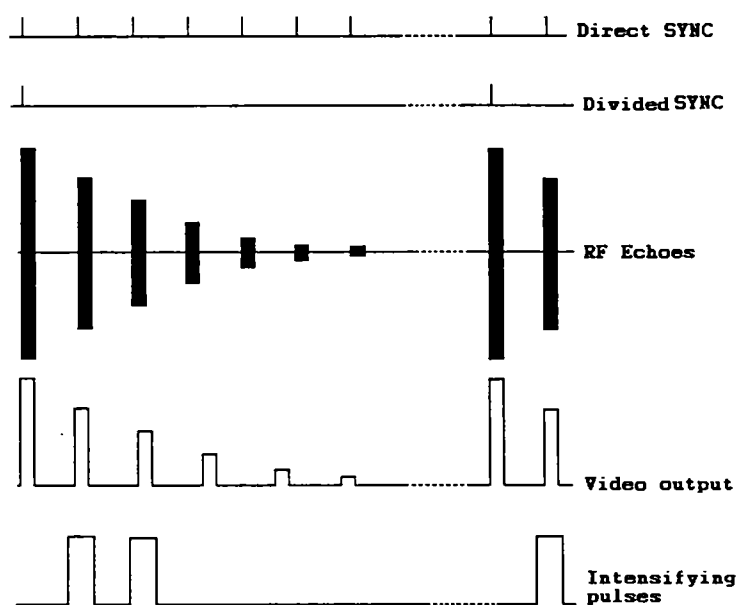


Fig. 2.4: Timing diagram of the various signals

2.4 Sample cell and accessories

Gold coated coaxial quartz transducers (Valpey-fisher) suitable for overtone operation are used for the present studies. The shear axis of y-cut transducer is perpendicular to the slight flat cut edge of the round crystals. A temperature controller (Lakeshore Model DR 82C) with platinum RTD sensor is used to control the temperature of the chamber where the crystal-transducer assembly is kept. A bath type cryostat [2.21] has been used for low temperature studies. A slow and uniform cooling with precise control of temperature is possible with this setup. The regions surrounding the liquid nitrogen and the sample cell are evacuated to attain very slow cooling rates. The schematic details of the cryostat are shown in Fig. 2.5.

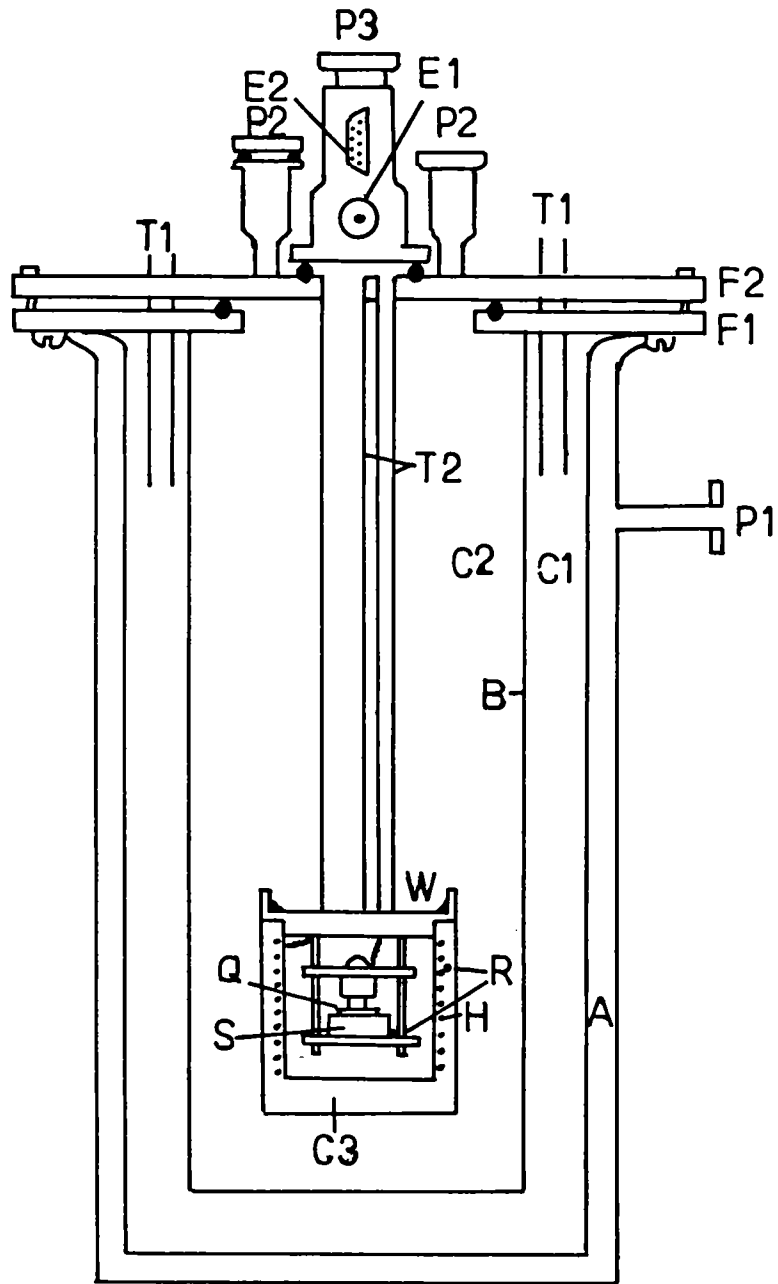


Fig. 2.5: Sectional view of the cryostat

[A-Double walled outer vessel, B-Single walled inner vessel, C1-Chamber1, C2-Chamber2, C3-Sample chamber, E1 & E2-Electrical I/O, F1 and F2-Flanges, H-Heater coil, P1, P2 and P3-Evacuation ports, Q-Transducer, R-Temperature sensor, S-Sample, T1 -Liquid nitrogen guide tube, T2 -Connection tube, W -Wood's metal seal]

The main parts of the cryostat are two coaxial stainless steel vessels A and B. Chamber A is a double-walled vessel and the space between the walls can be evacuated using a rotary pump through the port P1. Vessel B is single-walled and the space between vessels A and B (C1) can be filled with liquid nitrogen through the tubes T1 fixed on the flange F1. The sample holder is fixed at the end of a long tube fixed on the flange F2. The sample chamber (C3) can be evacuated through the port P3. H is a cylindrical heater covering the sample holder. The sample chamber can be sealed using Wood's metal (W) and can be evacuated through the port P3. Electrical leads are taken out through the side tube T2. E1 (BNC Jack) and E2 (D type connector) are two connectors provided to establish the electrical connection. The inner vessel B can be sealed at the top by the flange F2 using neoprene O-rings. P2 indicates the corresponding evacuation ports.

Transducer Q is properly bonded to the sample and it is kept in the sample holder. Heater and electrical connections are made. Sample chamber C3 is properly placed and it is sealed using Wood's metal. The top flange F2 and attached sample chamber are suitably placed to make proper sealing so that the vessel B and the region between the double-walled vessel A can be evacuated. After attaining the required vacuum, liquid nitrogen is gradually poured down into the region C1 through the tube T1.

Inner and outer regions surrounding the liquid nitrogen are kept at vacuum, which prevents heat absorption from outside. Similarly, the vacuum space inside the sample chamber C3 and vessel B prevents absorption of heat from the sample chamber so that it is suddenly cooled which results in cracking of the crystal.

The advantage of the cryostat is that it is a bath-type one, which can be used to cool the specimen kept in the sample chamber very slowly and steadily. After attaining the lowest temperature, power can be applied to the heater to increase the temperature of the sample. Two RTD sensors (R) are provided to sense and control the temperature of the sample S using a PID temperature controller. In this setup a cooling rate of 1K/min. or less can be attained and measurements can be made in the temperature range 80-300K. A photograph of the whole experimental setup including the cryostat is shown in Plate 2.1

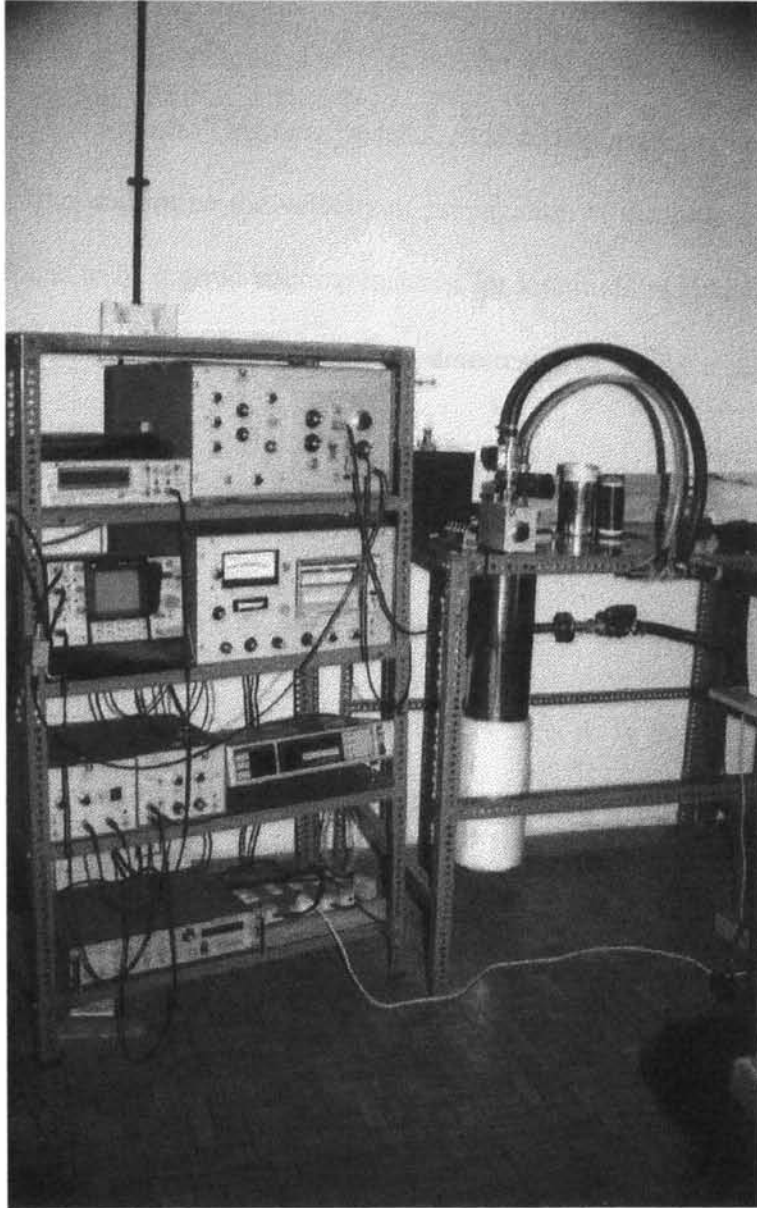


Plate 2.1
The photograph of the experimental setup

2.5 Low and high temperature measurements

The condition of perfect cycle-to-cycle overlap of the selected echoes will change with change in temperature of the sample. The CW oscillator is to be properly tuned to reestablish the initial condition. This new frequency value displayed by the frequency counter can be used to determine the velocity of propagation at the new temperature. Silicon grease is found to be a good bonding material for longitudinal measurements at room temperature as well as at relatively high temperatures up to 100° Celsius.

2.6 Bond correction in ultrasonic measurements

Usually a piezoelectric transducer of resonant frequency f and thickness $\frac{\lambda}{2}$ is bonded to one end of the sample with its opposite end free, where λ is the wavelength of ultrasonic waves generated by the transducer when operated at the resonant frequency. The thickness of the bonding medium is finite. The transducer is also unbacked. The presence of the bonding medium can alter the phase of the reflected wave when it gets reflected from the bonded end of the sample.

Consider a transducer of specific acoustic impedance Z_2 bonded to a sample of specific acoustic impedance Z_s using a bonding medium of specific acoustic impedance Z_1 as shown in Fig. 2.6. Let Z_d be the impedance offered at the termination (bond and transducer). Since the transducer is unbacked, the impedance seen by it at its back is that of air (Z_a) which is approximately zero. Based on the theory of lossless transmission lines, Z_d can be written as

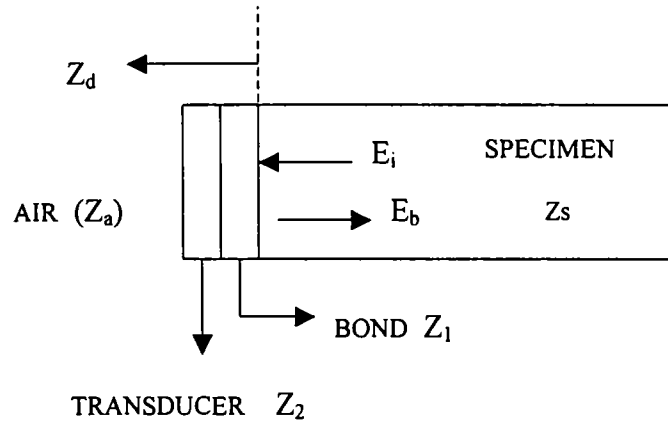


Fig 2.6(a): Sketch of specimen bond and transducer

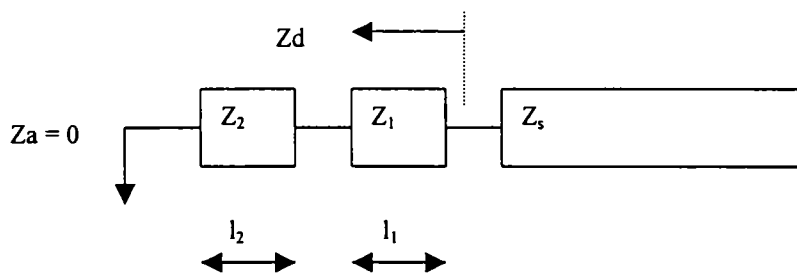


Fig. 2.6(b): Transmission line equivalent circuit

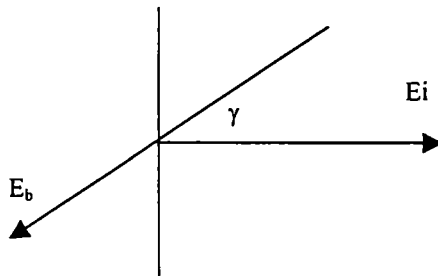


Fig. 2.6(c): Phase angle generated at each reflection of the echoes from the specimen/ bond / transducer interface

$$Z_d = jZ_e = jZ_1 \left[\frac{\frac{Z_1}{Z_2} \tan \beta_1 l_1 + \tan \beta_2 l_2}{\frac{Z_1}{Z_2} - \tan \beta_1 l_1 \tan \beta_2 l_2} \right] \quad (2.1)$$

Here l_1 and l_2 are the thickness of the bonding medium and transducer respectively.

The propagation constant in the bonding medium β_1 is defined as

$$\beta_1 = \frac{2\pi f}{v_1}, \quad (2.2)$$

where v_1 is the velocity of the acoustic wave in the bonding medium. Similarly β_2 , the propagation constant in the transducer can also be related to v_2 , the velocity of the wave in the transducer. The ratio of the reflected pressure (E_b) to the incident pressure (E_i) is defined as

$$\frac{E_b}{E_i} = \frac{Z_d - Z_s}{Z_d + Z_s}. \quad (2.3)$$

This is a complex quantity, since Z_d is imaginary ($Z_d = jZ_e$). Separating the real and imaginary parts, we have

$$\frac{E_b}{E_i} = \frac{Z_s^2 - Z_e^2}{Z_s^2 + Z_e^2} - j \frac{2Z_e Z_s}{Z_s^2 + Z_e^2}. \quad (2.4)$$

The phase angle γ upon reflection is given by

$$\tan \gamma = \frac{-2Z_e Z_s}{Z_s^2 - Z_e^2}. \quad (2.5)$$

Ultrasonic frequency f is a variable and hence one can change β_1 and β_2 by changing f . The bond thickness l_1 is unknown. The phase angle γ is the relevant measure of the effect of the transducer and bond upon the reflected wave.

McSkimin assumed that the measured travel time t_M is slightly higher than the true travel time t and is given by

$$t_M = pt - \frac{p\gamma}{2\pi f} + \frac{n}{f} \quad (2.6)$$

Here p is the number of round trips in the measurement. The phase angle change γ per reflection yields a fraction $\frac{\gamma}{2\pi}$ of the period of the RF as the increment in the time of travel. Also, during echo overlap, if a mismatch of n cycles occurs, the

corresponding error is $\frac{n}{f}$. The objective of the mathematical analysis is to find the overlap case with $n = 0$ and to estimate the error due to the bonding medium.

It is clear from the above expressions that both γ and t_M are functions of the frequency f . If round trip travel time (t_M) is measured at two different frequencies, say f_H (equal to the resonant frequency f_r) and f_L (equal to say $0.9 \cdot f_r$), they can be expressed as

$$t_H = pt - \frac{P\gamma_H}{2\pi f_H} + \frac{n}{f_H} \quad (2.7)$$

$$t_L = pt - \frac{P\gamma_L}{2\pi f_L} + \frac{n}{f_L} \quad (2.8)$$

If the same overlap condition is maintained (same n) by shifting the CW frequency slightly as the RF frequency is changed, we can write $t_L - t_H$ as

$$\Delta t_M = t_L - t_H = \frac{1}{f_L} \left[n - \frac{P\gamma_L}{2\pi} \right] - \frac{1}{f_H} \left[n - \frac{P\gamma_H}{2\pi} \right] \quad (2.9)$$

This expression represents the McSkimin's Δt criterion for finding the $n = 0$ case. If f_L, f_H, t_L and t_H are measured and γ_L and γ_H are computed using the values of $l_1, l_2, v_1, v_2, Z_1, Z_2$ and Z_S one can determine the possible value of Δt_M for the $n = 0$ case. Conversely, if $n = 0$ is set in the measurement, the measured value of Δt_M agrees with the theoretically calculated value.

The procedure to be followed to apply correction by the McSkimin's technique is listed below.

1. The full echo pattern generated by the RF pulse is made visible on the CRO screen. Estimate the time interval between successive echoes and adjust the CW frequency to have that time as its period.

2. Trigger the CRO using the CW output and adjust its frequency such that a plausible overlap is obtained. Every cycle of the latter echo must be smaller than the corresponding cycle of the earlier echo because of attenuation.
3. Measure T_L and T_H corresponding to RF frequency f_L and f_H , usually $0.9 f_r$ and f_r respectively.
4. Repeat step 3 for several possible adjacent overlaps, say three towards lower and three towards higher CW frequencies.
5. Compute Δt_M for each set of these measurements.
6. Compare Δt_M found experimentally with theory and choose the correct cycle to cycle matching case. The value of t_H , measured at $f_H = f_r$ will be the value of t_M with $n = 0$. This is the measured round trip travel time without correcting the phase lag due to the bonding medium.

A theoretical value for Δt_M cannot be obtained directly since the bond thickness is not known. Usually a graphical technique is adopted to estimate Δt_M . We can safely assume that the bond is thin and corresponding phase angle $\beta_1 l_1$ lies between 0 and 90°. Values of Δt_M can be computed for different bond angles ranging from 0 and 90° and a plot of Δt versus bond angle can be made for the $n = 0$ overlap condition. This gives a range of values for Δt for the given transducer, bond and sample combination. Now compare the values of Δt_M measured experimentally with the values of Δt plotted and determine the value of overlap case n corresponding to it. This can be taken as $n = 0$. Thus the correct case of overlap can be identified. Value of T_H and corresponding γ_H can be used to evaluate the round trip travel time eliminating the effect of the bonding medium.

A computer program developed in BASIC [2.22] to make these corrections numerically has been used to make the McSkimin Δt correction in our measurements.

2.7 Sample preparation techniques

In this section, growth of large crystals from supersaturated solution, preparation of oriented specimen for measurements and the associated instrumentation are described. Indexing of crystallographic planes and directions is easy if crystals are grown from solution. Five different crystals have been grown from solution by the slow evaporation or slow cooling techniques. Specimen with parallel planes perpendicular to selected crystallographic directions are required for the determination of all nine second order elastic stiffness constants of a crystal belonging to the orthorhombic system. Details of the technique adopted for the growth of each crystal studied in this thesis are given in the respective chapters.

2.7.1 Crystal growth from solution

Crystal growth from liquid [2.23] is the most widely used technique to grow large single crystals. Crystal growth from solution comes under this branch and requires less sophisticated instrumentation. Large single crystals can be grown by the slow evaporation or slow cooling technique. Very good books describing the various techniques to grow single crystals are available in literature [2.24-2.27]. If very large single crystals are required, a modified form of the slow evaporation technique [2.28] that allows convection of the steady state concentration is employed. The selection of the growth technique to be adopted depends on the solubility of the material and its temperature dependence. Slow cooling technique is the most suitable one when solubility of the material is very large and has high positive temperature coefficient of solubility. If the temperature coefficient of solubility is far less crystal growth by slow

evaporation technique can be employed. Schematic diagram of the crystal growth setup showing various parts of the unit is shown in Fig. 2.7. The accuracy with which temperature of the solution can be maintained decides the quality of the crystals grown.

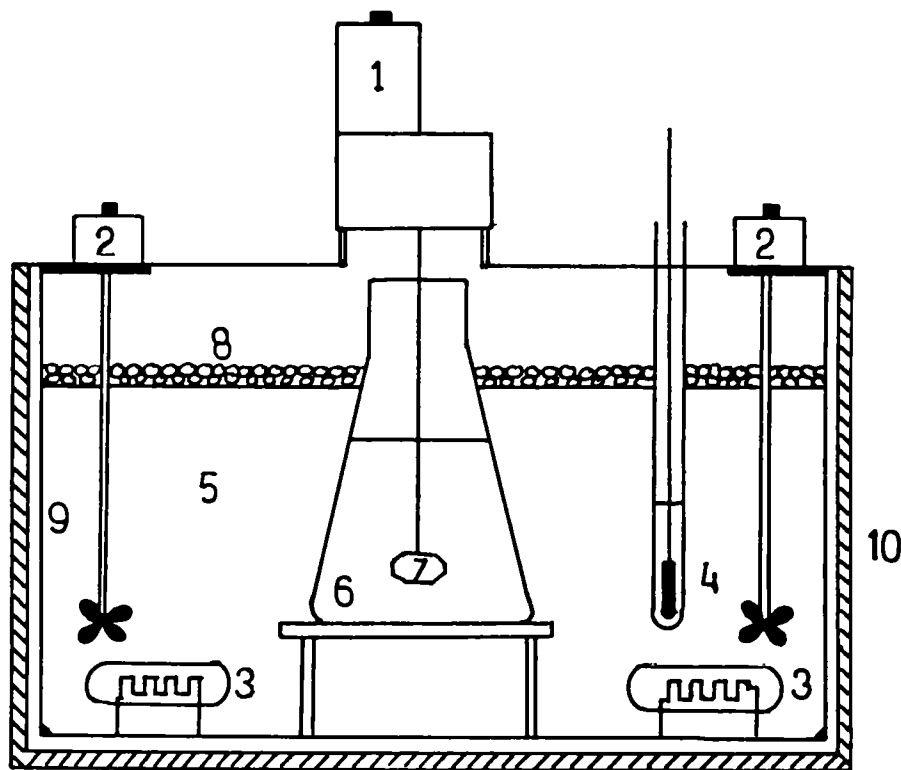


Fig. 2.7: Schematic of the solution growth setup

- | | | |
|-----------------------------------|----------------------|----------------|
| 1 Seed crystal rotation mechanism | 2 Bath stirrers | 3 Bath heaters |
| 4 Temperature sensor | 5 Bath liquid | 6 Solution |
| 7 Growing crystal | 8 Thermocol granules | 9 Glass tank |
| 10 Outer puff lining | | |

Spurious nucleation is a major problem in crystal growth from solution. High purity materials and solvents are essential to overcome this problem. Several techniques to purify the material to be crystallized, popular crystal growth techniques and preparation of oriented samples are discussed at length by Norbert Karl [2.29]. Usually, the materials to be crystallized are purified by repeated crystallization prior to

crystal growth. Triply distilled and de-ionized water is used as the solvent if salt is water-soluble.

Mixing of the solution can provide homogeneity of the solution and its concentration, which influences the growth of crystals. Several designs to achieve unidirectional mixing [2.30-2.33] and alternate mixing [2.34] are available in literature. Controller using accelerated rotation of seed crystal has also been used recently and design details are available in literature [2.35]. We have used alternate mixing technique with stop periods [2.36] between two reversal of the direction of rotation in growing our crystals.

Several designs of temperature controllers suitable for crystal growth applications have been reported in literature [2.37-2.39]. We have developed a temperature controller, which can be programmed to lower the temperature of the growth solution progressively so that crystals can be grown by the slow cooling technique under microprocessor (Intel 8085A) control. The rotation of the seed holder, with stop periods between two successive rotation reversals also, can be programmed. We have implemented the PID algorithm fully by software for this application. The design details of the temperature controller is described in detail in Appendix I. A diode sensor is used to monitor the temperature of the growth chamber periodically. An ADC (AD0809) converts the analog signal voltage into equivalent digital value. The gain of the amplifier is so adjusted that the digital output of the ADC is the equivalent of temperature in degree Celsius. The temperature of the bath is sampled once in every 30 seconds. The rate of cooling is computed from the values of initial and final temperatures and the time interval. The set temperature is progressively lowered and the error signal is manipulated suitably to implement the PID control algorithm. The count to be loaded into the register of the timer is evaluated to generate

the pulse width modulated output, which is used to control the power delivered to the heater. Periodically the bits are set or reset accordingly, to reverse the direction of rotation of the seed holder. The circuit design details and program developed to implement this temperature controller are discussed in detail in Appendix I.

References

- 2.1 W. P. Mason, IEEE Trans. on sonics and ultrasonics **SU-23** (1976) 224
- 2.2 D. I. Bolef, in *Physical acoustics* Vol.4 pt. A (ed.) W. P. Mason and R. N. Thurston (Academic Press, New York 1976)
- 2.3 D. I. Bolef and J. G. Miller, in *Physical acoustics* Vol.8 (ed.) W. P. Mason and R. N. Thurston (Academic Press, New York 1971)
- 2.4 T. A. Read, C. A. Wert and M. Metzger, in *Methods of experimental physics* Vol. 6A (ed.) K. Lark-Horovitz and V. A. Johnson (Academic Press, New York 1974)
- 2.5 W. P. Mason, in *Piezoelectric crystals and their applications to ultrasonics* (Van-Nostrand, Princeton 1950)
- 2.6 G. Rupprecht and W. Winter, Phys. Rev. **155** (1967) 1019
- 2.7 E. Schreiber, O. L. Anderson and N. Soga, in *Elastic constants and their measurements* (McGraw Hill, New York 1973)
- 2.8 A. Schaefer and L. Bergman, Naturwiss. **22** 1934) 685
- 2.9 H. J. McSkimin, J. Acoust. Soc. Am. **33** (1961) 12
- 2.10 H. J. McSkimin and P. Andreath, J. Acoust. Soc. Am. **34** (1962) 609
- 2.11 T. J. Moran and B. Lüthi, Phys. Rev. **187** (1969) 710
- 2.12 R. D. Holbrook, J. Acoust. Soc. Am. **20** (1948) 590
- 2.13 N. P. Cedrone, D. R. Curram, J. Acoust. Soc. Am. **26** (1954) 963

- 2.14 E. P. Papadakis, *J. Appl. Phys.* **35** (1964) 1474
- 2.15 E. P. Papadakis, in *Physical acoustics* Vol.12, (ed.) W. P. Mason and R. N. Thurston (Academic Press, New York 1976)
- 2.16 E. P. Papadakis, in *Physical acoustics* Vol.19, (ed.) R. N. Thurston and Allan D. Pierce (Academic Press, New York 1990)
- 2.17 R. Truell, C. Elbaum and B. B. Chick, in *Ultrasonic methods in solid state physics* (Academic Press, New York 1969)
- 2.18 E. V. Fuller, A. V. Granato, J. Holder and E. R. Naimon, in *Methods of experimental Physics* Vol. 11 (ed.) R V Coleman (Academic Press, New York 1974)
- 2.19 D. I. Bolef, in *Physical acoustics* Vol.4, pt. A (ed.) W. P. Mason and R. N. Thurston (Academic Press, New York 1976)
- 2.20 J. E. May, Jr., *IRE Natl. Conv. Rec.* **6** Pt.2 (1958) 134
- 2.21 R. Sreekumar, in *Investigations of phase transitions in selected high T_c superconductors and ferroelectrics using ultrasonic technique*, (Ph. D Thesis, Cochin University of Science and Technology 1993)
- 2.22 L. Godfrey and J. Philip, *Acoust. Letters*, **19** (1995) 11
- 2.23 J. C. Brice, *Prog. Cryst. Growth Charact.* **1** (1978) 255
- 2.24 J. C. Brice, in *The growth of crystals from liquids* (North Holland, Amsterdam 1973)
- 2.25 B. R. Pamplin, in *Crystal growth* (Pergamon Press, Oxford 1975)
- 2.26 J. J. Gilman, in *The art and science of growing crystals* (Wiley, New York 1963)
- 2.27 P. Santhanaraghavan and P. Ramasamy, in *Crystal growth, processes and methods* (Kru Publications, Chennai 1999)

- 2.28 I. F. Nicolau, *Kristall. und Technik* **9** (1974) 1331
- 2.29 Norbert Karl, in *Crystals, Growth properties and applications* Vol. **4** (Springer-Verlag, Berlin 1980)
- 2.30 Belonet C., *Acta Electronica* **16** (1973) 339
- 2.31 Belonet C. and Monnier M., *J. Cryst. Growth* **29** (1975) 109
- 2.32 J. R. Bourne, R. J. Davy, H. Cros and K. Hungerbehler, *J. Cryst. Growth* **34** (1976) 21
- 2.33 E. Janssen-van Rosmalen, Lunden, W. H. van den, E. Dobbing and D. Visser, *Kristall. und Technik* **13** (1978) 17
- 2.34 L. Vannay, *Kristall. und Technik* **14** (1979) K39
- 2.35 Aswani Karnal, Hari Om Mahawar and V K Wadhawan, *Ind. J. Pure Appl. Phys.* **36** (1998) 587
- 2.36 L. Godfrey, in *Ultrasonic study of the elastic properties and phase transitions in selected mixed sulphate crystals* (Ph.D. Thesis, Cochin University of Science and Technology 1994)
- 2.37 M. Grubic and R Strey, *J. Phys. E: Sci. Instrum.* **10** (1977) 142
- 2.38 L. Godfrey and J. Philip, *J. Phys. E: Sci. Instrum. (UK)* **22** (1989) 516
- 2.39 M. N. Bhusavalweala and Suchal Jariwala, *J. Inst. Soc. India* **25** (1994) 19

Chapter 3

Elastic properties of

sodium p-nitrophenolate dihydrate (NPNa)

single crystals

3.1 Introduction

The interest in understanding nonlinear optical phenomena started with the detection of second harmonic emission [3.1] from quartz about a year after the development of the first laser source. Since the middle of 1980's there has been an explosion of interest in the search for and development of nonlinear optical materials that are suitable for commercial device applications. To date, such materials find application in information processing, optical switching, optical frequency conversion and telecommunications [3.2-3.4]. Of the many systems studied, for example inorganic crystals and semiconductors, organic crystalline monomers and long chain polymers with delocalised π -electrons, no one species has proved to be all-encompassing, with advantages for one being negated by disadvantage for another. In recent years, organometallic compounds, through their unique characteristics such as diversity of metals, oxidation states, ligands and geometries have found success and brought a new dimension to this area. Extensive research done during the past decade indicate that

organic compounds often possess higher degree of optical nonlinearity than their inorganic counter parts. Some of the other advantages of organic materials are their inherent high nonlinearity, ease of synthesis, scope for altering the properties by functional substitutions, high damage resistance etc.

Sodium p-nitrophenolate dihydrate (abbreviated as NPNa) is a relatively new semiorganic nonlinear optical material. Minemoto *et al.* [3.5,3.6] have recently reported the linear optical properties and powder efficiency for second harmonic generation (SHG) of this material. Material synthesis, crystal growth and preliminary characterization of this crystal have also been done by them. They have reported that NPNa crystal has a d_{eff} value which is about 1.2 times that of potassium titanyl phosphate (KTP), or in other words the d_{eff} value of NPNa is 11.5 times the d_{36} value of potassium di-hydrogen phosphate (KDP) [3.7]. Davydov *et al.* [3.8] determined the powder efficiency for second harmonic generation in 1977. It is reported to be $1m\text{-NA}$ where $m\text{-NA}$ stands for the powder efficiency of meta-Nitro Aniline. An intra-cavity frequency doubling of a diode laser pumped Nd:YVO₄ laser have also been demonstrated by Minemoto *et al.* [3.9]. The d value of NPNa is reported to be the highest compared to a group of more than ten common NLO materials [3.10]. Effect of temperature on disorder and nature of hydrogen bonds have also been investigated using polarized Raman scattering experiments and reports are available in literature [3.11].

A more exact crystal structure determination of NPNa has been done recently by Sharma *et al.* [3.12]. NPNa is a metal complex of donor-acceptor substituted aromatic compound. Molecular structure and packing of NPNa molecules in planes parallel to the (100) plane are shown in Fig. 3.1(a) and Fig. 3.1(b) respectively. NPNa crystal has a layered structure with molecules packed in layers perpendicular to the

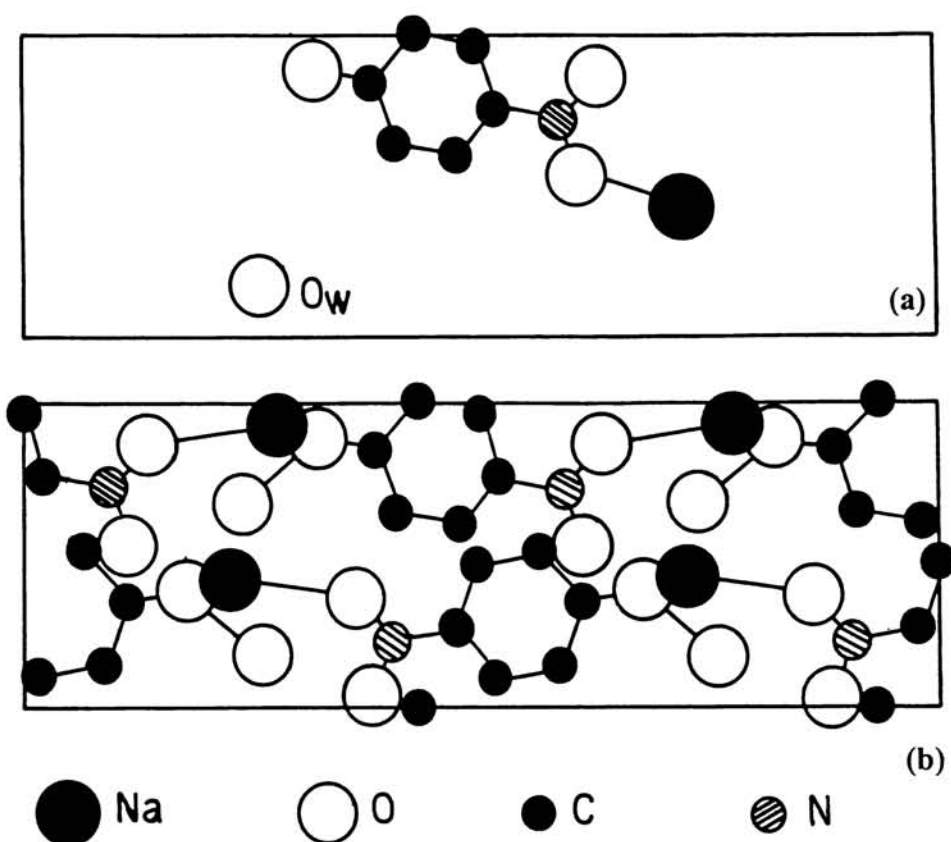


Fig. 3.1(a): Structure of NPNa molecule

Fig. 3.1(b): Packing of NPNa molecules in planes parallel to the (100) plane crystallographic a-axis. The bonding between sodium ion and nitrophenoxy ion is ionic in nature. It also interacts with the two oxygen atoms of the water of crystallization. The charge-transfer (CT) axis, defined as that along the donor-acceptor bonds, makes an angle of approximately 80° with the polar axis of the crystal. This alignment is not favorable to obtain the best nonlinear coefficients [3.13]. However, because of the presence of the extensive chains of these molecular dipoles, all aligned in the same direction, the functional units contribute additively to the macroscopic nonlinearity. This sort of molecular arrangement is highly favorable for optimum electrooptic effect [3.13].

A detailed account of the synthesis of the material, single crystal growth, crystal morphology, microhardness, defect characterization by chemical etching, synchrotron topography, and optical transmission studies is available in literature [3.14]. NPNa crystallizes into the orthorhombic structure with space group *Ima2*. The lattice parameters are reported to be $a = 6.892 \text{ \AA}$, $b = 19.692 \text{ \AA}$ and $c = 6.439 \text{ \AA}$ and has four molecules per unit cell. Good optical quality single crystals of reasonable size have been grown from methanol solution. The crystal does not exhibit any cleavage and has reasonably good hardness. The dielectric, thermal and optical properties of NPNa crystals have also been investigated earlier [3.15]. It is well documented in literature that the presence of dislocations, solvent inclusions and heterogeneous molecular inclusions which arise particularly from degraded solution during growth reduces the frequency conversion efficiency drastically and lowers the threshold for laser induced damage [3.16,3.17].

In this chapter we present the results of our measurement of the elastic properties of NPNa single crystal. All the nine second-order elastic constants have been determined by measuring the velocities of ultrasonic waves along various symmetry directions. Variation of selected elastic constants with temperature over a limited range have been measured and the results are presented. Phase velocity surfaces, slowness surfaces and group velocity surfaces have been plotted in different crystallographic planes to bring out the anisotropy in elastic properties for this crystal. The Young's modulus and linear compressibility surfaces also have been plotted. Details of the experiment, results obtained and a discussion of the results are presented in the following sections.

3.2 Sample preparation

NPNa material has been synthesized by mixing supersaturated solutions of nitrophenol and sodium hydroxide in the molar ratio 1:1. The yellow precipitate so obtained is washed and dried. It is further purified by several recrystallisations from water. The solubility of NPNa in methanol, already reported in literature [3.14], is shown in Fig. 3.2. Single crystals of NPNa have been grown from methanol solution by the slow evaporation or slow cooling method. NPNa is highly soluble in water but still it cannot be used as a good solvent to grow single crystals. Large rod shaped single crystals grown from aqueous solution loses its transparency within 30 minutes after its removal from the mother solution and are brittle in nature. It gets powdered on handling.

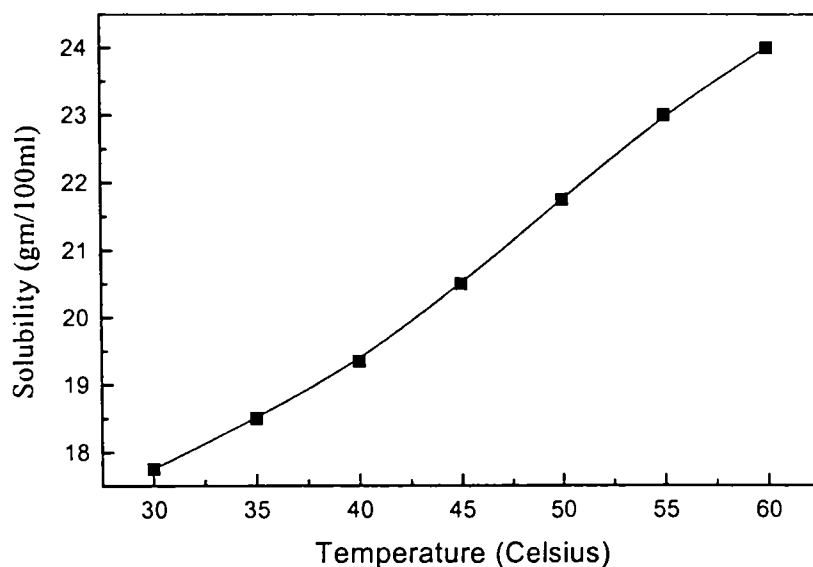


Fig. 3.2: Solubility curve of NPNa in methanol

Methanol is found to be a good solvent to grow bipyramidal crystals of NPNa which are optically clear and transparent. Supersaturated solution of NPNa in methanol is kept in jacketed vessel maintained at a temperature of 45°C. Temperature of the water bath is controlled to an accuracy of $\pm 0.01^\circ\text{C}$. Details of the setup to grow single

crystals from solution is already discussed in detail in chapter 2. Evaporation of the solvent has been controlled by providing suitable openings in the jacketed vessel. Attempts have also been made to grow single crystals of NPNa from N,N-dimethyl formamide (DMF) solution. Transparent, stable needle shaped single crystals can be easily grown from DMF solution since it is not so volatile compared to methanol.

The inter-planar angles have been evaluated from crystallographic data and are compared with those measured using an accurate contact goniometer. This helps one to fix the crystallographic directions and identify growth planes in the crystal grown from solution. The morphology of crystals grown from methanol solution, kept at a temperature 45°C is shown in Fig. 3.3. The crystal grows as a platelet in the a-c plane and is elongated in the a-direction.

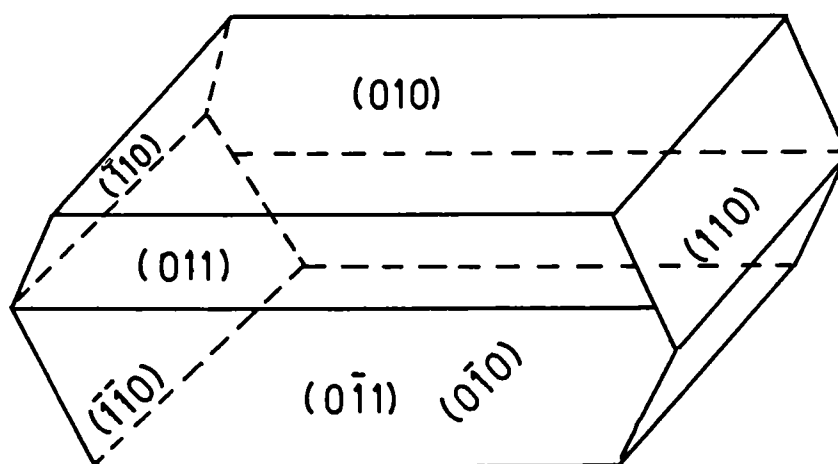


Fig. 3.3: Morphology exhibited by NPNa crystals grown from methanol solution at 45°C

If the crystals are grown at room temperature the shape of the crystal will be bipyramidal elongated in the b-direction. The prominent growth planes can be listed in their order of preference as $\{011\} > \{110\} > \{010\}$. Samples in the form of rectangular parallelepipeds for ultrasonic velocity measurements have been prepared

by cutting the bulk crystal using a slow speed diamond wheel saw. Our requirement of samples is shown in Fig. 3.4. These oriented samples have a pair of parallel planes perpendicular to the a [100], b [010], c [001], [110], [011] and [101] directions.

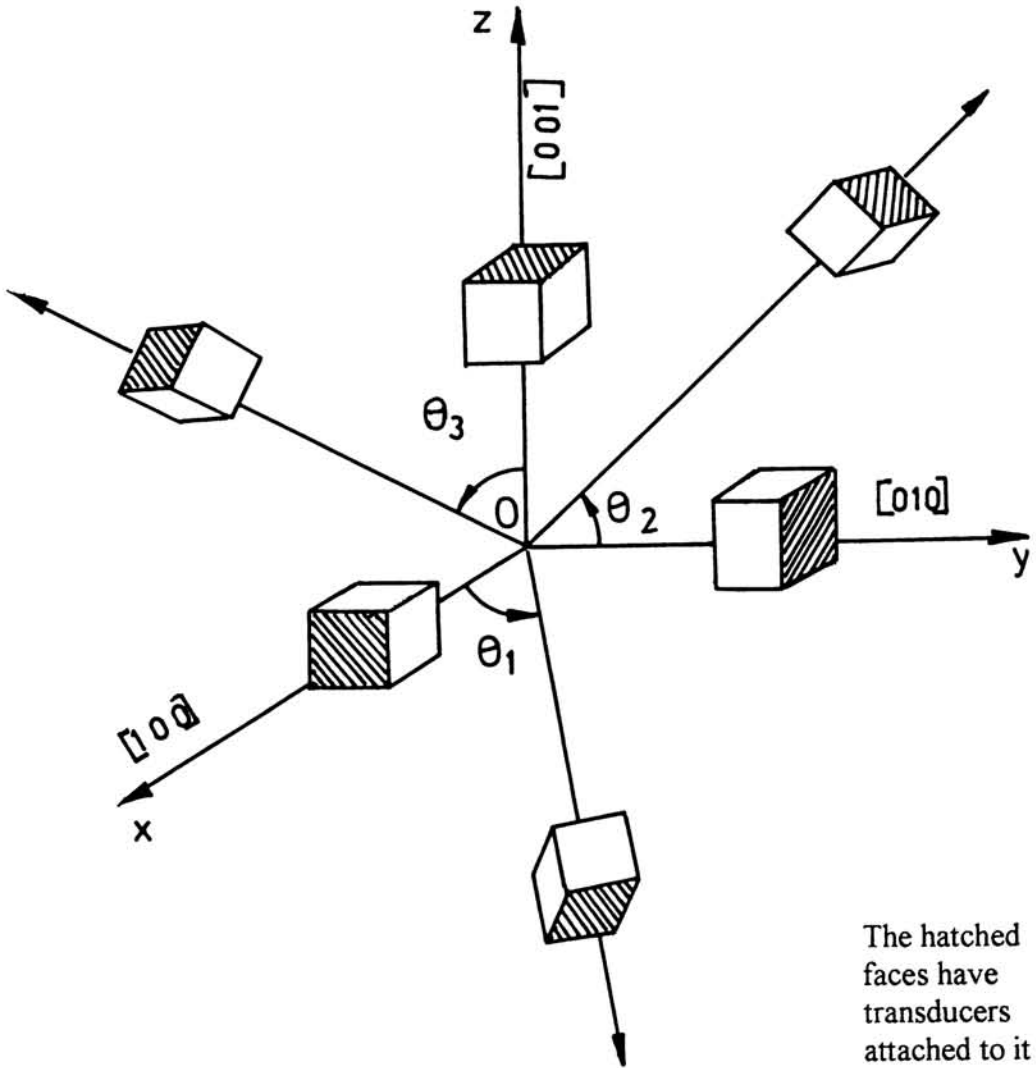


Fig. 3.4: Samples with different orientations required for ultrasonic measurements

Mostly the crystallographic directions need not be the same as the frame of reference for elastic properties. As per the IRE standards [3.18,3.19] for an orthorhombic crystal, x is taken parallel to a, y parallel to b and z parallel to c with $c < a < b$. Lattice parameters of NPNa obey this condition and hence the x, y, z frame of reference

coincides with the crystallographic axes. Samples prepared thus have been lightly polished without spoiling the parallelism between the opposite faces. Maximum care has been taken during polishing since even moisture present in the fingers is more than sufficient to dissolve a few layers of this crystal.

3.3 Ultrasonic velocity measurements

C_{11} , C_{22} , C_{33} , C_{44} , C_{55} , C_{66} , C_{12} , C_{23} and C_{13} are the nine elastic constants of a crystal belonging to the orthorhombic system. Twelve different mode velocity measurements are required to evaluate all these elastic constants from ultrasonic velocity data, which allows crosschecks on some of the critical values. X or Y-cut quartz transducers of resonant frequency 10MHz have been bonded to the crystal surface to admit mechanical vibrations generated by the transducer into the sample. Silicon grease is found to be a good bonding medium to transmit ultrasonic waves from the transducer to the sample. The same transducer detects the echo pulses reflected from the rear end of the sample. The travel time of the wave pulse through the sample has been determined accurately by the PEO technique. A more detailed description of the experimental setup and measurement details are given in chapter 2. The diagonal elastic constants ($i = j$) are related to the respective mode velocity in the crystal obeying a relation of the form $C_{ij} = \rho v^2$. These modes are pure modes. Velocities measured along [110], [011] and [101] directions are related to more than one elastic constant and are called mixed mode directions. Details of the modes measured, velocity of ultrasonic waves, corresponding elastic constants and the relation between these two are listed in Table 3.1. Corresponding elastic constants are also listed in the same table.

Table 3.1 Velocity of ultrasonic modes in NPNa crystals. L, T and QL represent longitudinal, transverse and quasi-longitudinal modes respectively. The relations between mode velocities and elastic constants are also given.

Sl No.	Mode	Direction of propagation	Direction of polarisation	Measured mode velocity (m/s)	Mode velocity - elastic constant relation	Elastic constant (GPa)
1	L	[100]	[100]	$v_1 = 4402 \pm 4$	$C_{11} = \rho v_1^2$	26.38 ± 0.05
2	L	[010]	[010]	$v_2 = 4032 \pm 4$	$C_{22} = \rho v_2^2$	22.11 ± 0.04
3	L	[001]	[001]	$v_3 = 5937 \pm 6$	$C_{33} = \rho v_3^2$	47.95 ± 0.10
4	T	[010]	[001]	$v_4 = 2259 \pm 2$	$C_{44} = \rho v_4^2$	6.94 ± 0.01
5	T	[001]	[010]	$v_5 = 2248 \pm 2$	$C_{44} = \rho v_5^2$	
6	T	[100]	[001]	$v_6 = 1518 \pm 2$	$C_{55} = \rho v_6^2$	3.14 ± 0.01
7	T	[001]	[100]	$v_7 = 1531 \pm 2$	$C_{55} = \rho v_7^2$	
8	T	[100]	[010]	$v_8 = 1470 \pm 2$	$C_{66} = \rho v_8^2$	2.94 ± 0.01
9	T	[010]	[100]	$v_9 = 1468 \pm 2$	$C_{66} = \rho v_9^2$	
10	QL	[110]	[QL]	$v_{10} = 5945 \pm 6$	$C_{12} = f_{ab}^{(a)}$	107.7 ± 1.08
11	QL	[011]	[QL]	$v_{11} = 5518 \pm 6$	$C_{23} = f_{bc}^{(b)}$	78.35 ± 0.78
12	QL	[101]	[QL]	$v_{12} = 3381 \pm 3$	$C_{13} = f_{ac}^{(c)}$	-2.53 ± 0.03

$$(a) f_{ab} = \{[c^2 C_{11} + s^2 C_{66} - \rho v_{10}^2] \{c^2 C_{66} + s^2 C_{22} - \rho v_{10}^2\} / c^2 s^2\}^{1/2} - C_{66}$$

$$(b) f_{bc} = \{[c^2 C_{22} + s^2 C_{44} - \rho v_{11}^2] \{c^2 C_{44} + s^2 C_{33} - \rho v_{11}^2\} / c^2 s^2\}^{1/2} - C_{44}$$

$$(c) f_{ac} = \{[s^2 C_{11} + c^2 C_{55} - \rho v_{12}^2] \{s^2 C_{55} + c^2 C_{33} - \rho v_{12}^2\} / c^2 s^2\}^{1/2} - C_{55}$$

(Here c and s are the cosine and sine of the angle of rotation from the respective axes.)

3.4 Temperature variation of elastic constants

Temperature dependence of elastic constants and ultrasonic attenuation can give very useful information about the properties of the material such as the existence of phase transitions resulting in elastic anomalies. The crystal-transducer assembly is kept in a temperature-controlled oven. As the temperature changes, one echo pulse drifts relative to the other laterally which is ultimately a change in the ultrasonic velocity in the sample. Dependence of the diagonal elastic constants on temperature are shown in Fig. 3.5(a) and 3.5(b).

3.5 Elastic anisotropy of NPNa crystal

Values of the second order stiffness constants of a crystal can be used to demonstrate the anisotropy in the elastic properties of a crystal by plotting the phase velocity, slowness, group velocity, Young's modulus and linear compressibility surfaces. Section of the phase velocity surfaces along the a-b, b-c and a-c planes are plotted in figures 3.6(a), 3.6(b) and 3.6(c) respectively. The pure shear (PS), quasi-shear (QS) and quasi-longitudinal (QL) modes have been shown separately by different symbols. Figures 3.7(a), 3.7(b) and 3.7(c) show the sections of the slowness (inverse phase velocity) surfaces along the a-b, b-c and a-c planes respectively. The quasi shear mode exhibits certain amount of anisotropy, which can be assessed from its shape. The group velocity or ray velocity surfaces can provide more information about the elastic properties of a crystal. The group velocity surfaces of NPNa are shown as sections along the a-b, b-c and a-c planes in Fig. 3.8(a), 3.8(b) and 3.8(c) respectively. The quasi shear mode

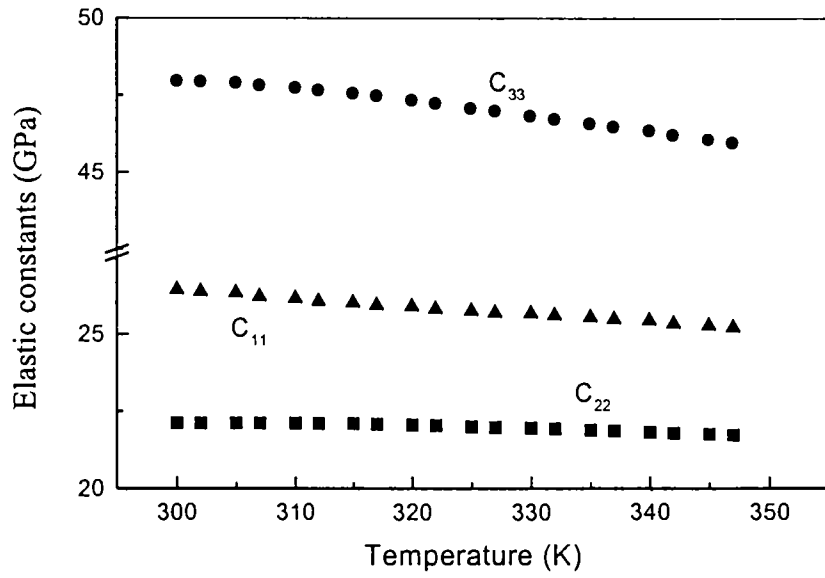


Fig. 3.5(a) : Dependence of elastic constants C_{11} , C_{22} and C_{33} on temperature.

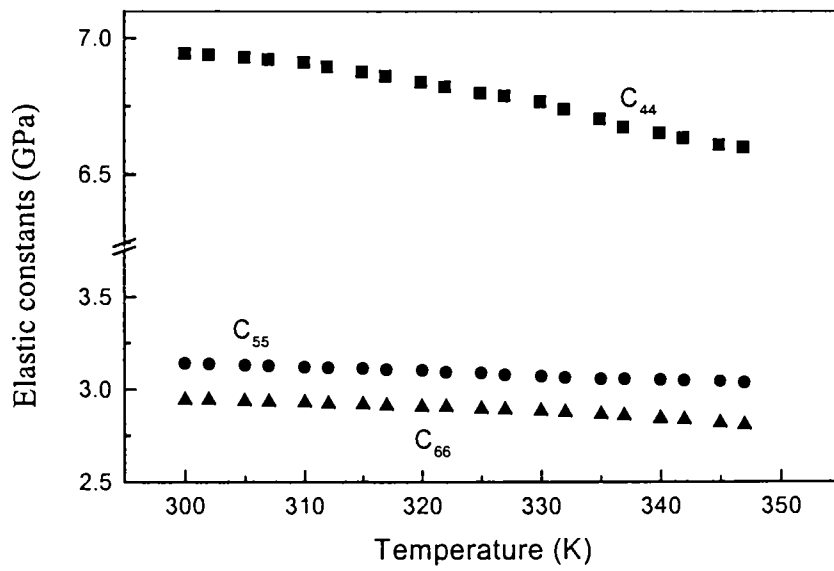


Fig. 3.5(b): Dependence of elastic constants C_{44} , C_{55} and C_{66} on temperature.

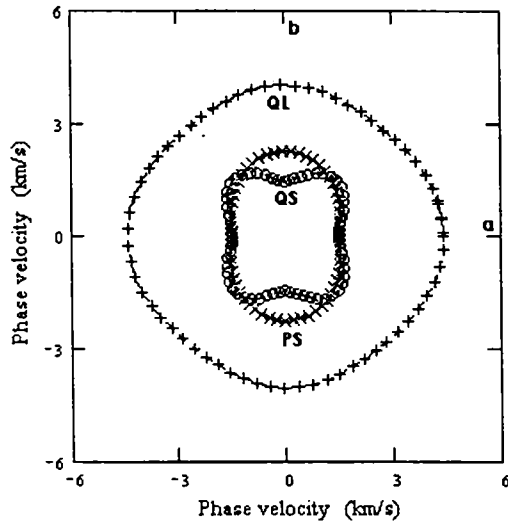


Fig.3.6(a) : Section of the phase velocity surfaces of NPNa along the a-b plane.

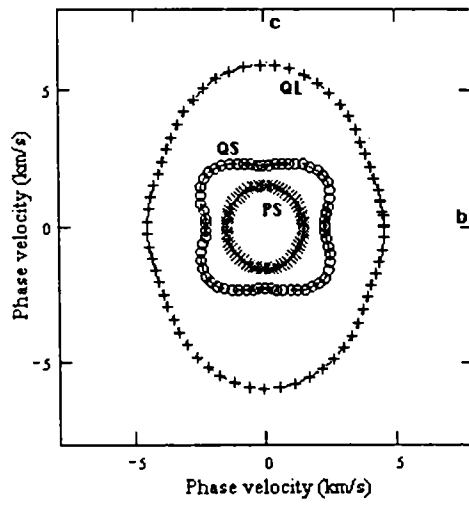


Fig.3.6(b) : Section of the phase velocity surfaces of NPNa along the b-c plane.

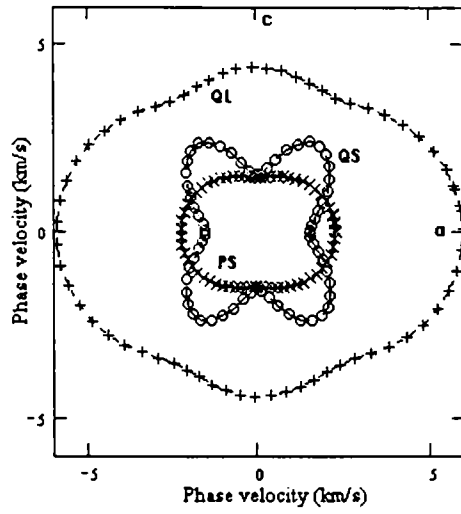


Fig.3.6(c) : Section of the phase velocity surfaces of NPNa along the a-c plane.

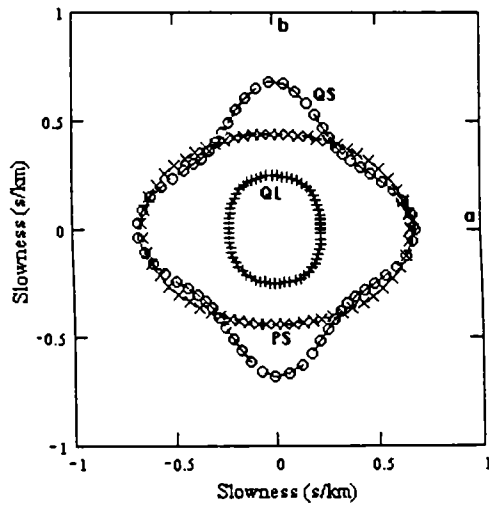


Fig.3.7(a) : Section of the slowness surfaces of NPNa along the a-b plane.

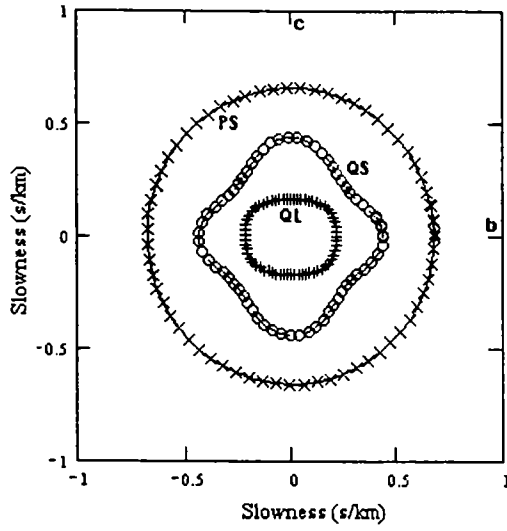


Fig. 3.7 (b): Section of the slowness surfaces of NPNa along the b-c plane

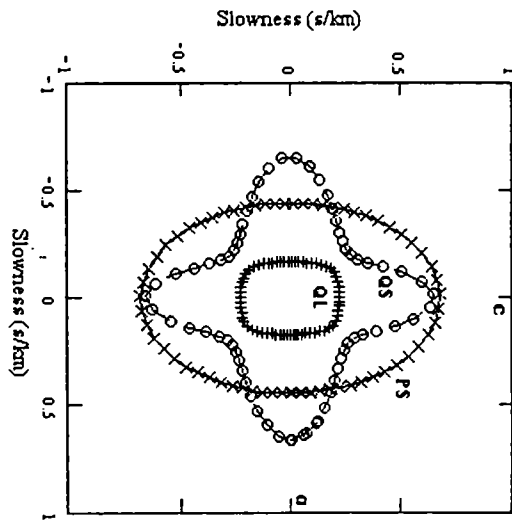


Fig. 3.7 (c): Section of the slowness surfaces of NPNa along the a-c plane

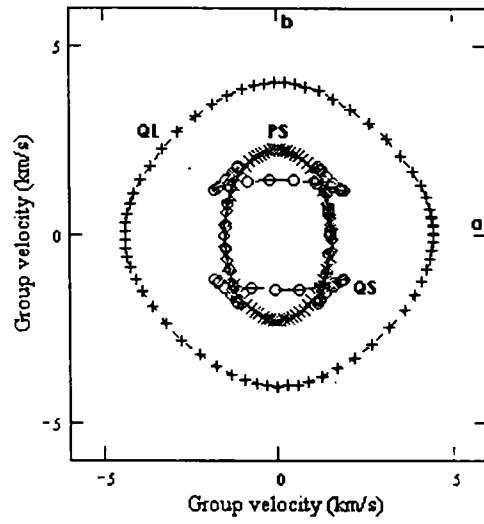


Fig.3.8(a) : Section of the group velocity surfaces of NPNa along the a-b plane.

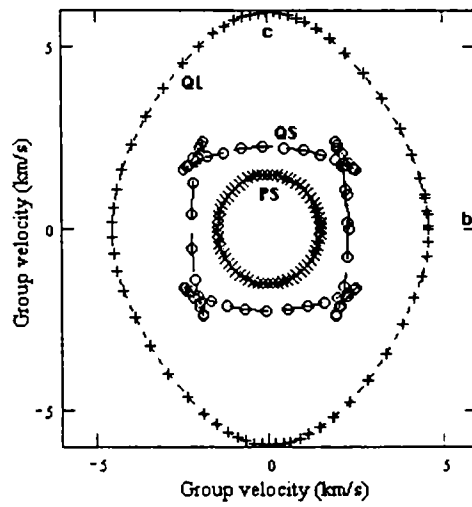


Fig.3.8(b) : Section of the group velocity surfaces of NPNa along the b-c plane.

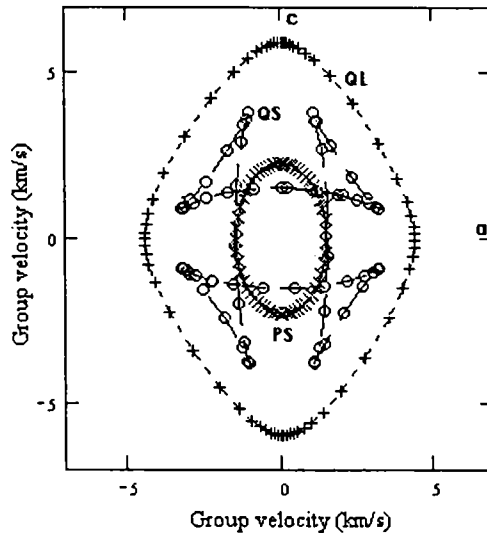


Fig. 3.8(c): Section of the group velocity surfaces of NPNa along the a-c plane exhibits cuspidal edges along the [110], [011] and [101] directions. It indicates that there can be more than one group velocity vector corresponding to a given phase velocity vector.

Behavior of a material under longitudinal stress is well understood when Young's modulus values are evaluated. Young's modulus is a direction dependent parameter and hence the shape of the surface generated by plotting Young's modulus values for various directions in the crystal can give more information about the anisotropy in the elastic properties. Fig. 3.9 shows sections of the Young's modulus surface along the a-b, b-c and a-c planes. Fig. 3.10 shows sections of the linear compressibility surface along the a-b, b-c and a-c planes.

3.6 Discussion and conclusion

All the nine second-order elastic constants of NPNa single crystals are reported in this chapter. The magnitude and sign of the elastic constants reflect the strength and nature

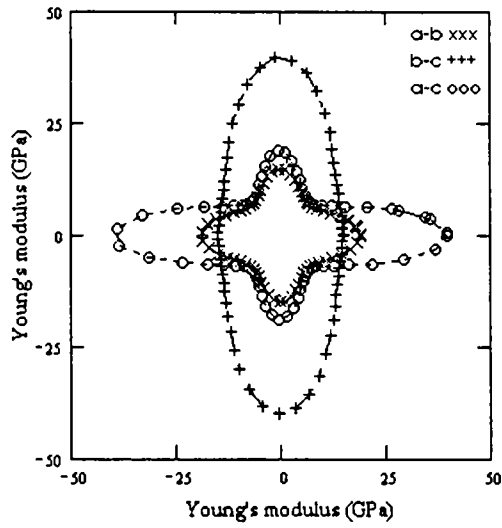


Fig.3.9 : Sections of the Young's modulus surface of NPNa along the a-b (xxx), b-c (+++) and a-c (ooo) planes.

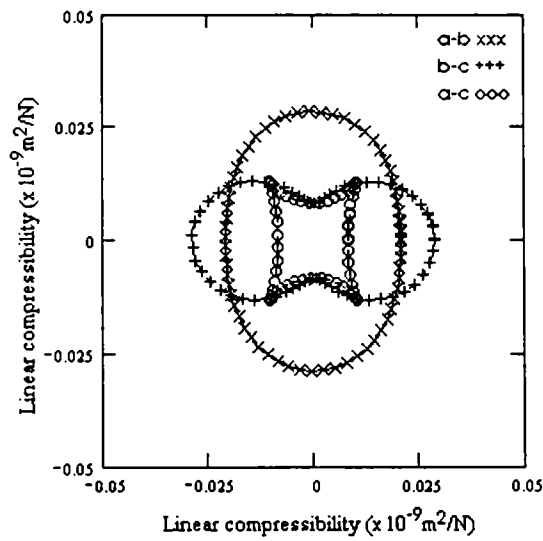


Fig.3.10 : Sections of the linear compressibility surface of NPNa along the a-b (xxx), b-c (+++) and a-c (ooo) planes.

of the inter-atomic forces in the crystal. All the elastic constants on which temperature variation measurements have been carried out, are found to decrease with temperature. This is the behavior exhibited by most solids. The temperature coefficients of elastic constants are rather small. It may be noted that none of the elastic constants exhibit any anomalous variation with temperature, indicating that this crystal does not undergo any phase transition in the temperature range over which measurements have been carried out. This observation is in agreement with other results reported on the sample.

It is rather interesting to note that this crystal exhibits significant anisotropy in its elastic properties. It may be noted that sections of the group velocity surfaces exhibit cuspidal edges along symmetry directions. These correspond to directions which a one-to-one correspondence between phase velocity vector and group velocity vector is lost, or more than one group velocity correspond to a single phase velocity. Such directions are expected to exhibit interesting phenomena such as conical refraction, phonon focussing etc. [3.20,3.21]. It would be interesting to study phonon focussing and enhancement in this sample by heat pulse techniques by keeping the sample at ultra low temperatures.

The Young's modulus and linear compressibility also show significant anisotropy in their values. This information would be of interest while using this crystal for various practical applications.

References

- 3.1 P. A. Franken, A. E. Hill, C. W. Peters and G. Weinreich, Phys. Rev. Lett. 7 (1961) 118
- 3.2 G. H. Wagnere, in *Linear and nonlinear optical properties of molecules* (VCH Weinheim Helvetica Chemica Acta Basel 1993)

- 3.3 D. J. Williams (ed), *Nonlinear optical properties of organic and polymeric materials* (ACS Symp. Ser. 1983), p233
- 3.4 S. R. Marder, J. E. Sohn and G. D. Stucky (ed), *Materials for nonlinear optics: Chemical perspective*, ACS Symp. Ser. 1991, p455
- 3.5 H. Minemoto, Y. Ozaki, N. Sonoda and T. Sasaki, *Appl. Phys. Lett.*, **63** (1993) 3565
- 3.6 H. Minemoto, N. Sonoda and K. Miki, *Acta Crystallogr. Sect. C* **48** (1992) 737
- 3.7 V. G. Dmitriev, G. G. Gurzadyan, and D. N. Nikogosyan, (ed), *Handbook of nonlinear optical crystals* (Springer Verlag, Berlin 1997) p294
- 3.8 B. L. Davydov, S. G. Kotovshchikov and V. A. Nefedov, *Sov. J. Quantum Electron.* **7** (1977) 129
- 3.9 H. Minemoto, Y. Ozaki, N. Sonoda and T. Sasaki, *J. Appl. Phys.* **76** (1994) 3975
- 3.10 Harneet Gahir, Prathima sen, Swapan Konar and Sen P. K., Sixth international Topical meeting on education and training in optics, Mexico 1998, Work 99E60 classification P(II)-9 Vol. **3831-96**
- 3.11 Carabotos-Nedelec, Constantin, Ben Salah, Mohammed Becker and Paul, in *Optical devices and diagnostics in materials Science*, Proceedings of SPIE Vol. **4098**
- 3.12 R. P. Sharma, S. Kumar, K. K. Bhasin and E. R. T. Tiekink, *Zeitschrift fur Kristallographie -New crystal structures* Vol. **212** (1997) 169
- 3.13 J. Zyss and J. L. Oudar, *Phys. Rev. A* **26** (1982) 2028
- 3.14 S. Brahadeeswaran, V. Venkataramanan, J. N. Sherwood and H. L. Bhat, *J. Mater. Chem.* **8** (1998) 613

- 3.15 S. Brahadeeswaran, H. L. Bhat, N. S. Kini, A. M. Omarji, P. Balaya and P. S. Goyal, *J. Appl. Phys.* **88** (200) 5935
- 3.16 R. T. Bailey, F. R. Cruickshank, D. Pugh and J. N. Sherwood, *J. Optoelectron.* **5** (1990) 89
- 3.17 V. Venkataramanan, J. N. Sherwood and H. L. Bhat, *SPIE Proceedings Vol. 3093* (International Society for Optical Engng. Washington, USA 1997)
- 3.18 I. R. E. Standards Committee, *Proc. IRE* **37** (1949) 1378
- 3.19 J. R. Neighbours and G. E. Schacher, *J. Appl. Phys.* **38** (1967) 5366
- 3.20 B. Taylor, H. J. Maris and C. Elbaum, *Phys. Rev. Lett.* **23** (1969) 416
- 3.21 B. Taylor, H. J. Maris and C. Elbaum, *Phys. Rev.* **B3** (1971) 1462

Chapter 4

Elastic properties of

Potassium acid phthalate (KAP) single crystals

4.1 Introduction

Many organic molecular crystals belonging to the orthorhombic system exhibit electro-optic [4.1], ferroelectric [4.2], photoconducting [4.3] and triboluminescence [4.4] properties. Some of these properties are structure sensitive and a correlation between piezoelectric and triboluminescence properties have been reported earlier [4.5]. The potassium salt of phthalic acid, potassium acid phthalate (KAP) or potassium hydrogen phthalate (KHP) or potassium biphthalate, with the chemical formula $C_8H_5O_4K$ finds application in soft x-ray spectroscopy due to its large $2d$ ($2d = 26.6\text{\AA}$) spacing [4.6,4.7]. It is also reported that it exhibits marked piezoelectric [4.8,4.9] and electrooptic [4.10] effects. The pyroelectric and electrical properties of pure and X-ray irradiated KAP crystals have been reported earlier [4.11,4.12]. These authors have reported that the crystal decomposes at about 520K. Optical properties of KAP crystals have been investigated by Comoretto *et al.* and the results are available in literature [4.13]. Even though the elastic properties of an isomorphous family member, thallium

acid phthalate have been reported earlier [4.14], there are no reports on the measurement of the elastic properties of this crystal.

Mniewicz *et al.* observed polariton dispersion in KAP by using near-forward Raman scattering technique [4.15]. The specular reflection spectra have been measured and associated optical functions have been evaluated in the 3 - 22 eV range by Romanyuk *et al.* [4.16]. The temperature dependence of cracking resistance and capture of water in KAP crystals [4.17] have been investigated earlier as part of the characterization of KAP crystals and optimization of growth conditions. KAP crystallizes into orthorhombic structure with lattice parameters $a = 6.46 \text{ \AA}$, $b = 9.60 \text{ \AA}$ and $c = 13.85 \text{ \AA}$ and has four molecules per unit cell, as reported by Okaya [4.18]. The space group is $Pca2_1$ and is noncentrosymmetric. KAP crystals have excellent cleavage, which is comparable to or even better than that of mica. Okaya [4.18] identified the cleavage plane as (001); but later van Enkevort *et al.* [4.19] assigned the value 13.85 \AA to b and accordingly the cleavage plane is indexed as (010). However, the assignment of these values to the lattice parameters a , b and c is not as per the IRE standards [4.20] for the determination of all the nine second-order elastic constants of an orthorhombic crystal.

Reports on studies of crystal growth [4.21,4.22], defect characterization by chemical etching [4.23], mechanism of layer growth and its micro morphology [4.24-4.26], effect of additives on crystal growth rate and morphology [4.22,4.27-4.29] and correlation between crystal structure and morphology [4.30,4.31] have been reported in literature. Large transparent inclusion-free crystals of KAP can be easily grown from aqueous solution either by the slow evaporation or slow cooling techniques.

In this chapter, we present the results of our measurement of the elastic properties of KAP single crystal. All the nine second-order elastic constants have been

determined by measuring the velocities of ultrasonic waves along various symmetry directions. Variation of selected elastic constants with temperature over a limited range have been measured and the results are presented. Phase velocity surfaces, slowness surfaces and group velocity surfaces have been plotted in different crystallographic planes to bring out the anisotropy in the elastic properties for this crystal. The Young's modulus and linear compressibility surfaces also have been plotted. Details of the experimental results obtained and a discussion of the results are presented in the following sections.

4.2 Sample preparation

Potassium hydrogen phthalate (KAP) is highly soluble in water and has high positive temperature coefficient of solubility [4.21]. Large single crystals of KAP have been grown by the slow cooling technique. Details of the crystal growth setup have been discussed at length in Chapter 2. Crystal of approximate size $40 \times 30 \times 15 \text{ mm}^3$ has been grown by this technique in a period of about 3 - 4 weeks. Large, transparent, inclusion-free crystals grown have $\{110\}$, $\{111\}$ family of planes and (010) plane developed fully well. The inter-planar angles measured using an accurate contact goniometer have been compared with the theoretically evaluated values, to fix the crystallographic directions and growth planes. The morphology of this crystal along with the laboratory axes for measurements are shown in Fig. 4.1. The laboratory axes x, y and z have been fixed according to the IRE standards as x parallel to a, y parallel to b and z parallel to c with $c < a < b$ [4.20]. Samples in the shape of rectangular parallelepipeds with parallel planes perpendicular to the a [100], b [010], c [001], [110], [011] and [101] directions (Fig. 3.4 in chapter 3) have been cut using a slow speed diamond wheel saw.

The sample faces of interest have been lightly polished without spoiling the parallelism between the opposite faces.

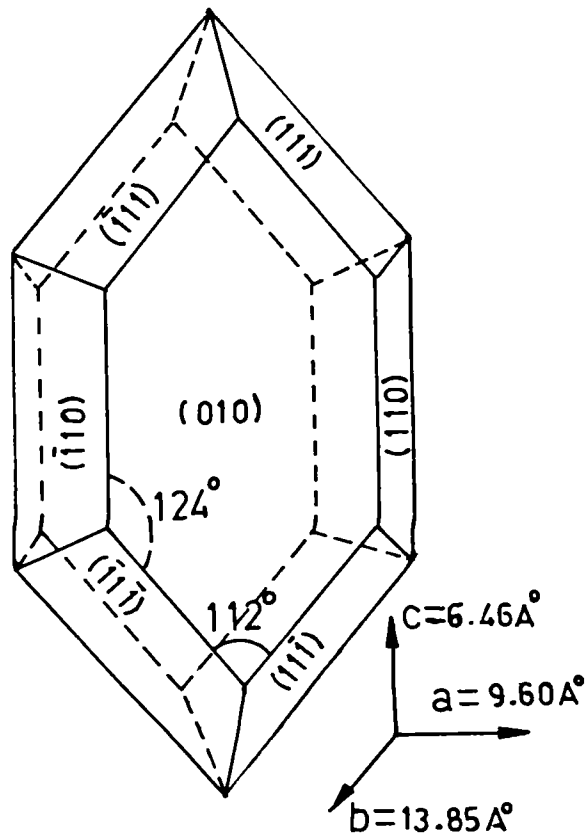


Fig. 4.1: Morphology exhibited by KAP single crystals

4.3 Ultrasonic velocity measurements

Evaluation of all the nine second-order elastic stiffness constants of an orthorhombic crystal require minimum 12 sound velocity measurements along selected crystallographic directions. This allows cross checking of some of the critical values. Ultrasonic pulse echo overlap (PEO) technique has been used to measure the round trip travel time through the sample. McSkimin Δt correction has been applied to eliminate the errors introduced in the measured travel times due to the presence of the bonding medium between the crystal and transducer. X and Y-cut quartz transducers of

resonant frequency 10MHz have been used to generate ultrasonic wave pulses. Silicon grease is found to be a suitable bonding medium to admit ultrasonic wave pulses generated by the transducer into the sample. The successive echo pulses generated by reflections from the rear end of the sample have been detected using the same transducer. A more detailed description of the measurement technique and setup are already given in Chapter 2. The density of KAP crystal has been measured to be equal to 1636 kg-m^{-3} .

4.4 Elastic constants of KAP crystal

Diagonal elastic constants ($i = j$) C_{11} , C_{22} , C_{33} , C_{44} , C_{55} and C_{66} have direct relation to the velocity of propagation of the respective mode as $C_{ij} = \rho v^2$ where ρ is the density of the crystal. These directions are usually pure mode directions. Velocities measured along any arbitrary direction in the a-b, b-c and a-c planes other than these pure mode directions can be used to evaluate the other three off-diagonal elastic constants C_{12} , C_{23} and C_{13} . These directions are called mixed mode directions because vibrations of particles constituting the medium will not be strictly longitudinal or transverse in nature. Velocities measured along these directions are related to more than one elastic constant. Description of the modes measured, values of velocity measured and relation between mode velocity and elastic constants are tabulated in Table 4.1. All the nine second order elastic stiffness constants and compliance constants and the respective Poisson's ratios evaluated are listed in Table 4.2. The accuracy of the measured diagonal elastic constants is better than 0.2% and that for the off-diagonal elastic constants is better than 1%, considering all possible sources of error in the measurements.

Table 4.1 Velocity of ultrasonic modes in KAP crystals. L, T and QL represent longitudinal, transverse and quasi-longitudinal modes respectively. The relations between mode velocities and elastic constants are also given.

Sl. No.	Mode	Direction of propagation	Direction of polarisation	Measured mode velocity (m/s)	Mode velocity - elastic constant relation
1	L	[100]	[100]	$v_1 = 3505.4 \pm 7$	$C_{11} = \rho v_1^2$
2	L	[010]	[010]	$v_2 = 3045.1 \pm 6$	$C_{22} = \rho v_2^2$
3	L	[001]	[001]	$v_3 = 3462.2 \pm 7$	$C_{33} = \rho v_3^2$
4	T	[010]	[001]	$v_4 = 2161.0 \pm 4$	$C_{44} = \rho v_4^2$
5	T	[001]	[010]	$v_5 = 2163.4 \pm 4$	$C_{44} = \rho v_5^2$
6	T	[100]	[001]	$v_6 = 1779.4 \pm 4$	$C_{55} = \rho v_6^2$
7	T	[001]	[100]	$v_7 = 1774.5 \pm 4$	$C_{55} = \rho v_7^2$
8	T	[100]	[010]	$v_8 = 2059.6 \pm 4$	$C_{66} = \rho v_8^2$
9	T	[010]	[100]	$v_9 = 2055.5 \pm 4$	$C_{66} = \rho v_9^2$
10	QL	[110]	[QL]	$v_{10} = 3261.2 \pm 7$	$C_{12} = f_{ab}^{(a)}$
11	QL	[011]	[QL]	$v_{11} = 3528.6 \pm 7$	$C_{23} = f_{bc}^{(b)}$
12	QL	[101]	[QL]	$v_{12} = 3163.2 \pm 6$	$C_{13} = f_{ac}^{(c)}$

$$(a) f_{ab} = \{[c^2 C_{11} + s^2 C_{66} - \rho v_{10}^2] \{c^2 C_{66} + s^2 C_{22} - \rho v_{10}^2\} / c^2 s^2\}^{1/2} - C_{66}$$

$$(b) f_{bc} = \{[c^2 C_{22} + s^2 C_{44} - \rho v_{11}^2] \{c^2 C_{44} + s^2 C_{33} - \rho v_{11}^2\} / c^2 s^2\}^{1/2} - C_{44}$$

$$(c) f_{ac} = \{[s^2 C_{11} + c^2 C_{55} - \rho v_{12}^2] \{s^2 C_{55} + c^2 C_{33} - \rho v_{12}^2\} / c^2 s^2\}^{1/2} - C_{55}$$

(Here c and s are the cosine and sine of the angle of rotation from the respective axes.)

Table 4.2 Elastic stiffness constants, compliance constants and Poisson's ratios of KAP crystal at room temperature (300K)

Elastic stiffness constants (GPa)	Elastic compliance constants ($\times 10^{-10} \text{ m}^2\text{-N}^{-1}$)	Poisson's ratios
$C_{11} = 20.10 \pm 0.040$	$S_{11} = 0.91 \pm 0.009$	
$C_{22} = 15.17 \pm 0.030$	$S_{22} = 1.37 \pm 0.013$	$\nu_{12} = 0.820$
$C_{33} = 19.61 \pm 0.040$	$S_{33} = 0.63 \pm 0.006$	$\nu_{21} = 0.550$
$C_{44} = 7.64 \pm 0.020$	$S_{44} = 1.31 \pm 0.013$	
$C_{55} = 5.18 \pm 0.010$	$S_{55} = 1.93 \pm 0.019$	$\nu_{23} = 0.300$
$C_{66} = 6.94 \pm 0.020$	$S_{66} = 1.44 \pm 0.014$	$\nu_{32} = 0.650$
$C_{12} = 11.11 \pm 0.100$	$S_{12} = -0.750 \pm 0.008$	
$C_{23} = 5.99 \pm 0.060$	$S_{23} = -0.410 \pm 0.004$	$\nu_{13} = -0.240$
$C_{13} = 0.23 \pm 0.010$	$S_{13} = 0.22 \pm 0.003$	$\nu_{31} = -0.350$

4.5 Temperature dependence of elastic constants

Study of the dependence of elastic stiffness constants on temperature allows one to detect any anomaly in the elastic properties at any specific temperature, which can be due to phase transition or related phenomena. The crystal-transducer assembly is kept in a temperature-controlled oven. The condition of perfect cycle-to-cycle matching of the overlapped echoes change with change in temperature, which is ultimately due to change in the round trip travel time. The tunable continuous wave oscillator is properly adjusted to reestablish the initial condition of overlap. The new frequency value enables one to evaluate the elastic constant at the new temperature. The dependence of C_{11} , C_{22} and C_{33} on temperature are shown in Fig. 4.2. C_{44} , C_{55} and C_{66} also show a similar behavior, and so is not included here.

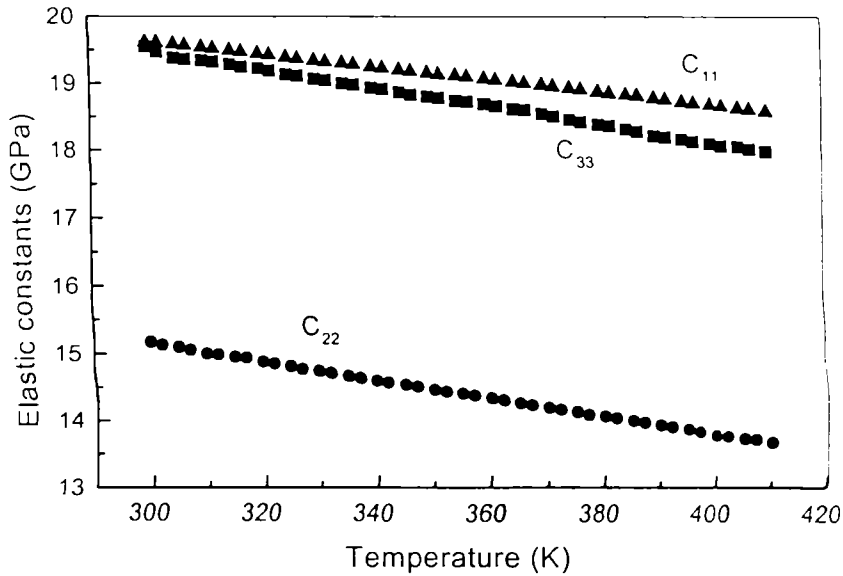


Fig. 4.2: Dependence of elastic constants C_{11} , C_{22} and C_{33} on temperature

4.6 Anisotropy of elastic wave propagation in KAP crystal

In order to demonstrate the anisotropy in the ultrasonic wave propagation characteristics of KAP, surface plots of the phase velocity, slowness or inverse phase velocity and ray velocity or group velocity have been drawn. Sections of the phase velocity surfaces along the a-b, b-c and a-c symmetry planes are shown in figures 4.3(a), 4.3(b) and 4.3(c) respectively. The pure shear (PS), quasi-shear (QS) and quasi-longitudinal (QL) modes are shown separately by different symbols. The crystal does not show marked anisotropy in ultrasonic wave propagation characteristics, which is clear from the shape of the contours. Sections of the slowness or inverse velocity surface do not exhibit large-scale anisotropy. The quasi-shear (QS) mode exhibits some anisotropy in elastic wave propagation. Sections of these surfaces along the a-b, b-c and a-c planes are shown in Fig. 4.4(a), 4.4(b) and 4.4(c) respectively. Sections of the group velocity surfaces along the a-b, b-c and a-c planes are shown in figures 4.5(a), 4.5(b) and 4.5(c) respectively.

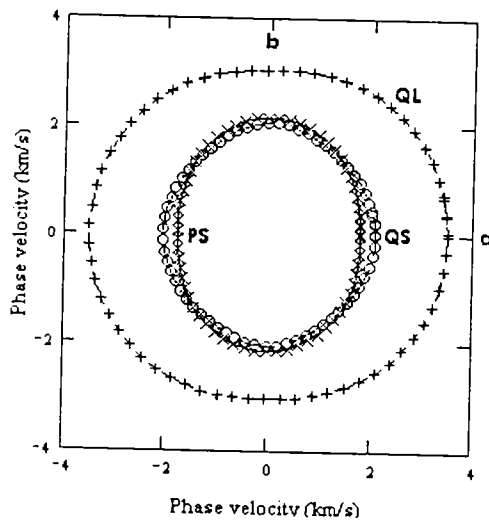


Fig. 4.3(a): Section of the phase velocity surfaces of KAP along the a-b plane.

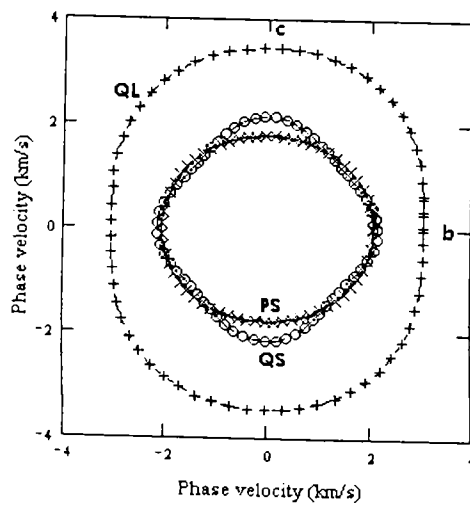


Fig. 4.3(b): Section of the phase velocity surfaces of KAP along the b-c plane

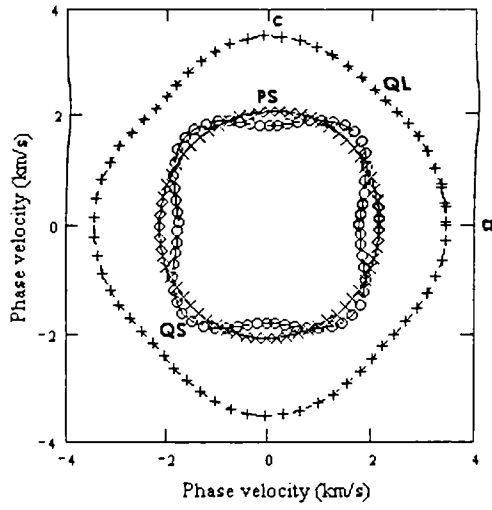


Fig. 4.3(c): Section of the phase velocity surfaces of KAP along the a-c plane.

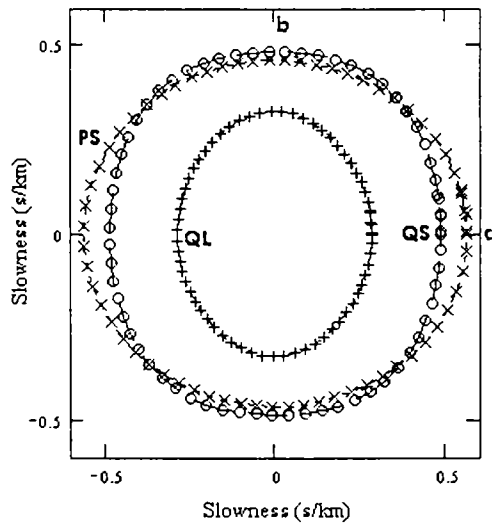


Fig. 4.4(a): Section of the slowness surfaces of KAP along the a-b plane.

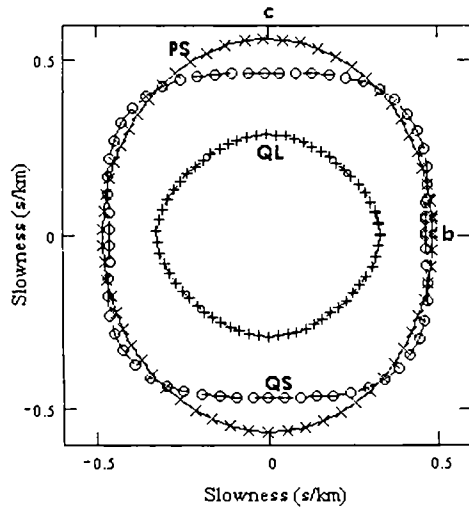


Fig. 4.4(b): Section of the slowness surfaces of KAP along the b-c plane.

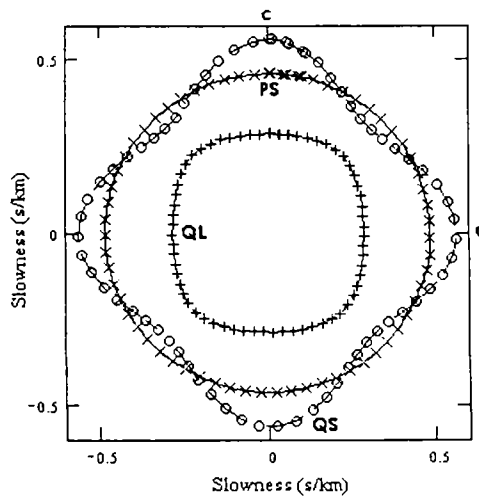


Fig. 4.4(c): Section of the slowness surfaces of KAP along the a-c plane.

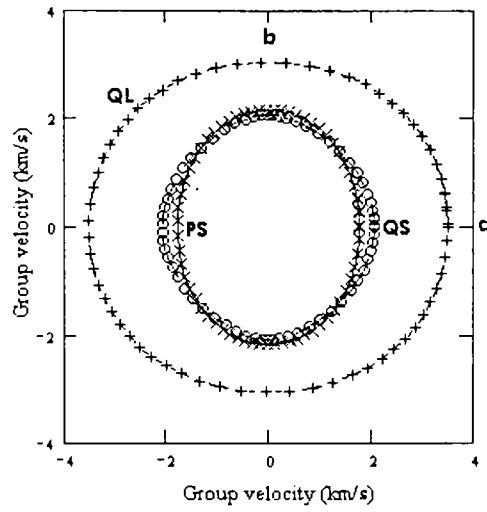


Fig. 4.5(a): Section of the group velocity surfaces of KAP along the a-b plane

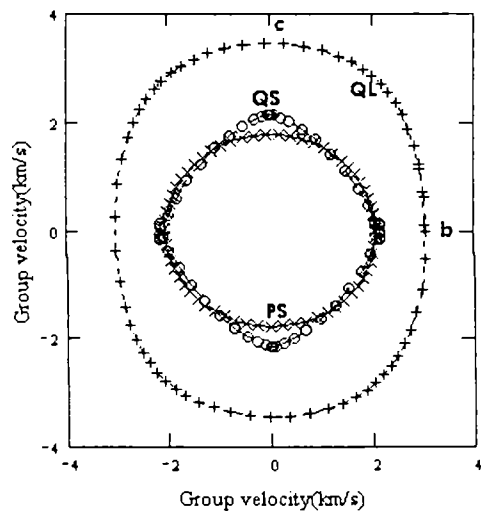


Fig. 4.5(b): Section of the group velocity surfaces of KAP along the b-c plane.

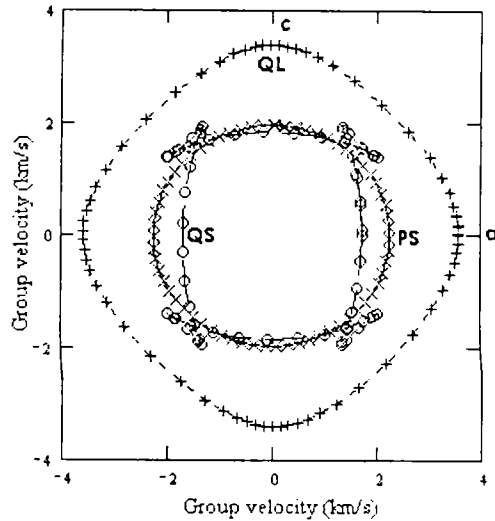


Fig. 4.5(c): Section of the group velocity surfaces of KAP along the a-c plane

The formation of cuspidal edges in these figures, provide very valuable information about anisotropy in the elastic properties of this crystal. Group velocity or ray velocity is the velocity with which energy is propagated in a crystal. This need not be collinear with the phase velocity vector. It may be noted that KAP exhibits cuspidal edges in group velocity surface for the quasi-shear mode.

Plotting of the Young's modulus and linear compressibility surfaces are two other useful techniques to demonstrate anisotropy in the elastic properties of a crystal. Sections of the Young's modulus surface along the a-b, b-c and a-c planes are shown in Fig. 4.6. Cross-sections of this surface is not perfectly circular indicating the presence of some amount of anisotropy in the longitudinal stress-strain response.

Linear compressibility, given by expression (1.74) in chapter 1 is a direction dependent parameter. Sections of the linear compressibility surface along the a-b, b-c and a-c planes are shown in Fig. 4.7. Here also the deviation from perfect circular shape indicates the extent of anisotropy in the linear compressibility of this crystal. Separate symbols have been used to indicate these sections along the a-b, b-c and a-c planes.

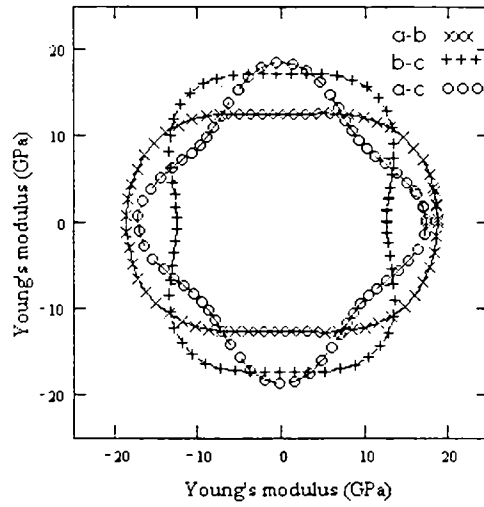


Fig. 4.6: Sections of the Young's modulus surface of KAP along the a-b (xxx), b-c (+++) and a-c (ooo) planes.

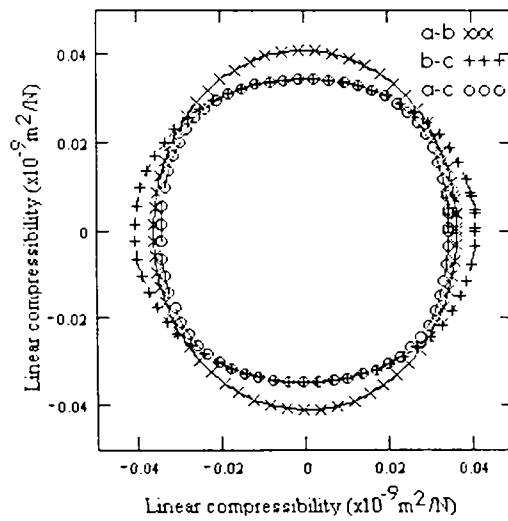


Fig. 4.7: Sections of the linear compressibility surface of KAP along the a-b (xxx), b-c (+++) and a-c (ooo) planes.

4.7 Discussion and conclusion

All the nine second order elastic stiffness and compliance constants of this crystal have been evaluated for the first time. The large number of clear echoes obtained in this crystal during ultrasonic measurements indicates that the crystals grown are free from structural imperfections and inclusions. Poisson's ratios have also been evaluated. The volume compressibility of this crystal is evaluated to be equal to $1.028 \times 10^{-10} \text{ m}^2 \text{ N}^{-1}$ and the corresponding bulk modulus is 9.73 GPa. Elastic constants, C_{11} , C_{22} and C_{33} gradually decrease with rise of temperature. Stretching of the lattice under longitudinal stress will be more in the presence of thermal energy and hence the longitudinal elastic constants C_{11} , C_{22} and C_{33} decrease steadily with rise of temperature. The shear elastic constants do not usually depend much on temperature. Shearing caused by tangential stress is not much affected by thermal energy. Dependence of C_{11} , C_{22} and C_{33} on temperature have been studied in the range 300-410K. Perfect cleavage along the (010) plane actually caused some difficulties in cutting oriented samples from the grown crystal. Very small stress exerted during handling is more than sufficient to cleave a portion of the crystal. The crystal is found not to exhibit any sort of large-scale anisotropy in the elastic properties.

References

- 4.1 J. L. Stevenson, J. Phys. D: Appl. Phys. **6** (1973) L13
- 4.2 C. J. Goldsmith and J. G. White, J. Chem. Phys. **31** (1959) 1175
- 4.3 J. Kommandeur, J. Phys. Chem. Solids **22** (1961) 339
- 4.4 J. I. Zink and W. Klumt, J. Am. Chem. Soc. **96** (1974) 4690
- 4.5 B. P. Chandra and N. Elyas, J. Phys. C: Solid state Physics **12** (1979) L695

- 4.6 D. Chopra, *Rev. Sci. Instrum.* **41** (1970) 1004
- 4.7 A. Bardeen and F. N. Huffman, *Rev. Sci. Instrum.* **34** (1963) 1233
- 4.8 I. S. Rez, *Cs. Cas. Fys.* **13** (1963) 31
- 4.9 I. S. Rez, A. S. Sonin, E. E. Tsepelevich and A. A. Filimonov, *Sov. Phys.-Crystallogr. (USA)* **4** (1960) 59
- 4.10 A. Miniewicz, M. Samoc, J. Dziedzic and R. Poprawski, *Proc. XI Mol. Cryst. Symp. Lugano 1985*, p.196.
- 4.11 K. B. R. Varma and A. K. Raychaudhuri, *J. Phys. D: Appl. Phys.* **22** (1989) 809
- 4.12 K. B. R. Varma, A. R. Raju and K. J. Rao, *Cryst. Res. Technol.* **23** (1988) 185
- 4.13 D. Comoretto, L. Rossi and A. Borghesi, *J. Materials Research* **12** (1997) 1262
- 4.14 M. Brissaud, L. Eyraud and P. Guerder, *Acoustica* **55** (1984) 160
- 4.15 A. Mniewicz, C. Ecolivet and Y. Marqueton, *Mater. Sci.(Poland)* **13** (1987) 169
- 4.16 N. A. Romanyuk and B. V. Andrievskii, *Ukr. Fiz. Zh.(USSR)* **30** (1985) 218
- 4.17 O. F. Pozdnyakov, B. P. Redkov, A. S. Smirnov, G. S. Belikova, V. R. Regel, N. L. Sizova and T. M. Okhrimenko, *Sov. Phys. Crystallogr. (USA)* **33** (1988) 588
- 4.18 Y. Okaya, *Acta Crystallogr.* **19** (1965) 879
- 4.19 L. A. M. J. Jetten, B. van der Hoet and W. J. P. van Enckevort, *J. Cryst. Growth* **62** (1983) 603
- 4.20 J. R. Neighbours and G. E. Schacher, *J Appl. Phys* **38** (1967) 5366
- 4.21 G. Bohm and K. Ulmer, *J. Cryst. Growth* **10** (1971) 175
- 4.22 K. Srenivasan, K. Meera and P. Ramasamy, *Cryst. Res. Technol.* **35** (2000) 291
- 4.23 Joy George and S. K. Premachandran, *J. Phys. D: Appl. Phys.* **14** (1981) 1277

- 4.24 G. I. Distler, E. I. Suvorova, Yu M. Gerasimov, E. I. Kortukova, T. M. Okhrimenko and G. S. Belikova, *Sov. Phys. Solid State (USA)* **27** (1985) 281
- 4.25 Yu M. Gerasimov, G. I. Distler, V. M. Kanevskii, E. I. Kortukova, E. I. Suvorova, T. M. Okhrimenko and G. S. Belikova, *Sov. Phys. Solid state (USA)* **29** (1984) 591
- 4.26 V. A. Kuznetsov, E. I. Suvorova and V. V. Volkov, *Sov. Phys. Solid State (USA)* **34** (1989) 929
- 4.27 P. Muruga-koothan, R. M. Kumar, P. M. Ushasree, R. Jayavel, R. Dhanasekhran and P. Ramasamy, *J. Cryst. Growth* **207** (1999) 325
- 4.28 V. A. Kuznetsov, T. M. Okhrimenko and Kh. S. Begdasarov, *Crystallography reports* ISSN 1063-7745, Vol. **41** (1996) 527
- 4.29 Zhao Quing-lan, Chen Jin-zhang and Huang Yi-sen, *Chin J. Phys (USA)* **32** (1983) 294
- 4.30 M. H. J. Hottenhuis, J. G. E. Gardeniers, L. A. M. J. Jetten and P. Bennema, *J. Cryst. Growth* **92** (1988) 171
- 4.31 M. H. J. Hottenhuis and C. B. Lucasius, *J. Cryst. Growth* **94** (1989) 708

Chapter 5

Elastic properties of Zinc tris (thiourea) sulphate (ZTS) single crystals.

5.1 Introduction

New nonlinear optical (NLO) frequency conversion materials with better physical properties can have significant impact on laser technology [5.1], optical communication [5.2], optical data storage technology [5.3] optical modulation etc. Recent efforts at producing new frequency conversion materials have been focussed primarily on increasing the NLO tensor d_{eff} coefficients to produce structures that can frequency double low peak power sources, such as diode lasers [5.4,5.5]. Also, emphasis has been given to develop highly transparent crystals suitable for frequency conversion of high-power lasers such as those used for internal confinement fusion [5.6]. These applications have unique and often competing materials requirements and illustrate that no single nonlinear optical material will be suitable for all these wide-ranging uses.

The search for new frequency conversion materials over the past has been concentrated primarily on organic compounds [5.4-5.8] and many NLO materials with high nonlinear susceptibilities have been synthesized. However, the realization of organic materials in the single crystal form in practical device applications has been hindered by their inadequate transparency, poor optical quality, lack of robustness, low laser damage threshold and above all, inability to grow large-size single crystals. The molecules in pure organic crystals are often coupled by only relatively weak Van der Waal's forces or hydrogen bonds, which result in poor mechanical properties.

Recently, a new class of materials known as metal organics or semi organics have been developed which are metal complexes of highly polarisable organic molecules having favorable physical properties such as high laser induced damage resistance, good transparency, large nonlinearity in optical properties and ease of single crystal growth. These are combinations of the properties of both organic and inorganic crystal constituents. Recently, the NLO properties of some products of thiourea [5.9-5.12] have attracted great interest. The thiourea molecule is an interesting inorganic matrix modifier due to its large dipole moment [5.13] and has ability to form an extensive network of hydrogen bonds. Unfortunately most thiourea complexes known so far are centrosymmetric. Only a few crystallize into an acentric space group, which is the most essential requirement of a material to be nonlinear optical.

A class of crystals incorporating urea and urea analogs in inorganic salts have been grown already. Zinc tris(thiourea) sulphate (ZTS) with chemical formula $Zn[CS(NH_2)_2]_3SO_4$, a prototype NLO coordination complex, has previously been identified as a potentially useful material for frequency doubling of near-IR laser radiation [5.9].

Structurally, ZTS crystal belongs to the orthorhombic system with space group $Pca2_1$ (point group-mm2) and has four molecules per unit cell [5.14]. The lattice parameters are reported to be $a = 11.126 \text{ \AA}$, $b = 7.773 \text{ \AA}$ and $c = 15.491 \text{ \AA}$. It has a less prominent cleavage along the (100) plane. The Zinc ion is tetrahedrally coordinated to three sulfur atoms present in the thiourea molecules and to one oxygen atom attached to a sulphate group. The thiourea molecules are planar and there is extensive intermolecular and intra-molecular hydrogen bonding between thiourea, amino hydrogen and sulphate oxygen [5.14,5.15]. The molecular structure and packing of the molecules in the unit cell as viewed approximately along the [010] direction are shown in Fig. 5.1 (a) and 5. 1(b), respectively.

Spectroscopic studies on the metal complexes of thiourea such as bis(thiourea) cadmium chloride and zinc tris(thiourea) sulphate single crystals have been reported in literature [5.16,5.17]. It has also been reported that there exists two low temperature phase transitions in ZTS, detected by Raman spectroscopic studies [5.15]. Raman measurements show drastic changes around 60K and 122K indicating the presence of two second-order phase transitions of order-disorder type. Ramabhadran *et al.* [5.18] have studied the electrooptic, piezoelectric and dielectric properties of this crystal. Reasons for its high polar nature [5.19] and high dielectric permittivity at low frequencies [5.20] are also reported in literature. Various thermal properties [5.21] such as thermal diffusivity, heat capacity etc. and laser damage studies [5.21-5.23] reveal that this crystal can be used in fabricating NLO devices.

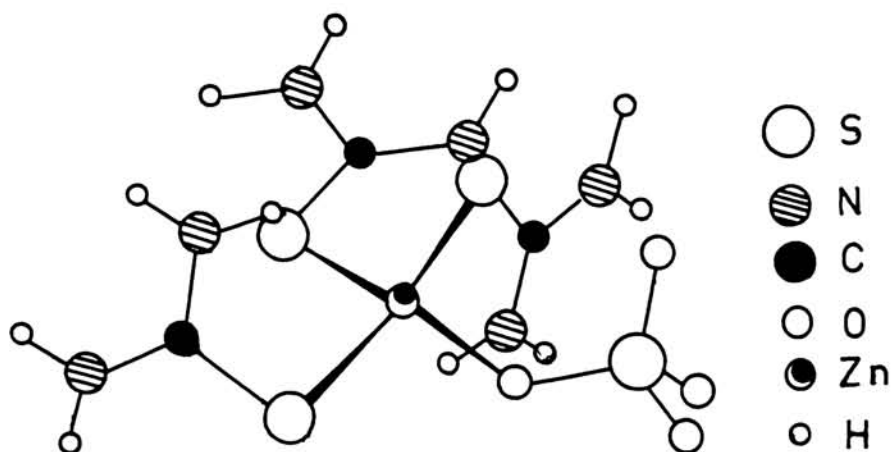


Fig. 5.1(a): Molecular structure of ZTS

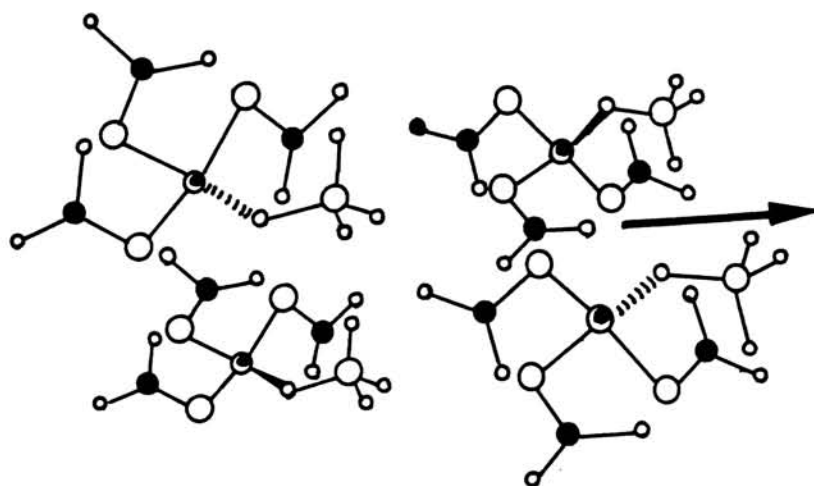


Fig. 5.1(b): Projection of ZTS crystal structure approximately along the $[010]$ direction showing the alignment of the molecular dipoles (Zn-O bonds).

(Arrows point along the c-axis and indicate the net dipole moment. The upper right and lower left molecules are below the plane of the upper left and lower right molecules. For clarity hydrogen atoms have been omitted in this projection)

A preliminary report of optical transmission and measurement of second and third order nonlinear optical (NLO) coefficients have been made by Newmann *et al.* [5.24]. Subsequently the values of d_{eff} , β_0 and the threshold for SHG have been reported [5.25]. The SHG efficiency, optical absorption, refractive index measurement, calculation of phase matching loci, non-critical wavelengths and their experimental verification have been done by Marcy *et al.* [5.9]. They have identified the principal dielectric axes (α , β , γ) and the ANSI / IEEE piezoelectric crystal coordinate system (x , y , z) and the crystallographic axes (a , b , c). These axes are shown in Fig. 5.2.

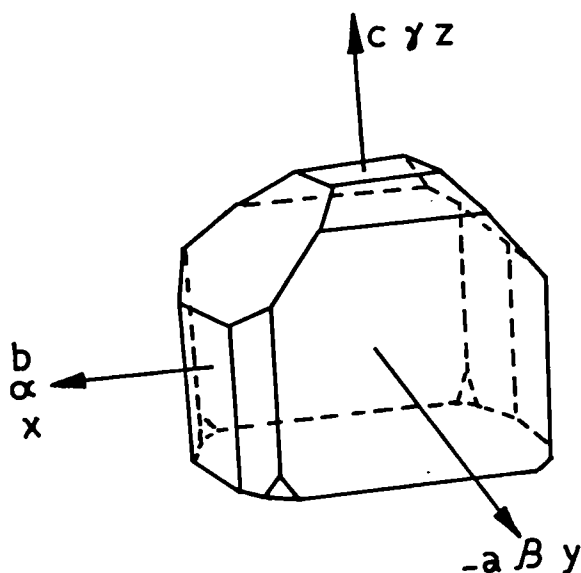


Fig. 5.2: Different systems of axes for ZTS crystals

It is also reported that the intensity of $0.532 \mu\text{m}$ second harmonic generated on a per particle basis by ZTS is about 1.2 times the intensity of that generated by potassium dihydrogen phosphate (KDP) having the same average diameter. This indicates that the nonlinear coefficients of ZTS are similar to those of KDP. Much better prospects for the practical application of ZTS are found after achieving non-critical Type-II phase

matching (along the a-axis) by temperature tuning. It is expected that maximum conversion efficiency could be achieved with crystals of length 3-5 cm.

Single crystal growth, defect characterization and other related studies of this crystal have been done by several researchers and reports are available in literature [5.10,5.26-5.31]. Studies of the slip system, surface anisotropy in micro hardness and its relation to inter atomic bonding are also investigated and reported [5.32,5.33].

It is reported that ZTS is thermodynamically stable up to 200°C following thermogravimetric analysis (TGA) and differential scanning calorimetry (DSC). Temperature dependence of dielectric constant over the frequency range 1-100kHz show no anomaly, which further confirms its stability. Measurement of the thermal expansion coefficient also does not indicate the presence of any structural phase transition before its decomposition at about 200°C.

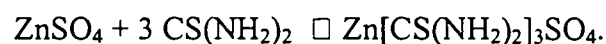
Single crystals of ZTS can be grown from aqueous solution either by the slow evaporation or by the slow cooling techniques where thiourea and $\text{ZnSO}_4 \cdot 7\text{H}_2\text{O}$ are dissolved in the molar ratio ranging from 1:1 to 6:1. Since thiourea has the coordinating capacity to form a variety of complexes, it would be safe to synthesize ZTS first and then grow single crystals from solution after purification by several recrystallizations. A more detailed study of the crystal growth and scaling of ZTS has been carried out by Cleveland Crystals Inc. in which crystals of size $13 \times 13 \times 62 \text{ mm}^3$ have been grown.

In this chapter we present the results of our measurement of the elastic properties of this crystal. All the nine second-order elastic constants of ZTS have been determined by measuring ultrasonic wave velocities along different symmetry directions. Other related parameters such as Poisson's ratios, volume compressibility etc. have also been determined. The phase velocity, group velocity and slowness

surfaces have been plotted in two dimensions to bring out the anisotropy in elastic wave propagation in this crystal. Variation of a few elastic constants with temperature, over a limited range are also presented. Details of the experimental technique, results obtained and a discussion of the results are outlined in the following sections.

5.2 Sample preparation

ZTS material for crystal growth has been synthesized from zinc sulphate and thiourea following the reaction



ZnSO_4 and thiourea taken in the molar ratio 1:3 are dissolved separately in triply distilled water, just sufficient to dissolve it. These solutions are mixed with vigorous stirring to avoid the formation of other complexes. The resultant precipitate of ZTS is washed and dried. This product obtained is purified by several re-crystallizations before attempting to grow single crystals. Fig. 5.3 indicates the solubility of ZTS in water at different temperatures, and one can see that the temperature coefficient of solubility is positive, but rather small. This implies that the best method to grow big-size single crystals is the slow evaporation technique, which is described already in Chapter 2. Single crystals of size nearly $20 \times 18 \times 0.8 \text{mm}^3$ have been grown over a period of about 5 weeks. The prominent growth planes have been identified and the morphology of the grown crystal is exhibited in Fig. 5.4. ZTS has a less prominent cleavage along the (100) plane. The inter-planar angles have been measured using an accurate contact goniometer and are compared with the values evaluated from crystallographic data to identify the crystal directions and growth planes.

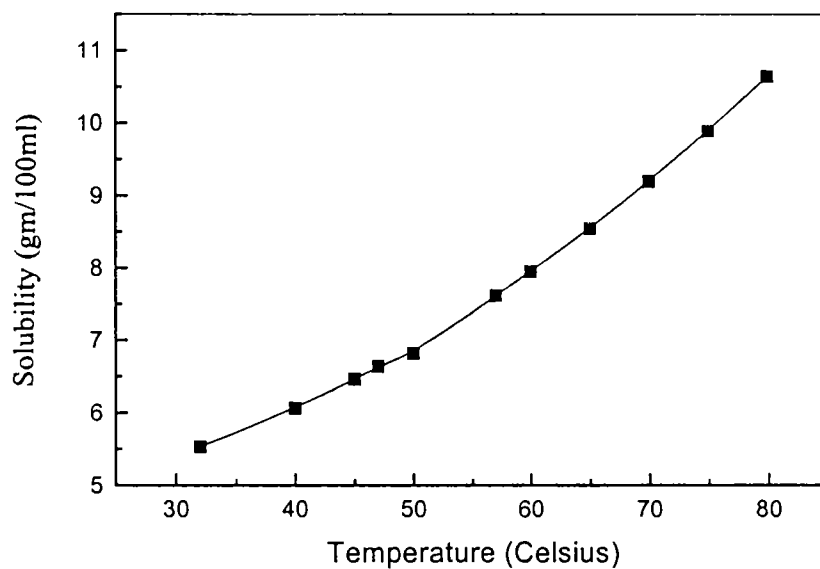


Fig. 5.3: Solubility curve of ZTS in water

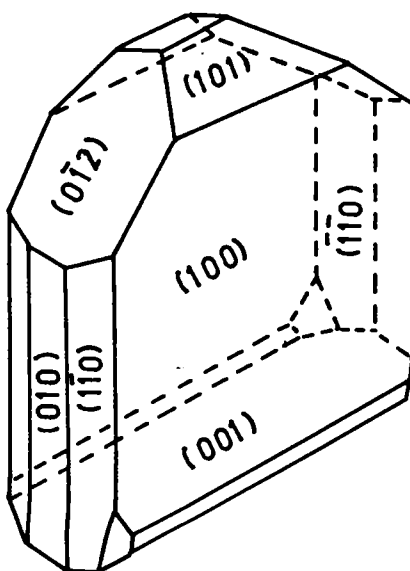


Fig. 5.4: Morphology of ZTS crystal grown from aqueous solution

The relative sizes of the growth planes can be expressed in the order $\{100\} > \{001\} > \{010\} > \{012\} > \{201\} > \{012\} > \{110\}$. After identifying the crystallographic directions, samples for measurements have been cut in the form of rectangular parallelepipeds with a pair of parallel planes perpendicular to the a [100], b [010], c [001], [110], [011] and [101] directions, as shown in Fig. 3.4 (in chapter 3) using a slow speed diamond wheel saw. The planes of interest have been lightly polished without spoiling the parallelism between the pair of planes.

5.3. Ultrasonic velocity measurements

Ultrasonic wave velocity measurements have been made along selected crystallographic directions for waves of longitudinal and transverse polarizations. The round-trip travel times through the sample cut along desired directions have been measured accurately using the pulse echo overlap (PEO) technique, already described in Chapter 2. To eliminate the errors introduced by the presence of the bonding medium between the transducer and sample and the incorrect identification of the condition of perfect match, McSkimin Δt correction has been applied. X and Y-cut quartz transducers of resonant frequency 10MHz are used to generate ultrasonic wave pulses and to detect the successive echoes after reflections from the rear end of the sample. Eighteen different mode velocity measurements can be measured along these specified directions. Out of this, twelve mode velocity measurements are sufficient to evaluate all the nine second-order elastic constants with cross checks possible on some of the critical values. Silicon grease is found to be a good bonding medium to fix the transducer onto the crystal surface and to admit ultrasonic wave pulses generated by it into the crystal medium. More technical details of these measurements are already described in Chapter 2.

5.4 Elastic constants of ZTS crystal

Velocities of propagation of ultrasonic waves through a medium are related to the second order elastic constants and the relations are given in Table 5.1.

Table 5.1 Velocity of ultrasonic modes in ZTS crystals. L, T and QL represent longitudinal, transverse and quasi-longitudinal modes respectively. The relations between mode velocities and elastic constants are also given.

Sl. No.	Mode	Direction of propagation	Direction of polarisation	Measured mode velocity (m/s)	Mode velocity - elastic constant relation
1	L	[100]	[100]	$v_1 = 3259 \pm 6$	$C_{11} = \rho v_1^2$
2	L	[010]	[010]	$v_2 = 4151 \pm 8$	$C_{22} = \rho v_2^2$
3	L	[001]	[001]	$v_3 = 3042 \pm 6$	$C_{33} = \rho v_3^2$
4	T	[010]	[001]	$v_4 = 2066 \pm 4$	$C_{44} = \rho v_4^2$
5	T	[001]	[010]	$v_5 = 2065 \pm 4$	$C_{44} = \rho v_5^2$
6	T	[100]	[001]	$v_6 = 2064 \pm 4$	$C_{55} = \rho v_6^2$
7	T	[001]	[100]	$v_7 = 2077 \pm 4$	$C_{55} = \rho v_7^2$
8	T	[100]	[010]	$v_8 = 2153 \pm 4$	$C_{66} = \rho v_8^2$
9	T	[010]	[100]	$v_9 = 2135 \pm 4$	$C_{66} = \rho v_9^2$
10	QL	[110]	[QL]	$v_{10} = 3863 \pm 8$	$C_{12} = f_{ab}^{(a)}$
11	QL	[011]	[QL]	$v_{11} = 3985 \pm 8$	$C_{23} = f_{bc}^{(b)}$
12	QL	[101]	[QL]	$v_{12} = 3241 \pm 6$	$C_{13} = f_{ac}^{(c)}$

$$(a) f_{ab} = \{[c^2 C_{11} + s^2 C_{66} - \rho v_{10}^2] \{c^2 C_{66} + s^2 C_{22} - \rho v_{10}^2\} / c^2 s^2\}^{1/2} - C_{66}$$

$$(b) f_{bc} = \{[c^2 C_{22} + s^2 C_{44} - \rho v_{11}^2] \{c^2 C_{44} + s^2 C_{33} - \rho v_{11}^2\} / c^2 s^2\}^{1/2} - C_{44}$$

$$(c) f_{ac} = \{[s^2 C_{11} + c^2 C_{55} - \rho v_{12}^2] \{s^2 C_{55} + c^2 C_{33} - \rho v_{12}^2\} / c^2 s^2\}^{1/2} - C_{55}$$

(Here c and s are the cosine and sine of the angle of rotation from the respective axes.)

[100], [010], and [001] directions are pure mode directions and hence each of the velocities measured along these directions are related to only one elastic constant. [110], [010], and [011] directions are mixed mode directions and hence the velocity of propagation of ultrasonic waves along these directions are related to several elastic constants. Ultrasonic wave velocities measured along different crystallographic directions are listed in Table 5.1 with polarization of the mode of propagation. The corresponding elastic stiffness constants, compliance constants and Poisson's ratios are tabulated in Table 5.2.

Table 5.2 Elastic stiffness constants, compliance constants and Poisson's ratios of ZTS crystal at room temperature (300K)

Elastic stiffness constants (GPa)	Elastic compliance constants ($\times 10^{-10} \text{ m}^2 \cdot \text{N}^{-1}$)	Poisson's ratios
$C_{11} = 19.65 \pm 0.039$	$S_{11} = 0.563 \pm 0.001$	
$C_{22} = 31.88 \pm 0.064$	$S_{22} = 0.388 \pm 0.001$	$\nu_{12} = 0.272$
$C_{33} = 17.12 \pm 0.034$	$S_{33} = 0.696 \pm 0.001$	$\nu_{21} = 0.188$
$C_{44} = 7.89 \pm 0.016$	$S_{44} = 1.266 \pm 0.003$	
$C_{55} = 7.88 \pm 0.016$	$S_{55} = 1.269 \pm 0.003$	$\nu_{23} = 0.257$
$C_{66} = 8.58 \pm 0.017$	$S_{66} = 1.166 \pm 0.002$	$\nu_{32} = 0.462$
$C_{12} = 7.19 \pm 0.070$	$S_{12} = -0.106 \pm 0.001$	
$C_{23} = 8.99 \pm 0.090$	$S_{23} = -0.179 \pm 0.002$	$\nu_{13} = 0.109$
$C_{13} = 3.99 \pm 0.040$	$S_{13} = -0.076 \pm 0.001$	$\nu_{31} = 0.135$

The density of the crystal is measured to be 1850 Kg-m^{-3} . The accuracy of the reported elastic constant values is estimated to be better than 0.2% in the diagonal elastic constants and 1% in the case of off-diagonal elastic constants.

5.5 Temperature dependence of elastic constants

In order to study the dependence of ultrasonic wave velocities on temperature, the crystal-transducer assembly is kept in an oven whose temperature is controlled accurately. As the temperature changes, the condition of perfect matching of the overlapped echoes changes. The tunable continuous wave oscillator is properly adjusted to establish the previous condition of perfect matching and the frequency output displayed on the frequency counter is noted. Temperature dependence of the elastic constants C_{11} , C_{22} and C_{33} are shown in Fig. 5.5(a) and that of C_{44} , C_{55} and C_{66} are shown in Fig. 5.5(b).

5.6 Anisotropy in elastic wave propagation in ZTS

In order to study the anisotropy of elastic properties of ZTS, various surface plots such as the phase velocity, slowness, group velocity, Young's modulus and linear compressibility have been drawn. The values of these parameters along the symmetry planes a-b, b-c and a-c have been plotted to demonstrate the anisotropy in elastic properties of this crystal. Sections of the phase velocity surfaces along the a-b, b-c and a-c planes are plotted in Fig. 5.6(a), (b) and (c) respectively. The pure shear (PS), quasi-shear (QS) and quasi-longitudinal (QL) modes are shown separately in each diagram. These contours are almost circular in shape, which indicates that this crystal does not show large-scale anisotropy in its ultrasonic (elastic) wave propagation characteristics.

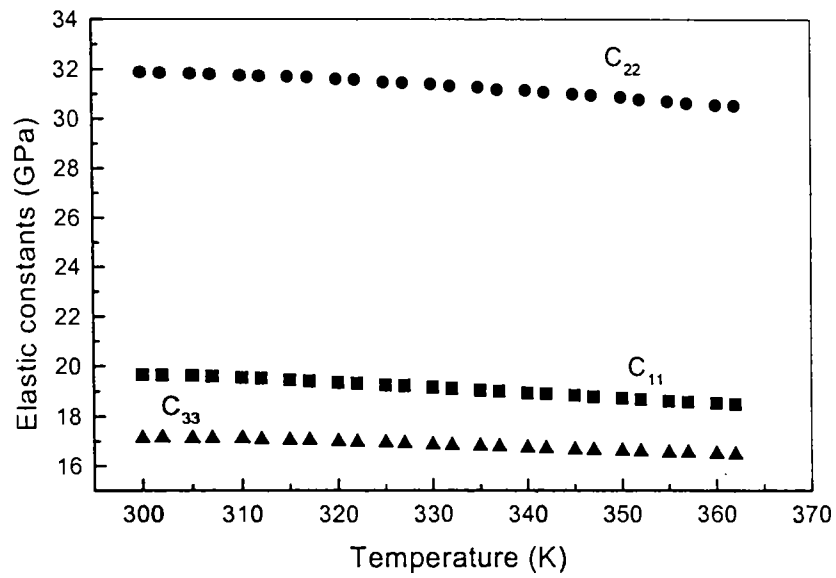


Fig.5.5(a) : Dependence of elastic constants C_{11} , C_{22} and C_{33} on temperature.

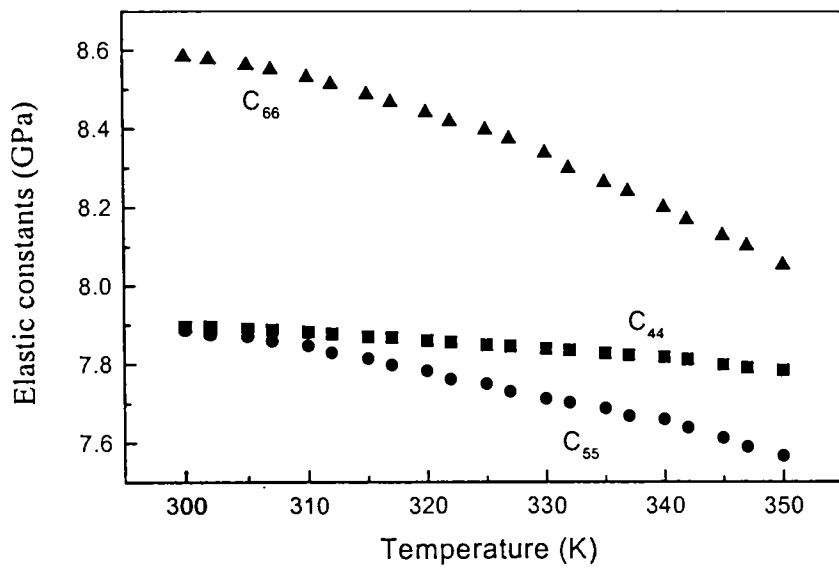


Fig.5.5(b) : Dependence of elastic constants C_{44} , C_{55} and C_{66} on temperature.

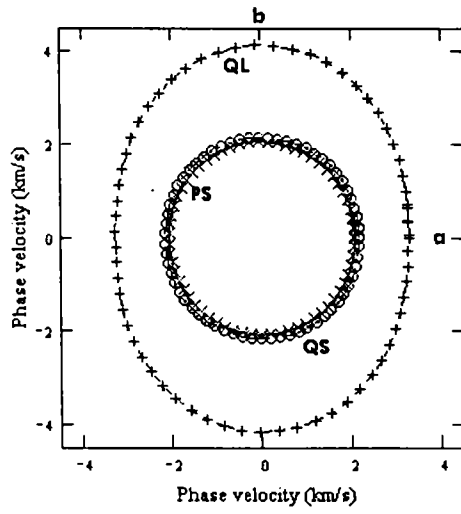


Fig. 5.6(a): Section of the phase velocity surfaces of ZTS along the a-b plane.

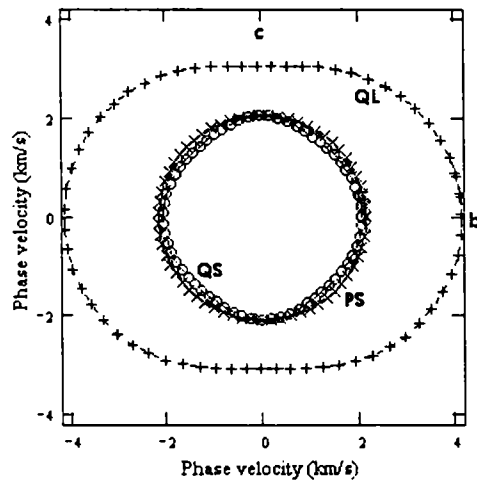


Fig. 5.6(b): Section of the phase velocity surfaces of ZTS along the b-c plane.

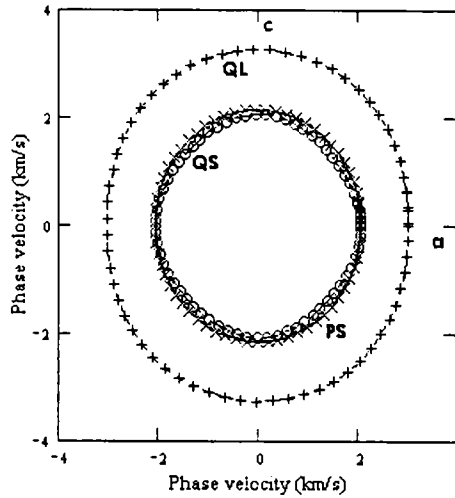


Fig. 5.6(c): Section of the phase velocity surfaces of ZTS along the a-c plane

Fig. 5.7(a), (b) and (c) show sections of the slowness surfaces along the a-b, b-c and a-c planes respectively, which are similar in nature. Ray velocity or group velocity is the velocity of propagation of the energy, which need not be collinear with the corresponding phase velocity. Sections of the ray velocity (group velocity) surface along the a-b, b-c and a-c planes are shown in Fig. 5.8(a), (b) and (c) respectively.

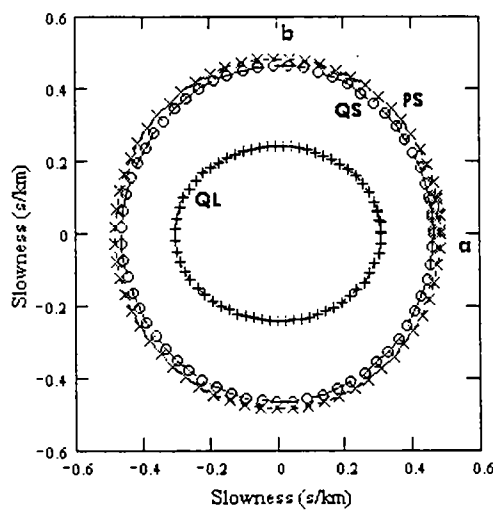


Fig. 5.7(a): Section of the slowness surfaces of ZTS along the a-b plane

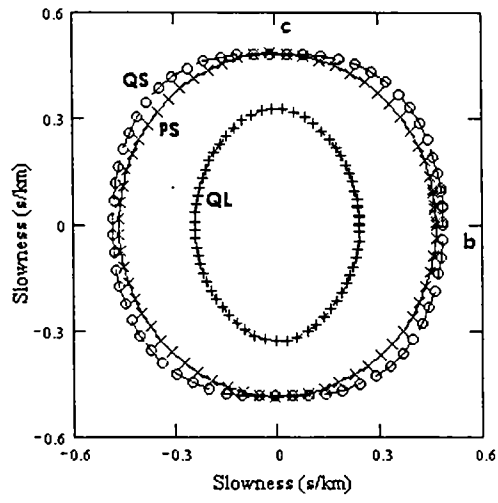


Fig. 5.7(b): Section of the slowness surfaces of ZTS along the b-c plane.

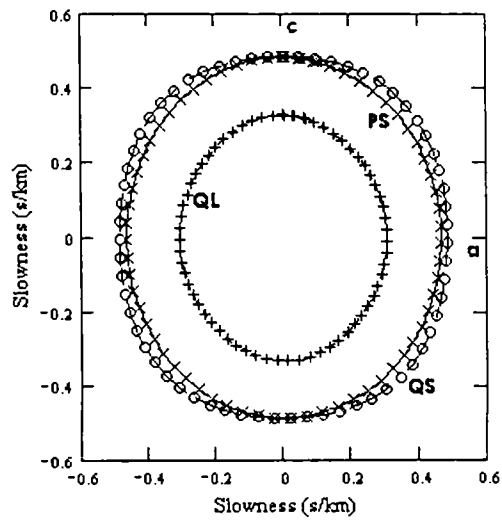


Fig. 5.7(c): Section of the slowness surfaces of ZTS along the a-c plane.

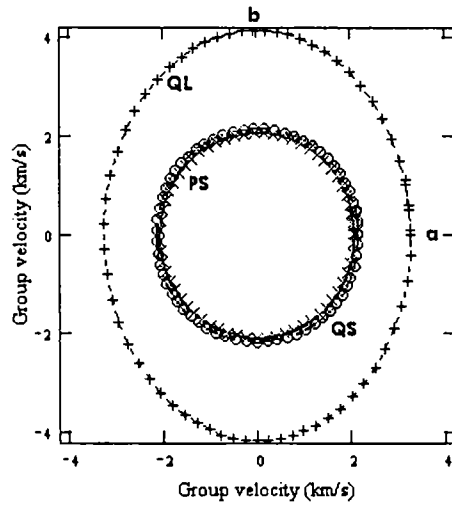


Fig. 5.8(a): Section of the group velocity surfaces of ZTS along the a-b plane.

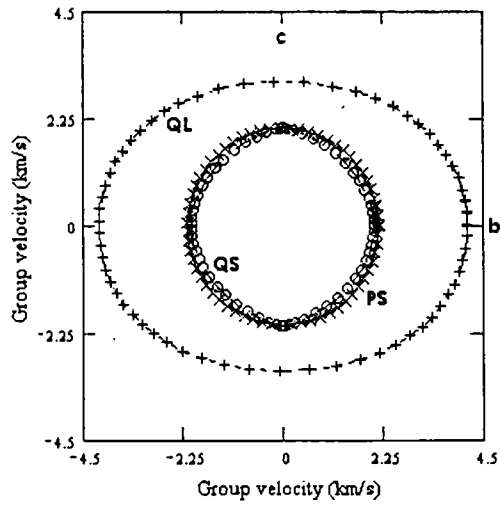


Fig. 5.8(b): Section of the group velocity surfaces of ZTS along the b-c plane.

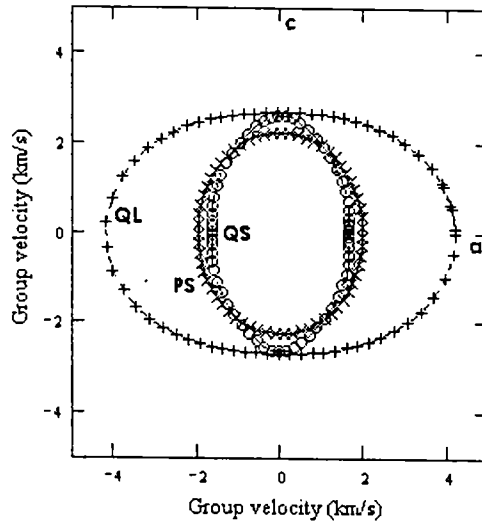


Fig. 5.8(c): Section of the group velocity surfaces of ZTS along the a-c plane

These figures indicate that ZTS single crystals show somewhat isotropic behavior as far as ultrasonic wave propagation is concerned.

Eq. 1.66 (in chapter 1) indicates that Young's modulus is a direction dependent parameter and hence the shape of the surface generated by plotting Young's modulus values for various directions will be very useful to demonstrate the anisotropy in elastic properties. Sections of the Young's modulus surface, along the a-b, b-c and a-c planes are shown in Fig. 5.9. The oval shape of these curves indicates the anisotropy in Young's modulus.

The presence of the direction cosines l , m and n in Eq.1.74 also indicate that the linear compressibility is also a direction dependent parameter. Sections of linear compressibility surface along the a-b, b-c and a-c symmetry planes are shown in Fig. 5.10. These are not circular in shape and hence the compressibility of this crystal along different directions in the crystal show clear anisotropy, when unit hydrostatic pressure is applied.

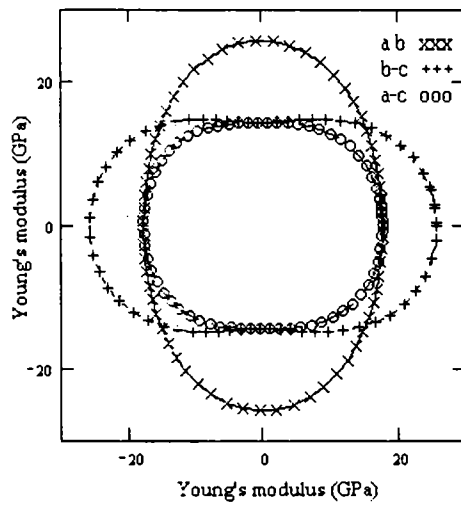


Fig. 5.9: Sections of the Young's modulus surface of ZTS along the a-b (xxx), b-c (+++) and a-c (ooo) planes.

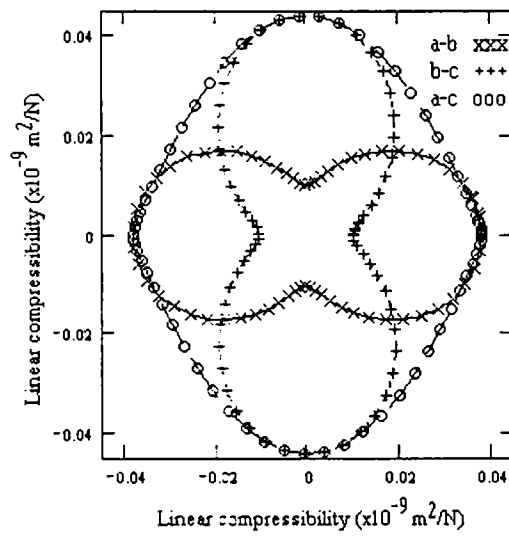


Fig. 5.10: Sections of the linear compressibility surface of ZTS along the a-b (xxx), b-c (+++) and a-c (ooo) planes.

5.7 Discussion and conclusion

All the nine second order elastic stiffness constants of Zinc tris(thiourea) sulphate single crystals are reported for the first time. Velocities of propagation of ultrasonic waves of both longitudinal and transverse nature along selected directions have been measured with the maximum possible accuracy and necessary computations have been done to evaluate all the nine second-order elastic stiffness and compliance constants of this crystal. These constants along with Poisson's ratios are tabulated in Table 5.2. The volume compressibility of this crystal has been evaluated using Eq. (1.71) as $0.926 \times 10^{-10} \text{m}^2 \text{N}^{-1}$ and the corresponding bulk modulus is 10.8GPa.

Elastic constants C_{11} , C_{22} and C_{33} are found to depend heavily on temperature. Longitudinal tensions along a, b and c directions cause the lattice to stretch along the respective directions. This enhances thermal expansion of the lattice. As temperature increases, the longitudinal strain corresponding to a fixed longitudinal stress increases, resulting in a decrease in the elastic constant values. C_{44} , C_{55} and C_{66} depend much less on temperature. Shearing caused by tangential forces and hence the corresponding shear elastic constants are practically not much affected by increase in temperature. C_{55} and C_{66} show a small decrease in their values with rise of temperature, whereas C_{44} remains practically unaffected.

Single crystals of ZTS grown from the aqueous solution are optically clear and transparent. Our results indicate that ZTS does not show any large-scale anisotropy in its elastic properties. Crystals are hard with no pronounced cleavage and hence are suitable for device fabrication, if other properties meet the desired requirements.

References

- 5.1 R. F. Belt, G. Gasshurov and Y. S. Liu, *Laser focus* **10** (1985) 110
- 5.2 R. S. Clark, *Photonic spectra* **22** (1988) 135
- 5.3 R. J. Gambino, *Bull. Mater. Res. Soc.* **15** (1990) 20
- 5.4 G. Khanarian, (ed.) in *Nonlinear optical properties of organic materials III*, Proc. Soc. Photo-opt. Instrum. Eng. (1990) 1337
- 5.5 S. Marder, G. Stucky and J. Sohn, (ed.), *New materials for nonlinear optics*, Vol.455 of ACS Symposium series (Am. Chem. Soc. Washington 1991)
- 5.6 S. P. Velsko, L.E. Davis, F. Wang, S. Monaco and D. Eimerl, in *Advances in nonlinear polymers and inorganic crystals, liquids and laser media*, Proc. Soc. Photo-opt. Instrum. Eng. **824** (1988) 178
- 5.7 D. S. Chemla and J. Zyss, (ed.), in *Nonlinear optical properties of organic materials and crystals* (Academic Press, New York 1987) Vol. 1 and 2
- 5.8 M. H. Lyens (ed.), in *Materials for nonlinear and electrooptics*, Vol. 103 of AIP Conference (American Institute of Physics, New York 1989)
- 5.9 H. O. Marcy, L. F. Warren, M. S. Webb, C. A. Ebberts, S. P. Velsko, G. C. Kennedy and S. C. Catella, *Applied Optics* **31** (1992) 5051
- 5.10 V. Venkataramanan, G. Dhanaraj, V. K. Wadhawan, J. N. Sherwood and H. L. Bhat, *J. Cryst. Growth* **154** (1995) 92
- 5.11 V. Venkataramanan, S. Maheswaran, J. N. Sherwood and H. L. Bhat, *J. Cryst. Growth* **179** (1997) 605
- 5.12 Xu Dong, Yuan Duo-rong, Zhang Nan, Hou Wen-bo, Liu Ming-guo, Sun Suo-ying and Jiang Min-hua, *J. Phys. D: Appl. Phys.* **26** (1993) B230
- 5.13 S. G. Bhat and S. M. Dharmaprakash, *Mater. Res. Bull.* **33** (1998) 833
- 5.14 G. D. Andreeti, L. Cavalca and A. Musatti, *Acta Cryst.* **B 24** (1968) 683

- 5.15 M. Oussaid, P. Becker, M. Kemiche and C. Carabatos-Nedelec, *Phys. Stat. Sol.* (b) **207** (1998) 103
- 5.16 S. Selvasekara Pandian, K. Vivekanandan, P. Kolandaivel and T. K. Gundu Rao, *Cryst. Res. Technol.* **32** (1997) 299
- 5.17 V. Venkataramanan, M. R. Sreenivasan, H. L. Bhat, *J. Raman Spectrosc.* **25** (1994) 805
- 5.18 U. B. Ramabhadran, D. E. Zelmon, G. C. Kennedy, *Appl. Phys. Lett.* **60** (1992) 2589
- 5.19 A. Yamaguchi, R. B. Penland, S. Mizuchima, T. J. Lane, C. Curran and J. V. Quagliano, *J. Am. Chem. Soc.* **80** (1958) 527
- 5.20 K. V. Rao, A. Smakula, *J. Appl. Phys.* **36** (1965) 2701
- 5.21 P. Kerkoc, V. Venkataramanan, S. Lochran, R. T. Bailey, F. R. Cruickshank, D. Pugh, J. N. Sherwood, R. Moseley, A. E. Goeta and C. W. Lechmann, *J. Appl. Phys.* **80** (1996) 6666
- 5.22 V. Venkataramanan, C. K. Subramanian and H. L. Bhat, *J. Appl. Phys.* **77** (1995) 6049
- 5.23 V. Venkataramanan, Ph.D Thesis, Indian Institute of Science, Bangalore India (1994)
- 5.24 P. R. Newman, L. F. Warren, P. Cunningham, T. Y. Chang, D. E. Cooper, G. L. Burdge, P. Polak-Dingels and C. K. Lowe-Ma, *Mater. Res. Soc. Symp. Proc.* **173** (1990) 557
- 5.25 H. O. Marcy, L. F. Warren, M. S. Webb, L. E. Davis and S. P Velsko, *CThR21, CLEO '91 Digest (IEEE)*
- 5.26 C. F. Desai and Sonal Gupta, *Surface Review and Letters* **6** (1999) 23

- 5.27 Sunil Varma, M. K. Singh, V. K. Wadhawan and C. H. Suresh, *Pramana: J. Phys.* **54** (2000) 879
- 5.28 P. M. Ushasree, R. Jayavel, C. Subramanyam and P. Ramasamy, *J. Cryst. Growth* **197** (1999) 216
- 5.29 G. Arunmozhi, R. Mohankumar, R. Jayavel, C. Subramanian, *Mater. Sci. Eng.* **B49** (1997) 216
- 5.30 P. M. Ushasree, R. Jayavel and P. Ramasamy, *Materials Chemistry and Physics* **61** (1999) 270
- 5.31 P. M. Ushasree, R. Jayavel, C. Subramanyam and P. Ramasamy, *Bulletin of Electrochemistry* **14**, (1998) 407
- 5.32 S. S. Gupta and C. F. Desai, *Cryst. Res. Technol.* **34** (1999) 1329
- 5.33 G. Ravi, S. Anbukumar and P. Ramasamy, *Mater. Chem. Phys.* **37** (1994) 180

Chapter 6

Elastic properties of Benzoyl glycine (BG) single crystals

6.1 Introduction

The nonlinear optical (NLO) properties of large organic molecules and polymers have been the subject of extensive theoretical and experimental investigations during the past two decades [6.1-6.3]. Organic NLO materials play an important role in second harmonic generation (SHG), frequency mixing, electro-optic modulation, optical parametric oscillation, optical bistability etc. [6.4]. Recently, a number of organic compounds with non-localized π -electron systems having large dipole moments have been synthesized to realize nonlinear susceptibilities far larger than well known inorganic nonlinear optical materials [6.5,6.6]. The basic features of nonlinear molecules are: (i) presence of highly conjugated and polarizable electronic systems, either linear, cyclic or a combination of both and (ii) occurrence of inter-molecular charge transfer, which could be modulated by a suitable choice of acceptor and donor substituents.

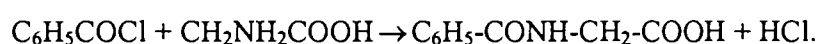
Moreover, one can in a similar way, adjust the transparency of the system (usually between 0.3 and 2 μm). The crystal must also be noncentro-symmetric to ensure molecular nonlinear response. From the fabrication and exploitation point of view, the other important aspects to be considered are (i) easy and inexpensive synthesis, (ii) desirable physio-chemical properties such as good radiation - thermal and chemical - resistance, (iii) ease of crystal growth etc. Moreover, the as grown crystal should exhibit satisfactory mechanical properties such as good strength and hardness for cutting and polishing of the crystal, which are essential for device fabrication.

A more detailed discussion of some of the important issues connected with crystal growth and characterization of some of the most important organic nonlinear optical crystals are available in literature [6.7]. A long list of organic molecular crystals exhibiting NLO property is available in literature [6.2,6.3,6.8]. Extensively studied molecular crystals belonging to this category are hexamethylenetetramine (HMT) [6.9], hippuric acid or benzoyl glycine [6.10] and benzil [6.11], for all of which a variety of optical properties are already known. However, applications of these crystals in device fabrication are rather limited due to poor chemical stability and red shift of the cut-off wavelength caused by the large organic n -conjugated group. Moreover, the large birefringence resulting from the stacking of the structure radical and several other factors lead to poor phase matching of optical waves in these materials.

Benzoyl glycine (BG) or hippuric acid with the chemical formula $\text{C}_6\text{H}_5\text{CO-NH-CH}_2\text{-COOH}$ is reported to be an excellent piezoelectric crystal [6.12] and NLO material [6.10,6.13]. The efficiency of second harmonic generation (SHG) is about 37% for this in single crystal form and it is much higher than that of potassium

dihydrogen phosphate (22%). A second harmonic output of wavelength $\lambda = 532$ nm of output power 7.7mW is reported to be obtained for an input power of 21mW using Q-switched, mode locked Nd: YAG laser ($\lambda = 1064$ nm) using BG single crystals. The SHG efficiency has been measured using the Kurtz's powder technique [6.14]. Also, the range of optical transparency of this crystal is reported to be much larger than that of other well-characterized organic NLO crystals such as 3-methyl-4-nitropyridine-1-oxide (POM), N-(4-nitrophenyl)-L-prolinol (NPP), vanillin etc. This indicates its stability for the generation and mixing of frequencies over a wide wavelength range of the electromagnetic spectrum. Thus this crystal can be efficiently used for the up conversion of IR radiation into visible green light. Scanning force microscopy of ion-irradiated benzoyl glycine single crystals has been done recently by Nagaraja *et al.* [6.13]. They have done surface characterization of BG crystals irradiated with Bi ions.

N-Benzoyl glycine has a formula weight 179.18 and melting point 187°C . It crystallizes into the orthorhombic structure with space group $P2_12_12_1$. The lattice parameters are reported to be $a = 9.112\text{\AA}$, $b = 10.566\text{\AA}$ and $c = 8.855\text{\AA}$ and has four molecules per unit cell [6.13]. It can be synthesized from GR grade benzoyl chloride and glycine according to the chemical reaction.



The product can be purified by recrystallisations from boiling water. Now, benzoyl glycine (GR grade) is readily available and hence the synthesis and purification processes can be avoided.

In this work we have measured the elastic properties of benzoyl glycine single crystals. All the nine second order elastic constants have been determined by measuring the velocities of ultrasonic waves of longitudinal and transverse

polarisations propagating along various symmetry directions. Temperature variation of selected elastic constants have been measured. Anisotropy in the propagation of elastic waves in this crystal has been brought out by plotting the phase velocity, slowness, group velocity, Young's modulus and linear compressibility surfaces. Details of the work are described in the following sections.

6.2 Sample preparation

The determination of all the nine second-order elastic stiffness constant require ultrasonic wave velocity data along preferred symmetry directions in the crystal. Single crystals of benzoyl glycine have been grown by the slow evaporation technique. N,N-dimethylformamide, $\text{HCON}(\text{CH}_3)_2$, is found to be a very good solvent for benzoyl glycine. Either the slow evaporation technique or slow cooling technique can be adopted to grow large single crystals from supersaturated solution. The variation of solubility (gm. /100ml) of benzoyl glycine with temperature is shown in Fig. 6.1. It can be seen that the solubility increases steadily with rise of temperature and hence, because of the large positive temperature coefficient of solubility, one can grow big-size crystals adopting the slow cooling technique. The elastic properties of this crystal have not been reported so far, where as optical and other characterization studies have been reported already.

The prominent growth planes have been identified by measuring the interplanar angles with an accurate contact goniometer and comparing it with the values evaluated from crystallographic data. The (100) and (010) planes are totally absent indicating that the growth rates along these directions are much larger. The morphology of the grown crystal is shown in Fig. 6.2.

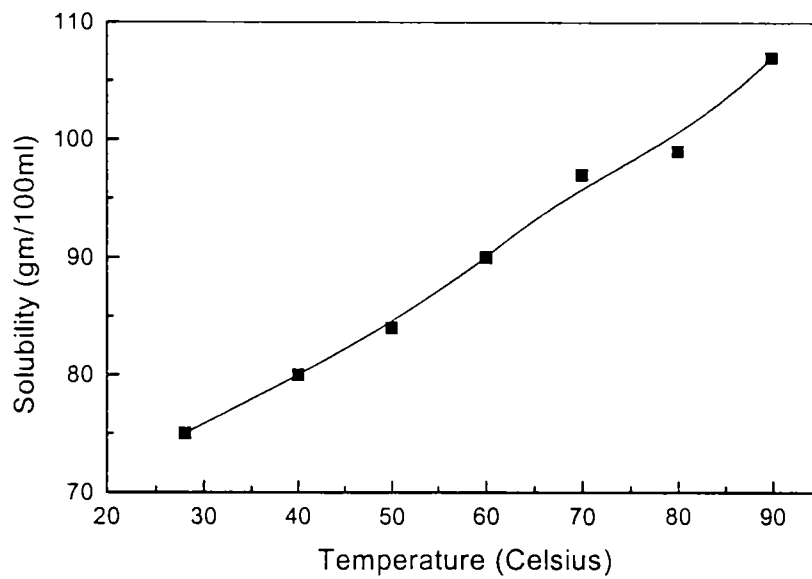


Fig. 6.1: Solubility curve of BG in N,N-dimethylformamide (DMF)

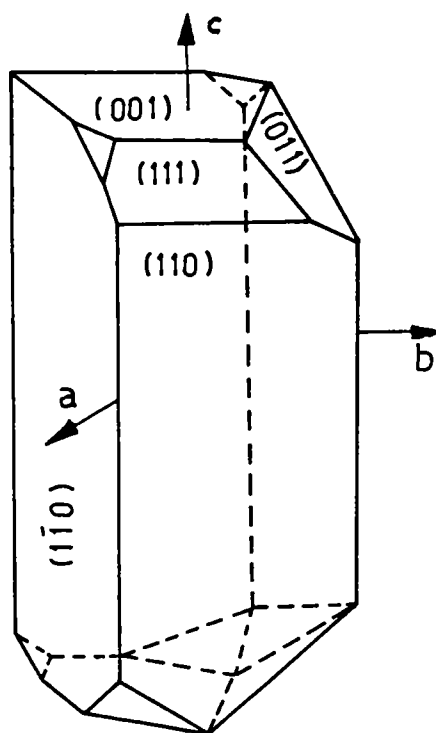


Fig. 6.2: Morphology exhibited by BG crystals grown from solution

The molecular structure and packing of molecules as viewed down along the c-axis are shown in Fig. 6.3(a) and Fig. 6.3(b) respectively.

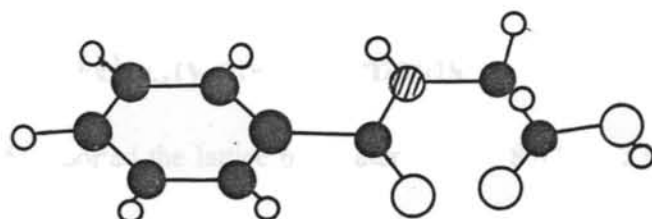


Fig. 6.3(a): The molecular structure of BG

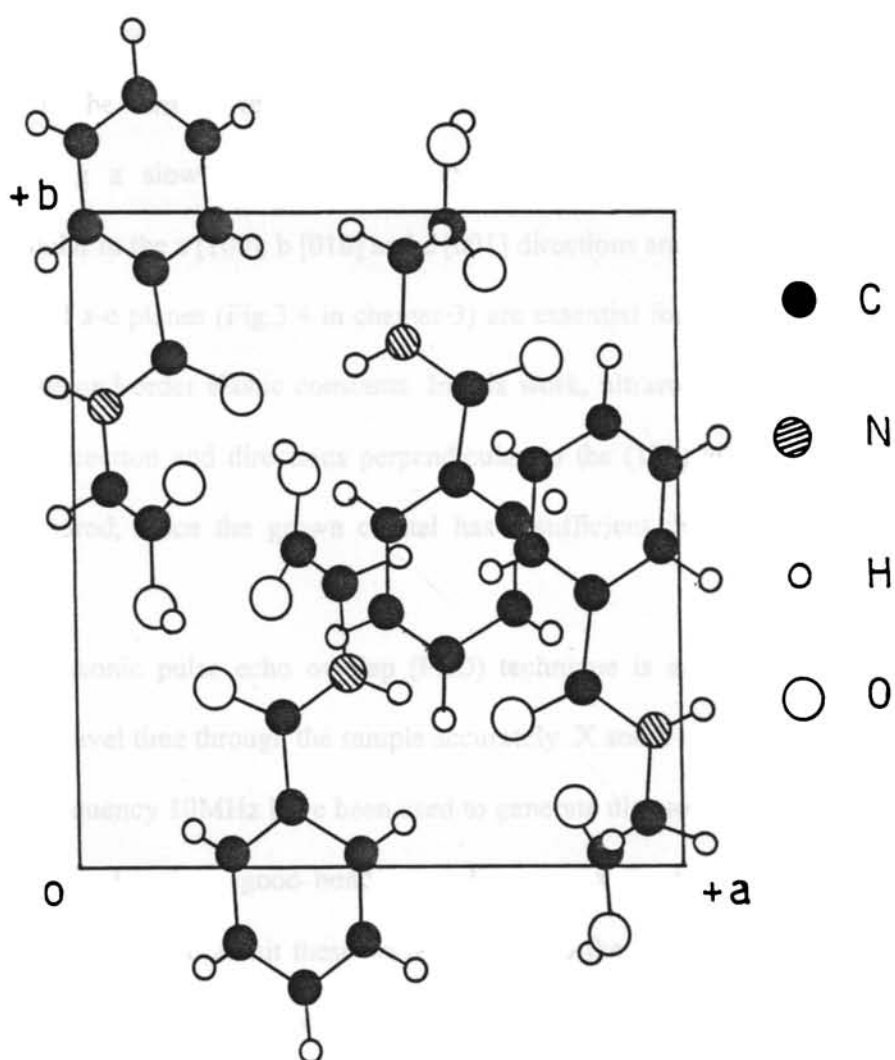


Fig. 6.3(b): Packing of benzoyl glycine molecules in the unit cell as viewed down along the c-axis

The thermo-gravimetric analysis of the grown crystal indicates that the crystal is stable up to its melting point (187 °C) and has no water of crystallization.

6.3 Ultrasonic velocity measurements

Ringhertz [6.15] reported the lattice parameters as $a = 8.874\text{Å}$, $b = 10.577\text{ Å}$ and $c = 9.177\text{Å}$ which is not according to the IRE standards [6.16]. The more exact crystallographic data was reported later by Nagaraja *et al.* [6.13] and according to them $a = 9.112\text{ Å}$, $b = 10.566\text{ Å}$ and $c = 8.855\text{ Å}$ which conforms to the IRE standards. Samples in the form of rectangular parallelepipeds have been cut from the grown crystal using a slow speed diamond wheel saw. Samples with parallel planes perpendicular to the a [100], b [010] and c [001] directions and any one direction in the a - b , b - c and a - c planes (Fig.3.4 in chapter 3) are essential for the determination of all the nine second-order elastic constants. In this work, ultrasonic wave velocity along the [110] direction and directions perpendicular to the (101) and (011) planes have been measured, since the grown crystal has insufficient thickness in the required direction.

Ultrasonic pulse echo overlap (PEO) technique is adopted to determine the round-trip travel time through the sample accurately. X and Y-cut quartz transducers of resonant frequency 10MHz have been used to generate ultrasonic wave pulses. Silicon grease is found to be a good bonding medium to fix the transducer on the crystal sample surface and to admit these wave pulses into the sample. The presence of the bonding medium can introduce some additional phase change and because of the progressive decrease in the amplitude of the successive echoes, the judgement of the condition of perfect overlap by visual evaluation also can introduce some error in the measured travel time. The analytical technique developed by McSkimin to eliminate

these errors was applied for better accuracy. More details of the measurement technique and McSkimin Δt correction are already described in Chapter 2.

6.4 Elastic constants of benzoyl glycine single crystals

The relationship of elastic constants to the measured mode velocities are listed in Table 6.1. Velocities of propagation of transverse and longitudinal ultrasonic waves along different symmetry directions are also listed in the same table.

Table 6.1 Velocity of ultrasonic modes in BG crystals. L, T and QL represent longitudinal, transverse and quasi-longitudinal modes respectively. The relations between mode velocities and elastic constants are also given.

Sl. No.	Mode	Direction of propagation	Direction of polarization	Measured mode velocity (m/s)	Mode velocity - elastic constant relationship
1	L	[100]	[100]	$v_1 = 2696 \pm 5$	$C_{11} = \rho v_1^2$
2	L	[010]	[010]	$v_2 = 4235 \pm 8$	$C_{22} = \rho v_2^2$
3	L	[001]	[001]	$v_3 = 3189 \pm 6$	$C_{33} = \rho v_3^2$
4	T	[010]	[001]	$v_4 = 1041 \pm 2$	$C_{44} = \rho v_4^2$
5	T	[001]	[010]	$v_5 = 1033 \pm 2$	$C_{44} = \rho v_5^2$
6	T	[100]	[001]	$v_6 = 1794 \pm 4$	$C_{55} = \rho v_6^2$
7	T	[001]	[100]	$v_7 = 1784 \pm 4$	$C_{55} = \rho v_7^2$
8	T	[100]	[010]	$v_8 = 2291 \pm 5$	$C_{66} = \rho v_8^2$
9	T	[010]	[100]	$v_9 = 2274 \pm 5$	$C_{66} = \rho v_9^2$
10	QL	[110]	[QL]	$v_{10} = 3852 \pm 8$	$C_{12} = f_{ab}^{(a)}$
11	QL	$\perp (011)$	[QL]	$v_{11} = 2988 \pm 6$	$C_{23} = f_{bc}^{(b)}$
12	QL	$\perp (101)$	[QL]	$v_{12} = 3146 \pm 6$	$C_{13} = f_{ac}^{(c)}$

$$(a) f_{ab} = \{[c^2 C_{11} + s^2 C_{66} - \rho v_{10}^2] \{c^2 C_{66} + s^2 C_{22} - \rho v_{10}^2\} / c^2 s^2\}^{1/2} - C_{66}$$

$$(b) f_{bc} = \{[c^2 C_{22} + s^2 C_{44} - \rho v_{11}^2] \{c^2 C_{44} + s^2 C_{33} - \rho v_{11}^2\} / c^2 s^2\}^{1/2} - C_{44}$$

$$(c) f_{ac} = \{[s^2 C_{11} + c^2 C_{55} - \rho v_{12}^2] \{s^2 C_{55} + c^2 C_{33} - \rho v_{12}^2\} / c^2 s^2\}^{1/2} - C_{55}$$

(Here c and s are the cosine and sine of the angle of rotation from the respective axes.)

The calculated values of second-order elastic stiffness constants, compliance constants and Poisson's ratios of BG are listed in Table 6.2. Data listed in this table is sufficient to evaluate the volume compressibility and bulk modulus of this crystal [6.17]. They are evaluated and found to have values equal to $1.371 \times 10^{-10} \text{m}^2 \cdot \text{N}^{-1}$ and 7.29 GPa respectively.

Table 6.2 Elastic stiffness constants, compliance constants and Poisson's ratios of BG single crystal at room temperature (300K)

Elastic stiffness constants (GPa)	Elastic compliance constants ($\times 10^{-10} \text{m}^2 \cdot \text{N}^{-1}$)	Poisson's ratios
$C_{11} = 9.33 \pm 0.019$	$S_{11} = 1.414 \pm 0.003$	
$C_{22} = 23.03 \pm 0.046$	$S_{22} = 0.498 \pm 0.001$	$\nu_{12} = 0.443$
$C_{33} = 13.06 \pm 0.026$	$S_{33} = 0.955 \pm 0.002$	$\nu_{21} = 0.156$
$C_{44} = 1.39 \pm 0.003$	$S_{44} = 7.189 \pm 0.004$	
$C_{55} = 4.13 \pm 0.008$	$S_{55} = 2.421 \pm 0.005$	$\nu_{23} = 0.090$
$C_{66} = 6.74 \pm 0.014$	$S_{66} = 1.484 \pm 0.003$	$\nu_{32} = 0.172$
$C_{12} = 4.95 \pm 0.050$	$S_{12} = -0.220 \pm 0.002$	
$C_{23} = 4.36 \pm 0.044$	$S_{23} = -0.086 \pm 0.001$	$\nu_{13} = 0.463$
$C_{13} = 4.76 \pm 0.047$	$S_{13} = -0.442 \pm 0.004$	$\nu_{31} = 0.312$

Also for demonstrating the anisotropy in elastic properties of this crystal, one can generate phase velocity, slowness and group velocity surfaces from this data. Young's

modulus and linear compressibility are two other parameters of interest, which are also direction dependent. The above data is sufficient to generate the Young's modulus and linear compressibility surfaces.

6.5 Temperature variation of elastic constants

The dependence of ultrasonic mode velocities on temperature have been measured by keeping the crystal-transducer assembly in a temperature-controlled oven. Slight variation in the surrounding temperature can produce shift in the position of one echo relative to the other when viewed in the overlapped condition. The CW frequency source has to be properly tuned to maintain the condition of perfect cycle-to-cycle matching of the overlapped echoes. This is ultimately a small change in the round-trip travel time. Usually for materials which do not exhibit any anomaly or undergo any phase transition, velocity and hence elastic constants gradually decrease as the temperature is increased. The temperature dependence of the three diagonal elastic constants C_{11} , C_{22} and C_{33} are shown in Fig. 6.4 (a). C_{44} , C_{55} and C_{66} also show a similar dependence, which are shown in Fig. 6.4 (b).

6.6 Elastic anisotropy in BG crystals

In order to demonstrate the anisotropy in elastic properties, the phase velocity, slowness and group velocity surfaces have been generated using a program written in MATHCAD. Sections of these surfaces along the a-b, b-c and a-c planes are enough to visualize the entire surface. Sections of the phase velocity surfaces along the a-b, b-c and a-c planes are shown in Fig. 6.5 (a), (b) and (c) respectively. The pure shear (PS),

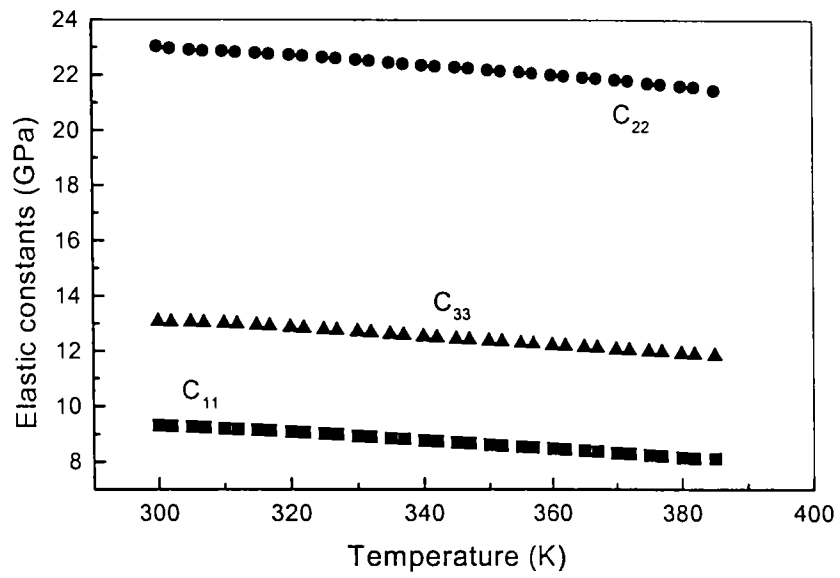


Fig.6.4(a) : Dependence of elastic constants C_{11} , C_{22} and C_{33} on temperature.

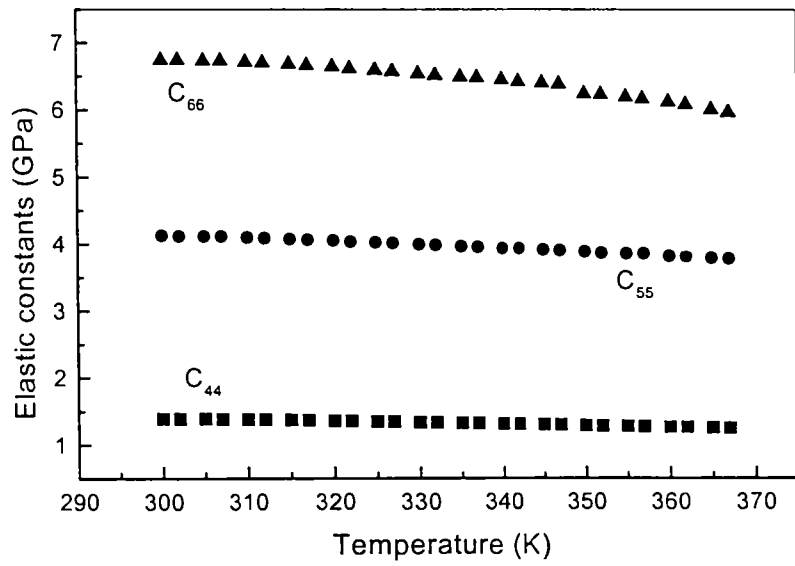


Fig.6.4(b) : Dependence of elastic constants C_{44} , C_{55} and C_{66} on temperature.

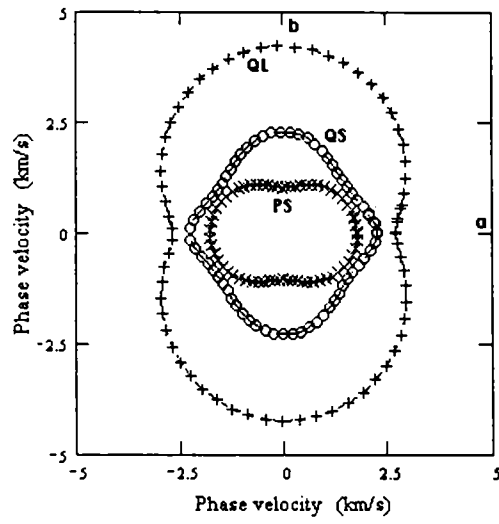


Fig. 6.5(a): Section of the phase velocity surfaces of BG along the a-b plane.

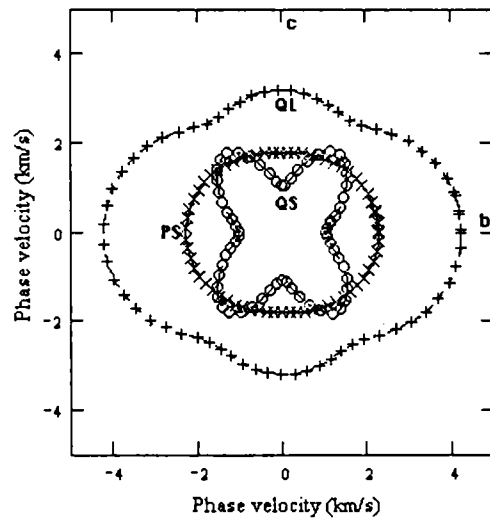


Fig. 6.5(b): Section of the phase velocity surfaces of BG along the b-c plane.

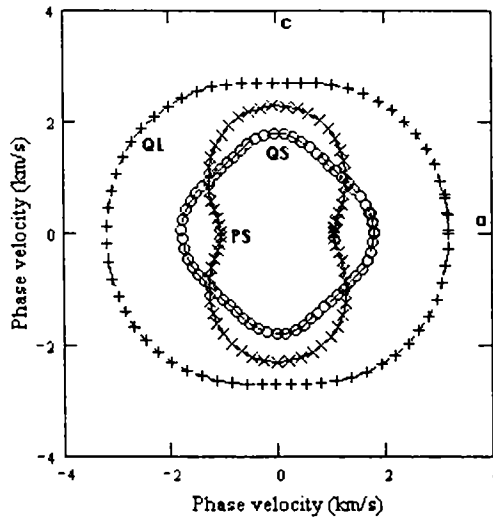


Fig. 6.5(c): Section of the phase velocity surfaces of BG along the a-c plane
 quasi-shear (QS) and quasi-longitudinal (QL) modes are shown separately in these figures. The shapes of these sections indicate the extent of anisotropy in the elastic properties of this crystal.

The inverse velocity surface or slowness surface can give more information regarding the elastic anisotropy. Figures 6.6 (a), (b) and (c) show the sections of the slowness surfaces along the a-b, b-c and a-c planes respectively.

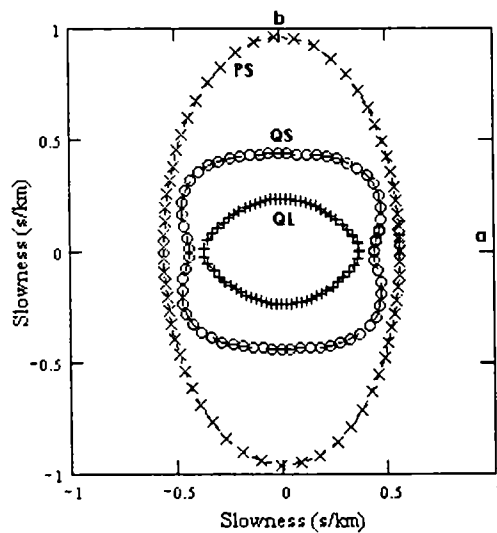


Fig. 6.6(a): Section of the slowness surfaces of BG along the a-b plane

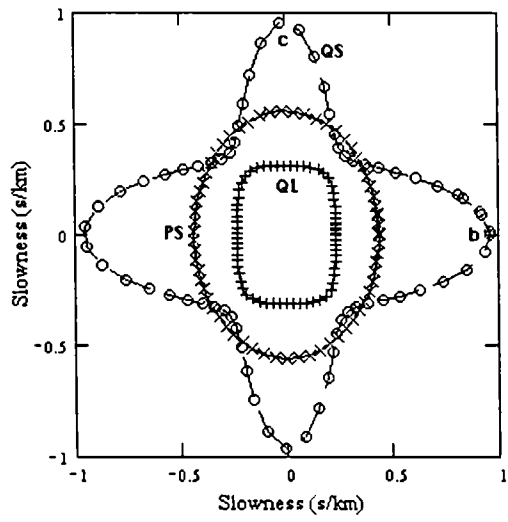


Fig. 6.6(b): Section of the slowness surfaces of BG along the b-c plane.

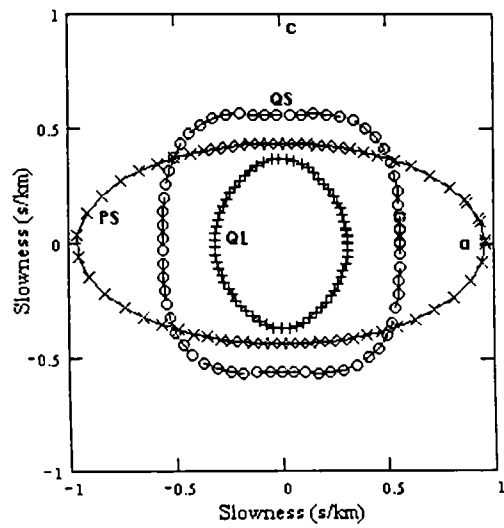


Fig. 6.6(c): Section of the slowness surfaces of BG along the a-c plane.

Group velocity surfaces can also be plotted to understand more about the anisotropy in elastic properties of single crystals. It may be noted that wave propagation, particularly the quasi-shear mode is highly anisotropic in this crystal. Sections of these surfaces along the a-b, b-c and a-c planes are shown in Fig. 6.7 (a), (b) and (c) respectively. The quasi-shear mode exhibits cuspidal edges along the symmetry directions in the group velocity surfaces. Along these directions the phase velocity and group velocity do not have a one-to-one correspondence and they are not collinear. More than one group velocity vector correspond to a phase velocity vector and the wave propagation is highly anisotropic in these directions. These features are reflected in the slowness surfaces also.

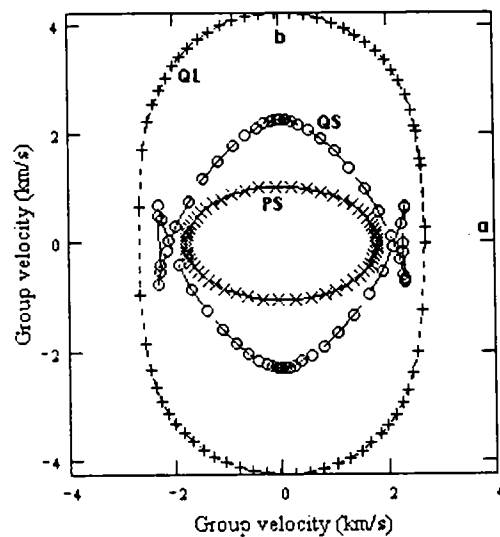


Fig. 6.7(a): Section of the group velocity surfaces of BG along the a-b plane

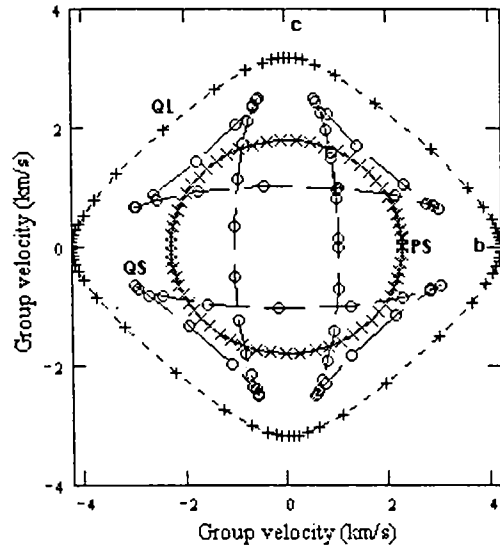


Fig. 6.7(b): Section of the group velocity surfaces of BG along the b-c plane

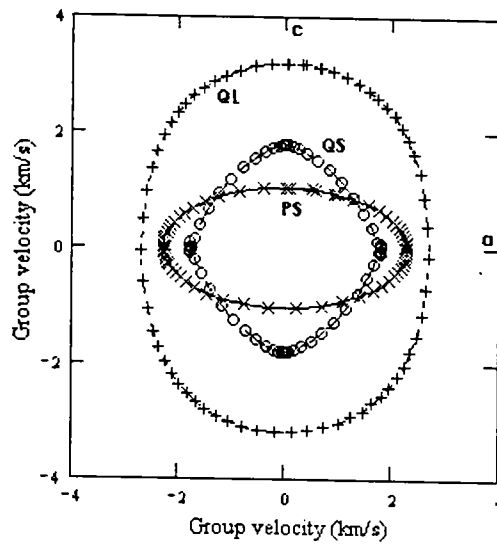


Fig. 6.7(c): Section of the group velocity surfaces of BG along the a-c plane

Eq.1.66 indicates that Young's modulus is also a direction dependent parameter. One can generate a surface by plotting values of the Young's modulus for all orientations. Sections of this surface along the a-b, b-c and a-c planes are shown in Fig. 6.8. Young's modulus along the b-direction is much larger than that along other directions. This indicates that the strain that can be produced along the b-direction applying stress is very small compared to other directions, indicating the presence of very strong intermolecular forces of attraction in this direction.

Linear compressibility is also a similar direction dependent parameter for which a surface can be generated. Sections of this surface along the a-b, b-c and a-c planes have been shown in Fig. 6.9. Here also the compressibility of this crystal by the application of unit hydrostatic pressure along the b-direction is much lower compared to the a and c directions.

6.7 Discussion and conclusion

N,N-dimethylformamide is found to be an ideal solvent for growing benzoyl glycine single crystals from solution. The rate of evaporation is very small compared to other organic solvents and hence one can control the spurious nucleation and other related difficulties. Crystals of size nearly $70 \times 25 \times 8 \text{ mm}^3$ have been grown over a period of around 4-5 weeks. Since, a (100) and b (010) planes are totally absent in the grown crystal, one must be extremely careful during the cutting of the crystals. The {110} set of planes is well developed. The density of the crystal is measured to be 1284 kg-m^{-3} . All the nine second order elastic constants of benzoyl glycine are reported for the first time. Here C_{22} is much larger than C_{11} and C_{33} indicating that the intermolecular forces along the b-direction is much stronger than that along the a and c directions.

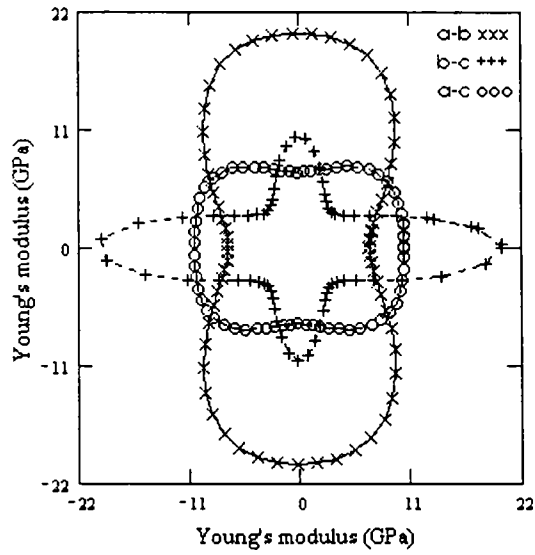


Fig. 6.8: Sections of the Young's modulus surface of BG along the a-b (xxx), b-c (+++) and a-c (ooo) planes.

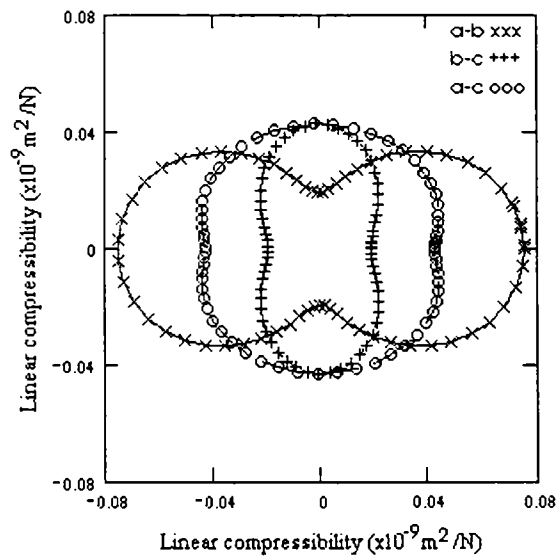


Fig. 6.9: Sections of the linear compressibility surface of BG along the a-b (xxx), b-c (+++) and a-c (ooo) planes.

The dependence of the diagonal elastic constants on temperature, do not show any anomaly in the range 300-375 K indicating the absence of any phase transition in this temperature range. This crystal is not known to exhibit any phase transition in this temperature range as already reported. Elastic constants C_{11} , C_{22} and C_{33} , normally called longitudinal elastic constants, depend more heavily on temperature compared to the shear elastic constants, C_{44} , C_{55} and C_{66} [6.18]. Thermal energy aids the lattice to expand more in the direction of the applied linear stress which ultimately results in a decrement in values of the elastic constants when applied stress is constant. The shear strain is not significantly affected by the rise of temperature and hence dependence of C_{44} , C_{55} and C_{66} on temperature is less.

Benzoyl glycine crystals are stable up to its melting point and are non-hygroscopic. It is very interesting to see the anisotropy exhibited in the elastic properties indicating the presence of strong intermolecular forces of attraction along the b-direction.

References.

- 6.1 N. Bloembergen, *J. Nonlinear Opt. Phys. Mater.* **15** (1996) 1
- 6.2 V. G. Dmitriev, G. G. Gurzadyan and D. N. Nikogosyan, *Hand book of nonlinear optical crystals* (Springer Verlag, New York 1997)
- 6.3 N. J. Long, *Angew. Chem. Int. Ed. Engl.* **34** (1995) 21
- 6.4 J. Badan, R. Hierle, A. Perigaud and J. Zyss, *Nonlinear optical properties of organic molecules and polymeric materials*, Am. Chem. Soc. Symp. Ser. 233 (ed) D. J. Williams (Am. Chem. Soc., Washington, DC 1993)
- 6.5 D. S. Chemla and J. Zyss (ed) *Nonlinear optical properties of organic molecules and crystals*, Vol. 1 and 2 (Academic Press, New York 1987)

- 6.6 R. A. Hann and D. Bloor (ed) *Organic materials for nonlinear optics* (Royal Society of Chemistry, 1989)
- 6.7 J. F. Nicoud and R. J. Twieg, *Nonlinear optical properties of organic molecules and crystals*, Vol. 1, D. S. Chemla and J. Zyss (ed) (Academic Press, New York 1987) p. 264.
- 6.8 Xu Dong, Yuan Duo-rong, Zhang Nan, Hou Wen-bo, Liu Ming-guo, Sun Nuoying and Jiang Min-hua, *J. Phys. D: Appl. Phys.* **26** (1993) B230
- 6.9 Heilmeyer, G. H. Ockman, Braunstein and Kramer D. A., *Appl. Phys. Lett.* **5**, (1964) 229
- 6.10 Orlov R. Y., *Sov. Phys.: Crystallogr. (Engl. Transl.)* **11**, (1966) 410
- 6.11 Gott J. R., *J. Phys.* **B4** (1971) 116
- 6.12 I. S. Rez, A. S. Sonin, E. E. Tsepelevich and A. A. Filimonov, *Sov. Phys.: Crystallogr.* **4** (1960) 59
- 6.13 H. S. Nagaraja, V. Upadhyaya, P. Mohan Rao, P. Sreeramana Aithal and A. P. Bhat, *J. Cryst. Growth* **193** (1998) 674
- 6.14 S. K. Kurtz and T. T. Perry, *J. Appl. Phys.* **39** (1968) 3798
- 6.15 H. Ringertz, *Acta Crystallogr.* **B27** (1971) 285
- 6.16 J. R. Neighbours and G. E. Schacher, *J. Appl. Phys.* **38** (1967) 5366
- 6.17 J. F Nye in *Physical properties of crystals* (Oxford University Press, London, 1957)
- 6.18 Soon-Chul kim and T. H Kwon, *Phys. Rev.* **B45** (1992) 2105

Chapter 7

Elastic properties of di-Ammonium hydrogen citrate (DAHC) single crystals

7.1 Introduction

Many organic crystals having orthorhombic structure exhibit ferroelectric [7.1,7.2], electrooptic [7.3], photoconducting [7.4] and triboluminescence [7.5] properties. The ammonium salt of citric acid, di-Ammonium hydrogen citrate (DAHC) with chemical formula $C_6H_{14}N_2O_7$ and formula weight 226.19 has been reported to be piezoelectric and triboluminescent [7.6,7.7]. This is a noncentrosymmetric crystal with orthorhombic structure and space group $Pn2b$ having lattice parameters $a = 10.767 \text{ \AA}$, $b = 14.736 \text{ \AA}$ and $c = 6.165 \text{ \AA}$ and has four molecules per unit cell [7.8]. Good quality single crystals of reasonable size can be grown quite easily by layering supersaturated aqueous solution with ethyl alcohol. Alcohol absorbs water from the solution and thereby supersaturation increases leading to the development of nuclei. It further grows and thus small single crystals can be grown easily. Not much work has been reported

earlier on characterization of this crystal. Crystal growth, defect characterization by etching studies and dielectric properties of this crystal have been studied earlier by J. George *et al.* [7.9]. The deformation and fracture characteristics of this crystal has also been investigated by them employing microhardness indentation technique [7.10]. The hardness, fracture toughness and brittleness of this crystal in the (001) and (110) planes have been estimated for various ranges of load. It has a less prominent cleavage along the (110) plane. The density of this crystal is measured to be 1383 kg-m^{-3} . Compared to other organic crystals, this crystal is reported to be much harder (Hardness = 0.68GPa.) and the serious disadvantage of this crystal is its hygroscopic nature. The elastic properties of this crystal has not yet been reported earlier in literature. A more detailed report on the growth and characterization of this crystal is available in literature [7.9].

In this chapter we present the results of our work on the elastic properties of DAHC measured using ultrasonic technique. Single crystals of DAHC have been grown in the laboratory. All the nine second-order elastic constants of this crystal have been determined by measuring ultrasonic (longitudinal and transverse) wave velocities along symmetry directions. The phase velocity surfaces, Young's modulus surface and linear compressibility surface have been plotted to understand the anisotropy in wave propagation in this crystal. Temperature variation of selected elastic constants have been measured and reported. Details of the work are presented in the following sections

7.2 Sample preparation

Large single crystals of DAHC have been grown by the slow evaporation technique. The solubility of DAHC in water is very high and hence the slow evaporation technique is the best method to grow large single crystals. Crystals of size nearly 60 x

35 x 12mm³ have been grown by this technique over a period of 4-5 weeks. The growth speed in the b-direction is very low and maximum along the a-direction. The lattice parameters reported are according to the IRE standards [7.11] and hence can be used to evaluate the inter-planar angles to identify the symmetry planes and directions in the crystal. With the aid of an accurate contact goniometer, the inter-planar angles were measured and the morphology of the crystal has been identified. The order of preference of the growth planes can be represented observing their relative size as (010) > (100) > (101) > (011). The molecular formula and morphology of the DAHC single crystal are shown in Fig.7.1 and Fig.7.2 respectively.

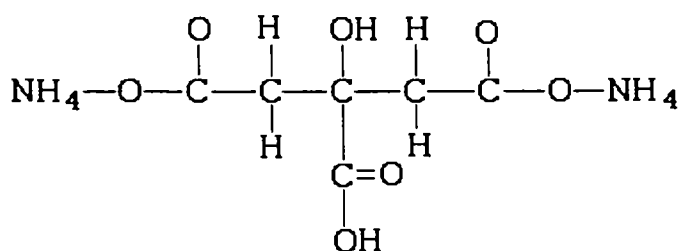


Fig. 7.1: Molecular formula of di-ammonium hydrogen citrate

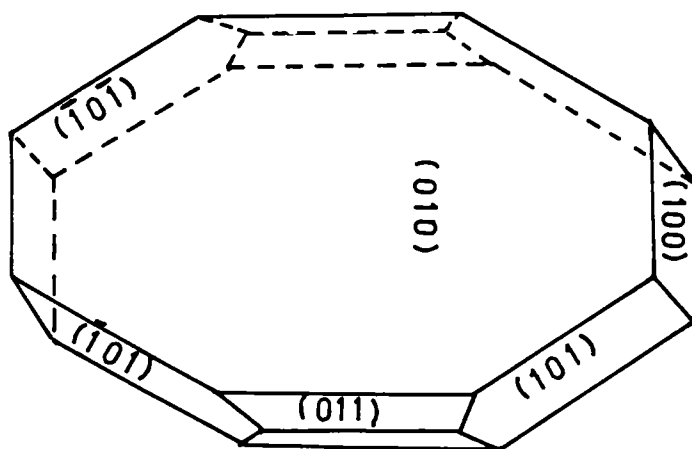


Fig. 7.2: Morphology of di-ammonium hydrogen citrate single crystals

Samples for ultrasonic measurements have been prepared in the shape of rectangular parallelepipeds by cutting the grown crystal with a slow speed diamond wheel saw. The well-developed growth planes have been taken as reference planes to orient the crystal for proper cutting. Samples with parallel planes perpendicular to the [100], [010] and [001] directions have been cut to measure velocities of propagation of ultrasonic wave pulses of longitudinal and transverse polarisations, which can directly yield all the six diagonal elastic constants. Three other samples with parallel planes perpendicular to any one direction along the a-b, b-c and a-c planes are necessary to determine C_{12} , C_{23} and C_{13} . Samples with parallel planes perpendicular to the [110], [011] and [101] directions (see Fig. 3.4 in chapter 3) have been prepared for this taking care to attain as best parallelism between the opposite planes as possible. These planes were lightly polished preserving the parallelism for accurate velocity measurements.

7.3 Ultrasonic velocity measurements

Twelve selected mode velocity measurements are sufficient to evaluate all the nine second-order elastic constants of an orthorhombic crystal. Pulse modulated ultrasonic waves are allowed to propagate through the crystal sample which leads to the generation of a series of echoes of exponentially decreasing amplitudes. X and Y cut quartz transducers of resonant frequency 10MHz bonded to the sample generates ultrasound vibrations in the crystal and in turn functions as the detector to receive the successively reflected echo pulses. Silicon grease serves as a good bond to fix the transducer on the crystal surface and easily transfer the mechanical vibrations generated by the transducer into the crystal medium. Pulse echo overlap technique developed by May [7.12] and later modified to the present form by Papadakis [7.13] have been used to determine the round trip travel time through the sample. A detailed

account of the different techniques adopted to measure ultrasonic wave velocity is available in literature [7.14] and is outlined in Chapter 2. Velocities of propagation of the different modes are directly related to the second order elastic constants. A direct relation of the form $C_{ij} = \rho v^2$ exists in the case of all diagonal elastic constants ($i = j$) and these modes are all pure modes. [110], [011] and [101] directions are mixed mode directions and the velocities measured along these directions are related to more than one elastic constant. The relationship between the elastic constants and relevant ultrasonic wave velocities for orthorhombic crystals are available in literature [7.15] and is summarized in Chapter 1.

McSkimin developed an analytical technique to eliminate the errors introduced in the measured travel times by the presence of the bonding medium between the transducer and crystal and the incorrect identification of the condition of perfect match by the visual examination of the overlapped echoes. This technique has been applied to measure the round trip travel times with the maximum possible accuracy (Chapter 2).

7.4 Elastic constants of DAHC single crystals

Velocities of propagation of the different ultrasonic modes along different symmetry directions and mode velocity-elastic constant relationship are tabulated in Table 7.1. The corresponding elastic stiffness constants, compliance constants and Poisson's ratios are listed in Table 7.2. It can be seen that, the crystal does not exhibit any sort of large-scale anisotropy in the elastic properties. The accuracy in the measured elastic constants is estimated to be 0.2% in the case of diagonal elastic constants and around 1% in the case of off-diagonal elastic constants.

Table 7.1 Velocity of ultrasonic modes in DAHC crystals. L, T and QL represent longitudinal, transverse and quasi-longitudinal modes respectively. The relations between mode velocities and elastic constants are also given.

Sl. No.	Mode	Direction of propagation	Direction of polarization	Measured mode velocity (m/s)	Mode velocity - elastic constant relationship
1	L	[100]	[100]	$v_1 = 4240 \pm 8$	$C_{11} = \rho v_1^2$
2	L	[010]	[010]	$v_2 = 4524 \pm 9$	$C_{22} = \rho v_2^2$
3	L	[001]	[001]	$v_3 = 4284 \pm 8$	$C_{33} = \rho v_3^2$
4	T	[010]	[001]	$v_4 = 2267 \pm 5$	$C_{44} = \rho v_4^2$
5	T	[001]	[010]	$v_5 = 2243 \pm 4$	$C_{44} = \rho v_5^2$
6	T	[100]	[001]	$v_6 = 2133 \pm 4$	$C_{55} = \rho v_6^2$
7	T	[001]	[100]	$v_7 = 2135 \pm 4$	$C_{55} = \rho v_7^2$
8	T	[100]	[010]	$v_8 = 2197 \pm 4$	$C_{66} = \rho v_8^2$
9	T	[010]	[100]	$v_9 = 2212 \pm 4$	$C_{66} = \rho v_9^2$
10	QL	[110]	[QL]	$v_{10} = 4129 \pm 8$	$C_{12} = f_{ab}^{(a)}$
11	QL	[011]	[QL]	$v_{11} = 4341 \pm 8$	$C_{23} = f_{bc}^{(b)}$
12	QL	[101]	[QL]	$v_{12} = 4250 \pm 8$	$C_{13} = f_{ac}^{(c)}$

$$(a) f_{ab} = \{[c^2 C_{11} + s^2 C_{66} - \rho v_{10}^2] \{c^2 C_{66} + s^2 C_{22} - \rho v_{10}^2\} / c^2 s^2\}^{1/2} - C_{66}$$

$$(b) f_{bc} = \{[c^2 C_{22} + s^2 C_{44} - \rho v_{11}^2] \{c^2 C_{44} + s^2 C_{33} - \rho v_{11}^2\} / c^2 s^2\}^{1/2} - C_{44}$$

$$(c) f_{ac} = \{[s^2 C_{11} + c^2 C_{55} - \rho v_{12}^2] \{s^2 C_{55} + c^2 C_{33} - \rho v_{12}^2\} / c^2 s^2\}^{1/2} - C_{55}$$

(Here c and s are the cosine and sine of the angle of rotation from the respective axes.)

Table 7.2 Elastic stiffness constants, compliance constants and Poisson's ratios of DAHC crystal at room temperature (300K)

Elastic stiffness constants (GPa)	Elastic compliance constants ($\times 10^{-10} \text{ m}^2\text{-N}^{-1}$)	Poisson's ratios
$C_{11} = 24.86 \pm 0.019$	$S_{11} = 5.46 \pm 0.011$	
$C_{22} = 28.30 \pm 0.046$	$S_{22} = 3.66 \pm 0.007$	$\nu_{12} = 0.157$
$C_{33} = 25.38 \pm 0.026$	$S_{33} = 5.28 \pm 0.011$	$\nu_{21} = 0.105$
$C_{44} = 7.10 \pm 0.003$	$S_{44} = 14.08 \pm 0.028$	
$C_{55} = 6.29 \pm 0.008$	$S_{55} = 15.90 \pm 0.032$	$\nu_{23} = 0.048$
$C_{66} = 6.67 \pm 0.014$	$S_{66} = 15.00 \pm 0.030$	$\nu_{32} = 0.069$
$C_{12} = 4.78 \pm 0.050$	$S_{12} = -0.576 \pm 0.005$	
$C_{23} = 3.74 \pm 0.044$	$S_{23} = -0.254 \pm 0.003$	$\nu_{13} = 0.497$
$C_{13} = 12.59 \pm 0.047$	$S_{13} = -2.625 \pm 0.026$	$\nu_{31} = 0.481$

7.5 Temperature dependence of elastic constants

Dependence of ultrasonic wave velocities and hence elastic constants on temperature have been studied by keeping the crystal-transducer assembly in a temperature-controlled oven. Since no reports are available on the detection of a phase transition or elastic anomaly in the temperature range 300-380K, study of only the transverse wave modes is done for this crystal. Usually elastic constants C_{11} , C_{22} and C_{33} may depend heavily on temperature whereas C_{44} , C_{55} and C_{66} depend less heavily [7.16]. The temperature dependence of C_{44} , C_{55} and C_{66} is shown in Fig. 7.3.

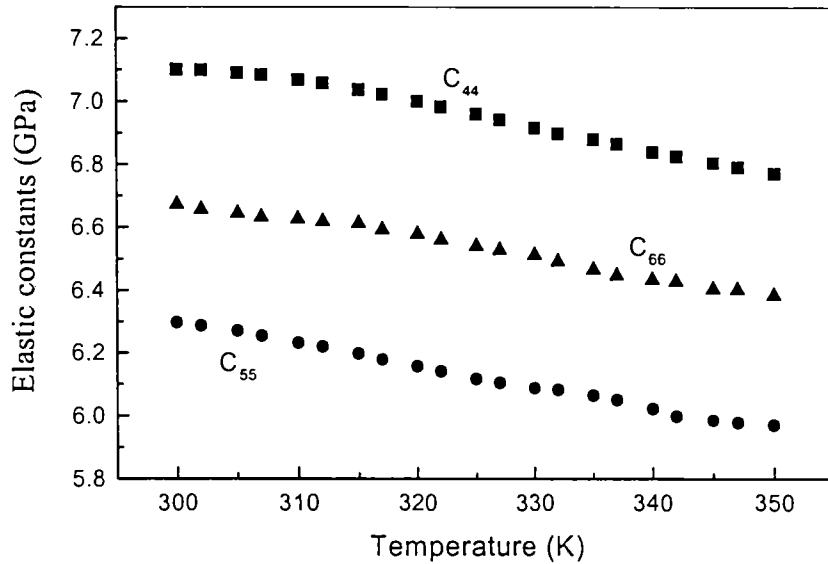


Fig. 7.3: Dependence of elastic constants C_{44} , C_{55} and C_{66} on temperature

7.6 Elastic anisotropy in DAHC crystal

DAHC single crystals show less anisotropy in the elastic properties. Longitudinal elastic constants C_{11} , C_{22} and C_{33} have values, more or less same in magnitude. C_{44} , C_{55} and C_{66} also show the same nature. In order to demonstrate the anisotropy in elastic properties, phase velocity, slowness and group velocity surfaces have been plotted using compliance constant data. Sections of these surfaces along the prominent symmetry planes are very useful to demonstrate anisotropy in elastic wave propagation. The sections of the phase velocity surfaces along the a-b, b-c and a-c planes are shown in Fig. 7.4(a), (b) and (c) respectively. The three modes - pure shear (PS), quasi-shear (QS) and quasi-longitudinal (QL) - are shown by separate plots. Elastic anisotropy in large-scale is not exhibited by this crystal. Slowness or inverse phase velocity surfaces are highly informative. Sections of these surfaces along the symmetry planes a-b, b-c and a-c are shown in Fig. 7.5(a), (b) and (c) respectively.

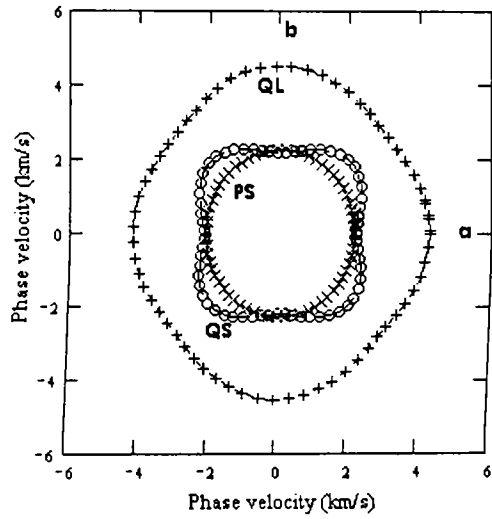


Fig. 7.4(a): Section of the phase velocity surfaces of DAHC along the a-b plane.

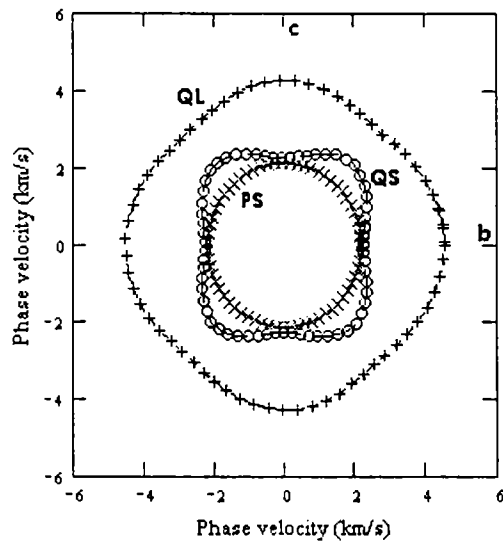


Fig. 7.4(b): Section of the phase velocity surfaces of DAHC along the b-c plane.

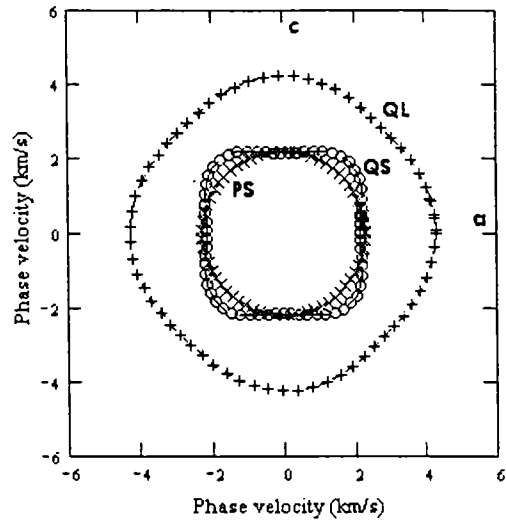


Fig. 7.4(c): Section of the phase velocity surfaces of DAHC along the a-c plane.

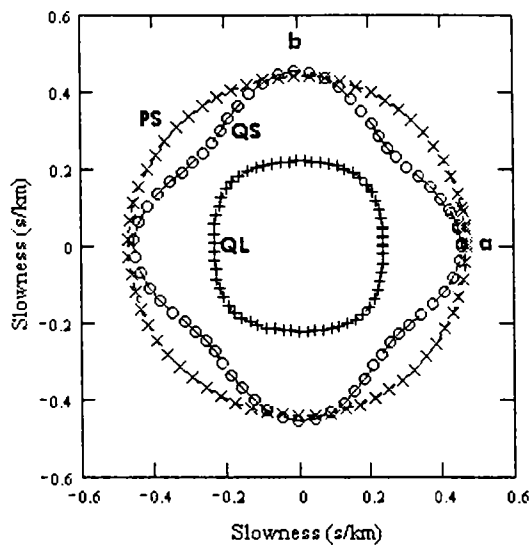


Fig. 7.5(a): Section of the slowness surfaces of DAHC along the a-b plane.

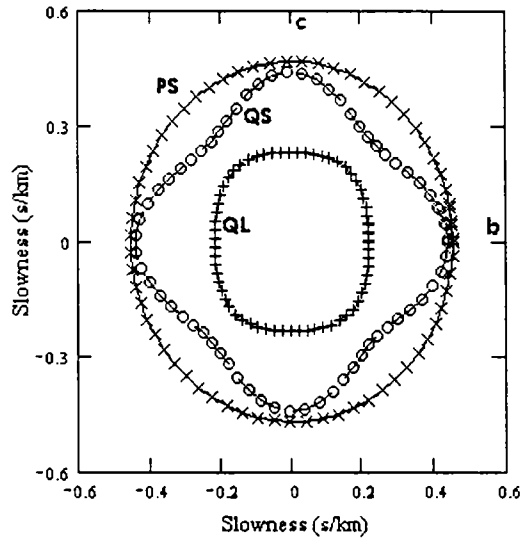


Fig. 7.5(b): Section of the slowness surfaces of DAHC along the b-c plane.

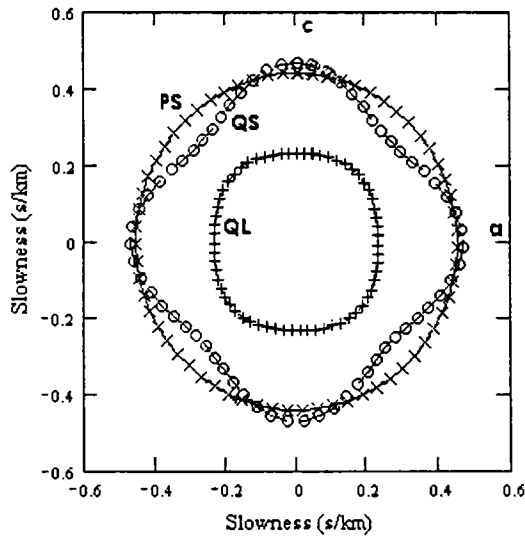


Fig. 7.5(c): Section of the slowness surfaces of DAHC along the a-c plane.

The three modes - pure shear (PS), quasi-shear (QS) and quasi-longitudinal (QL) - are shown by separate plots. The quasi-shear mode shows some anisotropy, which is clear from the shape of the curve.

Velocity of propagation of the modulation envelope called the ray velocity is the velocity with which energy propagates. The corresponding ray velocity vector need not be collinear with the phase velocity vector. The surface generated by plotting ray velocity for all directions can reveal more interesting aspects of the anisotropy in elastic properties of a crystal. Fig. 7.6(a), (b) and (c) show sections of these surfaces along the symmetry planes a-b, b-c and a-c respectively. It may be noted that the group velocity surfaces for the quasi-shear mode exhibit cuspidal edges along the $[110]$, $[011]$ and $[101]$ symmetry directions indicating that in these directions a one-to-one correspondence between phase velocity vector and group velocity vector does not exist. A phase velocity vector in these directions corresponds to more than one group velocity vector. One can expect very interesting phenomena such as conical refraction, phonon magnification etc., to occur in these directions [7.17,7.18].

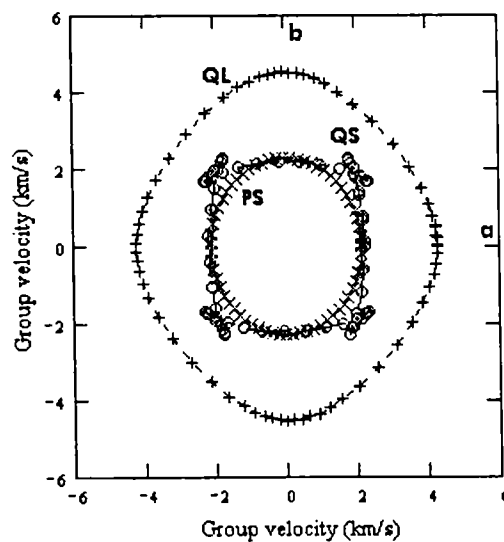


Fig. 7.6(a): Section of the group velocity surfaces of DAHC along the a-b plane

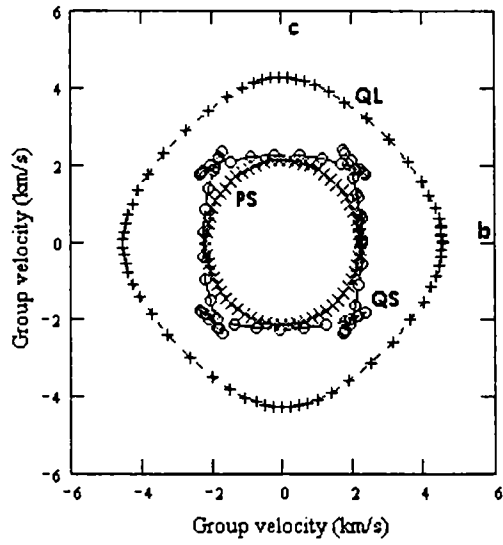


Fig. 7.6(b): Section of the group velocity surfaces of DAHC along the b-c plane

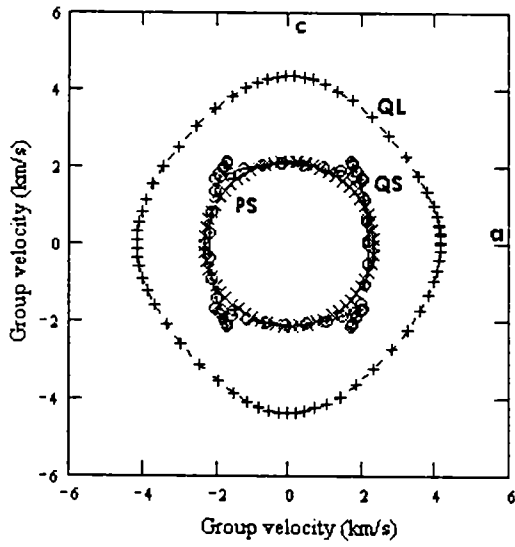


Fig.7.6(c): Section of the group velocity surfaces of DAHC along the a-c plane

Young's modulus [7.19] E in any direction in a crystal can be given as

$$E = (S_{11}n_1^4 + 2S_{12}n_1^2n_2^2 + 2S_{13}n_1^2n_3^2 + S_{22}n_2^4 + 2S_{23}n_2^2n_3^2 + S_{33}n_3^4 + S_{44}n_2^2n_3^2 + S_{55}n_1^2n_3^2 + S_{66}n_1^2n_2^2)^{-1}$$

Direction cosines, n_1 , n_2 and n_3 in the expression for Young's modulus E indicate that it is a direction dependent parameter. The strain produced in any direction in the crystal will be different in magnitude for the same longitudinal stress applied in one direction. Anisotropy in the elastic properties of a crystal can be demonstrated by plotting the Young's modulus surface. Sections of this surface along the symmetry planes a-b, b-c and a-c are plotted in Fig. 7.7. Young's modulus is minimum in the a-c plane.

Linear compressibility [7.19] β is also found to be a direction dependent parameter, since direction cosines n_1, n_2 and n_3 are present in the expression for β (Eq. 1.74). The linear compressibility surface can be easily generated from the elastic compliance data. For a better understanding of the direction dependence of linear compressibility, sections of this surface along the a-b, b-c and a-c planes have been drawn and are shown in Fig. 7.8. It can be noted that these curves are almost circular in shape. The crystal exhibits more or less isotropic behavior in its elastic properties.

Expressions for volume compressibility and bulk modulus are available in literature [7.19]. Volume compressibility of DAHC single crystal is evaluated to be equal to $0.75 \times 10^{-10} \text{ m}^2\text{-N}^{-1}$ and its bulk modulus works out to be 13.34 GPa.

7.7 Discussion and conclusion

Growth of single crystals of DAHC from the aqueous solution is rather difficult because of its very high solubility. Even the filtering of the solution is not so easy.

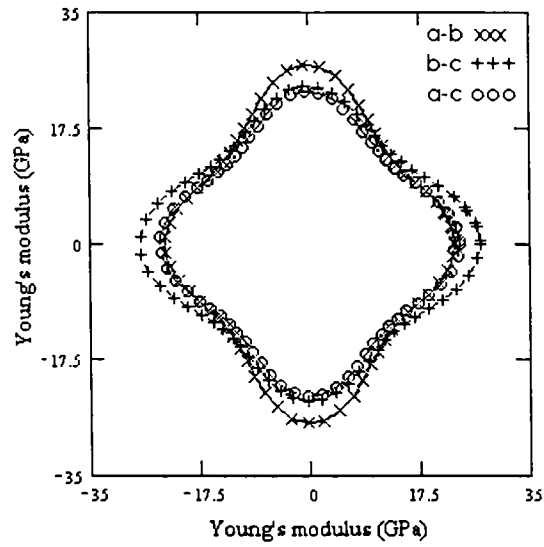


Fig. 7.7 : Sections of the Young's modulus surface of DAHC along the a-b (xxx), b-c (+++) and a-c (ooo) planes.

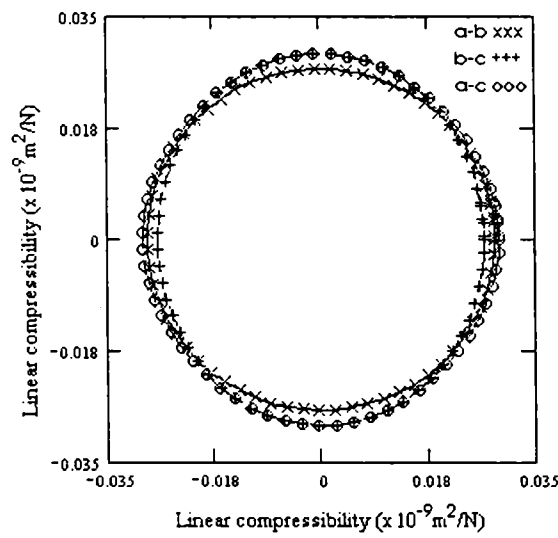


Fig. 7.8 : Sections of the linear compressibility surface of DAHC along the a-b (xxx), b-c (+++) and a-c (ooo) planes.

Clear transparent single crystals of size nearly $60 \times 35 \times 12 \text{ mm}^3$ have been grown over a period of about five weeks.

Longitudinal elastic constants C_{11} , C_{22} and C_{33} relate longitudinal stress to longitudinal strain. Thermal energy can enhance lattice expansion and hence the magnitude of the strain produced for a given stress can be more at higher temperatures. Correspondingly the elastic constants gradually decrease as the temperature is increased. The shear constants C_{44} , C_{55} and C_{66} need not show such a pronounced dependence because the shear strain is practically not much affected by change in temperature. DAHC single crystal does not exhibit any elastic anomaly or sudden change in the temperature range 300-350K indicating that there exist no phase transitions in this range of temperature. Dependence of only the shear constants (C_{44} , C_{55} and C_{66}) on temperature are studied here.

Very precise control of temperature is essential for the growth of single crystals of DAHC. Large good quality transparent single crystals have been grown from supersaturated solution by the slow evaporation technique. All the nine second-order elastic constants of this crystal have been determined for the first time. Anisotropy in elastic wave propagation in this crystal have been studied and reported.

References

- 7.1 C. J. Goldsmith and J. G. white, J. Chem. Phys. **31** (1959) 1175
- 7.2 R. G. Kepler, Ann. Rev. Phys. Chem. **29** (1978) 497
- 7.3 J. L. Stevenson, J. Phys. D: Appl. Phys. **6** (1973) L13
- 7.4 J. Kommandeur, J. Phys. Chem. Solids **22** (1961) 339
- 7.5 J. I. Zink and W. Klumt, J. Am. Chem. Soc. **96** (1974) 4690
- 7.6 B. P. Chandra and M. Elyas, J. Phys. **C12** (1979) L695

- 7.7 I. S. Rez, A. S. Sonin, E. E. Tsepelevich and A. A. Filimonov, *Sov. Phys: Crystallogr.* **4** (1960) 59
- 7.8 W. E. Love and J. L. Patterson, *Acta Crystallogr.* **13** (1960) 426
- 7.9 J. George and George Peter, *J. Mater. Sci.* **20** (1985) 3150
- 7.10 George Peter, Ph.D Thesis (Cochin University of Science and Technology, 1986).
- 7.11 J. R. Neighbours and G. E. Schacher, *J. Appl. Phys.* **38** (1967) 5366
- 7.12 J. E. May Jr., *IRE Natl. Conv. Rec.* **6**, Pt. 2 (1958) 134
- 7.13 E. P. Papadakis, *J. Appl. Phys* **35** (1964) 1474
- 7.14 E. P. Papadakis in *Physical Acoustics* (ed.) W. P. Mason and R. N. Thurston (Academic Press, New York 1976) Vol. **XII**, p. 227
- 7.15 H. J. McSkimin in *Physical Acoustics* (ed.) W. P. Mason (Academic Press, New York 1964) Vol. **I** Pt. **A**, p. 327
- 7.16 Soon-Chul Kim and T. H. Kwon, *Phys. Rev.* **B45** (1992) 2105
- 7.17 B. A. Auld in *Acoustic fields and waves in solids* (John Wiley and Sons, New York 1973) Vol. **1**
- 7.18 G. A. Northorp and J. P Wolfe, *Phys. Rev.* **B22** (1980) 6196 and references therein
- 7.19 J. F. Nye in *Physical properties of crystals* (Oxford University Press, London 1957)

Chapter 8

Summary and conclusion

A variety of single crystals find application in several technological fields. Of late newer and newer materials are synthesized to test the suitability of these crystals for various technological applications. Nonlinear optical crystals are a new class of materials, which are suitable to generate second harmonic of optical radiation and many related applications. A long list of organic, inorganic and semiorganic or organometallic class of materials synthesized is available in literature. Growth of single crystals of these materials with required dimensions and purity is a challenging task. The physio-chemical characterization of these crystals is essential to assess their suitability in device fabrication. Mechanical properties such as microhardness, elastic properties and resistance to laser induced damages have to be studied prior to device fabrication.

Five different single crystals having orthorhombic structure have been grown in bulk form for the investigations presented in this thesis. These crystals are either nonlinear optical or semiorganic in nature. All the nine second-order elastic constants of all these crystals have been determined for the first time. Sodium p-nitrophenolate dihydrate (NPNa), hippuric acid or benzoyl glycine (BG) and zinc tris (thiourea) sulphate (ZTS) single crystals are potential nonlinear optical crystals. Growth conditions for growing bulk crystals have been optimized. Crystals of reasonably good

size have been grown by the solution growth technique. Crystallographic directions and growth planes have been properly identified by measuring inter-planar angles using an accurate contact goniometer and are compared with values evaluated from crystallographic data. Laboratory axes (x, y, and z) have been fixed according to the IRE standards before cutting the single crystal. As per this convention x is taken parallel to a, y is taken parallel to b and z is taken parallel to c where the condition $c < a < b$ is satisfied. Twelve selected ultrasonic mode velocity measurements have been carried out in all cases to evaluate all the nine second-order elastic constants. Poisson's ratios, volume compressibility and bulk modulus have been evaluated for all these crystal samples.

Dependence of the diagonal elastic constants on temperature have been studied in all cases. It is found that the dependence of the longitudinal elastic constants C_{11} , C_{22} and C_{33} on temperature is more compared to the shear elastic constants C_{44} , C_{55} and C_{66} . Reasons for this behavior are out lined in the thesis. None of these crystals exhibit any anomaly in the elastic properties in the range of temperature over which measurements have been carried out. These samples have not been reported to exhibit any kind of phase transition in this range of temperature, and our measurements confirm this.

Demonstration of the anisotropy in the ultrasonic (elastic) wave propagation characteristics of these crystals have been done by plotting surfaces of phase velocity, slowness or inverse velocity and group velocity or ray velocity. Sections of these three-dimensional surfaces along the a-b, b-c and a-c planes have been drawn for better clarity. Deviation from perfect circular shape indicates anisotropy in elastic wave propagation. It is found that elastic anisotropy is more pronounced for the quasi-shear mode, which is the general behavior exhibited by most crystals.

Inverse velocity (slowness) surfaces are also very informative. In some aspects, the group velocity surfaces are also more informative. The formation of cuspidal edges has been found in few crystal samples, which is an interesting phenomenon. The ray velocity (or group velocity) need not be collinear with the phase velocity vector and there need not have a one-to-one correspondence between these two. The significance of the formation of cuspidal edges in these crystals has been explained in relevant chapters.

Young's modulus and linear compressibility are two other important direction dependent parameters. Surfaces generated by plotting these values for all orientations in the crystal sample can demonstrate the anisotropy in the elastic properties of a crystal better. Sections of these surfaces along the a-b, b-c and a-c planes are shown for all these five single crystal samples. The extent of deviation from perfect circular shape determines the anisotropy in the elastic properties of a crystal. Single crystals of benzoyl glycine and NPNa exhibit marked anisotropy in their elastic properties.

Large number of new materials have been synthesized recently which are reported to be nonlinear optical crystals. Efficiency for second harmonic generation (SHG) in most of these cases is very high compared to, the well-characterized KDP crystals. Reports are available on the synthesis, growth of single crystals and crystallographic data on many crystals. It is very important to investigate their elastic properties before they are put into any use. Thiourea is one such sample, which has the ability to form a variety of complexes with other compounds and hence there is plenty of scope for work in this line. Single crystals of these materials are usually grown from supersaturated solution by the slow evaporation or slow cooling techniques. Well-developed growth planes are very advantageous in orienting the crystal.

AMA, m-chloronitrobenzene, m-bromonitrobenzene, POM, NPP etc. are some of the very important NLO crystals grown from solution. L-histidine tetrafluoro borate, bis(thiourea) cadmium chloride, L-arginine flouride, zinc thiourea chloride, CsGeCl₃ etc. are some of the recently reported NLO crystals. The elastic properties of these and many other important crystals have not been studied so far. There is lot of scope for doing very important and useful work in this direction.

It would be interesting to extent ultrasonic measurements on nonlinear optical crystals to low temperatures. From a basic, research point of view it would be very valuable to measure variations in elastic properties with applied electric field in these crystals. These measurements will give interesting information about electro-acoustic (phonon) interactions. There is lot of scope for doing front line research in this area.